Next Generation On-Line Dynamic Security Assessment

Final Project Report

Power Systems Engineering Research Center

Empowering Minds to Engineer
the Future Electric Energy System

Next Generation On-Line Dynamic Security Assessment

Parts I and II

Final Project Report

Parts I and II Project Team

Vijay Vittal, Project Leader

Feng Ma and Guanji Hou, Graduate Students

Arizona State University

PSERC Publication 11-09

November 2011

Information about this project

Vijay Vittal
Ira A. Fulton Chair Professor
Department of Electrical Engineering
Arizona State University
PO Box 875706
Tempe, AZ 85287-5706
Tel: 480-965-1879
Fax: 480-965-0745
Email: vijay.vittal@asu.edu

Power Systems Engineering Research Center

The Power Systems Engineering Research Center (PSERC) is a multi-university Center conducting research on challenges facing the electric power industry and educating the next generation of power engineers. More information about PSERC can be found at the Center's website: http://www.pserc.org.

For additional information, contact:

Power Systems Engineering Research Center
Arizona State University
577 Engineering Research Center
Tempe, Arizona 85287-5706
Phone: 480-965-1643
Fax: 480-965-0745

Notice Concerning Copyright Material

Acknowledgements

This is Parts I and II of the final report for the Power Systems Engineering Research Center (PSERC) research project titled “Next Generation On-Line Dynamic Security Assessment.” (PSERC project S-38) We express our appreciation for the support provided by PSERC’s industrial members and by the National Science Foundation under the Industry/University Cooperative Research Center Program.

We specifically thank:

- Jianzhong Tong – PJM
- Eugene Litvinov – ISO New England
- Jinan Huang – Institut de Recherche d'Hydro-Québec (IREQ)
- Doug McLaughlin – Southern Co.
- Sharma Kolluri – Entergy
- Dede Subakti – California Independent System Operator (CAISO).

Executive Summary

This project addresses five elemental aspects of analysis for the enhanced performance of on-line dynamic security assessment. These five elemental components include: a) A systematic process to determine the right-sized dynamic equivalent for the phenomenon to be analyzed, b) Employing risk based analysis to select multi-element contingencies, c) Increased processing efficiency in decision-tree training, d) Using efficient trajectory sensitivity method to evaluate ability for changing system conditions, and e) Efficient determination of the appropriate level of preventive and/or corrective control action to steer the system away from the boundary of insecurity. An overview of the work accomplished in each part is presented below:

Part I. Determination of the right-sized dynamic equivalent (work done at Arizona State University)

To account for the challenges associated with rapid expansion of modern electric power grid, power system dynamic equivalents have been widely applied for the purpose of reducing the computational effort of dynamic security assessment. Dynamic equivalents are commonly developed using a coherency based dynamic equivalencing approach in which a study area and external area are first demarcated. Then the coherency patterns of the generators in the external areas are determined. A commonly used method is to introduce faults on the boundary of the study area and to group the generator with similar dynamic responses in the external area. Other methods, such as slow coherency-based method and weak-link method have also been proposed. As a result, the coherent generators in the external area are equivalenced. Network reduction is then performed at the interface between the study area and the external area to suitably interconnect the equivalent generators. In the process of building a dynamic equivalent, the definition of the retained area can significantly impact the effectiveness of the final reduced system. As more components are included in the retained area, more attributes related to the dynamic characteristics of the study area can be retained. In conventional dynamic equivalencing applications, the study area and external area are arbitrarily determined without examining the phenomenon of interest with respect to the system dynamic behavior. An improperly defined retained area boundary can result in detrimental impact on the effectiveness of the equivalenced model in preserving dynamic characteristics of the original unreduced system. Additionally, under realistic situations, generator coherency information obtained under one particular operating condition might not be applicable to another operating condition. For a new system condition the process of re-evaluating the generator coherency is time-consuming, especially for large-scale power systems. Therefore significant strides can be made if an efficient technique can be developed to predict the variation in coherency behavior as system condition changes.

The approach that has been implemented in this project first considers the system representation that is available in the control center and for which the supervisory control and data acquisition (SCADA) implementation is available. The boundary of this system representation is then transferred to the planning case being considered for dynamic equivalencing. This represents the initial boundary of the study area. Tie-line interfaces between the study area and external area are identified. Then three criteria, namely the

power transfer distribution factors (PTDFs), the estimated generator rotor acceleration during the fault duration, and the oscillatory mode participation factors are applied to identify the critical generators in the initial external area that exert significant impacts on the dynamic performance of the study area. Based on this determination, the buffer area to be additionally retained can be formed by including these identified generators. The coherent generators in the new external area are then equivalenced, followed by network reduction and load aggregation. The proposed approach is efficient in the sense that the criteria, such as PTDFs and mode participation factors can be readily assessed in many commercial software packages (e.g. PowerWorld, PSS/E, and DSA Tools); while the rotor acceleration-based criterion can be readily computed without the need of time-domain simulation.

To account for the impacts of system condition change on dynamic equivalents, an eigensensitivity-based approach has been proposed in this project to trace the changes in generator slow coherency patterns. Instead of computing the slow coherency patterns from scratch for a new operating condition, the proposed method aims at capturing the significant changes in generator slow coherency after either generation level, load level, or system topology is changed. Based on the predicted coherency patterns, the retained area boundary is adjusted by including the critical generators in the initial external area that become tightly coherent with the initial retained area. The advantages of the proposed approach in saving computational time and improving the equivalencing accuracy for varied operating condition are significant.

The research conducted also reveals that the improvement resulting from revising the retained area boundary might become insignificant when the retained area is already large enough. This limitation is important in today's environment because detailed information regarding the component models and system topologies in the entire system is often inaccessible to a signal entity under the restructured environment. To address this issue, a novel hybrid dynamic equivalent, consisting of both a coherency-based equivalent and an artificial neural network (ANN)-based equivalent, has been proposed. The ANN-based equivalent complements the coherency-based equivalent at the retained area boundary buses. It is designed to compensate for the discrepancy between the full system and the conventionally reduced system. The test on a portion of the WECC system shows that the hybrid dynamic equivalent method can improve the accuracy of the coherency-based equivalent for both the trained and untrained cases. Additionally, the measurements collected by the synchronized phasor measurement units (PMUs) also allow the proposed method to improve the dynamic models for on-line dynamic security assessment (DSA).

The approaches developed have been tested on a large portion of the WECC system and on a test case provided by ISO-NE which includes a significant portion of the Eastern interconnection. The techniques developed have also used in conjunction with the new version of DYNRED developed by Powertech Labs. This represents significant large scale testing of the method and demonstrates its capability of technology transfer to PSERC member companies. The student working on this portion of the project also performed a summer internship at ISO-NE where the method was applied to the ISO-NE system and demonstrated.

Part II. Trajectory sensitivity analysis to determine stability limits under changing system conditions (work done at Arizona State University)

Currently some utilities have existing time domain simulation based approaches to perform DSA in near real time. However, when the network topology or the operating condition changes significantly in a short time horizon, the derivation of the stability limits is computationally burdensome. In this part of research effort, an approach to compute stability limits based on a computationally enhanced trajectory sensitivity analysis has been developed to improve the computational efficiency and accuracy. The most attractive advantage of the trajectory sensitivity approach is that it can provide valuable insights into system responses due to parameter changes within a very short time at the expense of only a negligible amount of extra computational burden.

Firstly, various system parameters sensitivity calculation software packages have been implemented. The implementations include sensitivity to system generation change, load change, load modeling parameters change, generator control parameters change, network topology change and FACTs control parameters change. A Graphic User Interface (GUI) is also developed to simplify the usage. The implementations are fully tested by comparing the approximated system variable trajectories based on the base case with the actual perturbed trajectories obtained by running repeated time domain simulation for the changed condition. The results show the correctness of the implementation and enhanced performance of the trajectory sensitivity method.

Secondly, the computational efficiency problem is also addressed. The trajectory sensitivity method requires augmenting the existing system differential algebraic equations (DAEs) with a new set of sensitivity DAEs corresponding to each system parameter changes. This increases the computation burden. A high performance parallel computing platform has been utilized to reduce this burden. It is observed that each parameter sensitivity calculation is independent of other parameter sensitivity calculations. Moreover, they share the same Jacobian matrices for the solutions. Therefore, when multiples element sensitivities are evaluated, they can be performed in this cluster simultaneously. The test of this cluster shows great efficiency improvement.

The third issue tackled in this research effort is the linear approximation accuracy. The application basis of the trajectory sensitivity method is the first order linear approximation. When there is a small change in certain parameter, the system responses for this changed condition can be approximated based on the base case and the sensitivities evaluated along the base case. However, there is no quantitative measurement on the relation between the linear approximation accuracy and the perturbation size. In this research effort, it is found that there is a relationship between the bound on the linear approximation error and the bound on the product of the maximum normalized sensitivity and the perturbation size. This relationship appears to be system independent and system operating point independent. Thus, the error-perturbation size analysis method based on this finding serves as a general application guide to evaluate the accuracy of the linear approximation.

The uncertainty problem of power system modeling is also addressed using the trajectory sensitivity method. Currently most widely used methods mainly rely on the Monte Carlo type simulation to estimate the probability distribution of the outputs. These methods

require repeated simulations for each possible set of values of load models. Therefore, these approaches are computationally intensive. The trajectory sensitivity analysis can provide an alternative approach to deal with this problem. When load modeling parameter uncertainty is considered, the possible system operational boundary can be obtained by linear approximation with load parameter sensitivity information evaluated along a base case simulation in the time horizon. Based on this operational boundary, the amount of control needed to maintain the system voltage stability should not be fixed. Rather it should be within a certain defined range. An example to study the uncertainty of the composite load modeling and its effect on the system voltage stability problem is given.

The applicability of the trajectory sensitivity approach to a large realistic network is demonstrated in detail. This work applies the trajectory sensitivity analysis method to the WECC system. Several typical power system stability problems have been addressed:

1. The angle stability problem

A systematic preventive control analysis method in terms of generation rescheduling to maintain the system transient angle stability is developed and demonstrated

2. The voltage stability problem

The trajectory sensitivity approach is used to determine the system operational boundary corresponding to a set of uncertain parameters. Several preventive control actions are then determined according to this operational boundary rather than one fixed operating point. This consideration provides border information for control decision making

3. Interface real power flow limit calculation

The trajectory sensitivity method is also applied to calculate the interface real power flow limit. First the generation limits of the key generators in the interface are calculated utilizing the trajectory sensitivity method. Then the flow limit through the interface can be determined by the limits of the key generators and their PTDFs.

All these approaches have been demonstrated on a large realistic model of the WECC system. The software was developed in conjunction with an open source time domain software package called PSAT. All the elements of the development can be easily transported to any member company for demonstration and use.

Project Publications

[1] F. Ma, and V. Vittal, "Right-sized power system dynamic equivalents for power system operation," to appear in the *IEEE Trans. on Power Syst*, TPWRS.2011.2138725.

[2] F. Ma, X. Luo, and V. Vittal, "Application of dynamic equivalencing in large-scale power systems," to appear in the proceeding of *IEEE PES 2011 General Meeting*, Detroit, MI, July 24–28, 2011, Paper no. 2011GM0804.

[3] G. Hou, and V. Vittal, "Cluster computing-based trajectory sensitivity analysis application to the WECC system," *IEEE Trans. on Power Syst*., v. 26, No. 3, pp. 1 – 8, 2011.

Student Theses

[1] F. Ma, “Improved Coherency-based Dynamic Equivalent,” PhD Dissertation, Arizona State University, November 2011.

[2] G. Hou, “Trajectory Sensitivity Based Dynamic Security Assessment,” PhD Dissertation, May 2012.

Part I

Determination of the Right-Sized Dynamic Equivalent

Vijay Vittal
Feng Ma – Graduate Student
Arizona State University

Information about this project

Vijay Vittal
Ira A. Fulton Chair Professor
Department of Electrical Engineering
Arizona State University
PO Box 875706
Tempe, AZ 85287-5706
Tel: 480-965-1879
Fax: 480-965-0745
Email: vijay.vittal@asu.edu

Power Systems Engineering Research Center

The Power Systems Engineering Research Center (PSERC) is a multi-university Center conducting research on challenges facing the electric power industry and educating the next generation of power engineers. More information about PSERC can be found at the Center's website: http://www.pserc.org.

For additional information, contact:

Power Systems Engineering Research Center
Arizona State University
577 Engineering Research Center
Tempe, Arizona 85287-5706
Phone: 480-965-1643
Fax: 480-965-0745

Notice Concerning Copyright Material

Table of Contents

List of Figures

List of Tables

Glossary

a_i	Rotor acceleration rate of generator *i*
a_{opt}	Optimal step length in the corrector procedure for eigensolution estimation
b_{ij}	Primitive susceptance of line from bus *i* to bus *j*
d_{ij}	Slow coherency index between generator *i* and generator *j*
g_{ij}	Primitive conductance of line from bus *i* to bus *j*
n_{ANN}	Number of buses connected to ANN-based equivalent
p_{ki}	Participation factor of the k^{th} state variable in the i^{th} mode
t_f	Fault duration
x_{ij}	Primitive reactance of line from bus *i* to bus *j*
x'_{di}	Transient reactance of generator *i*
$\mathbf{b}(i)$	Bias vector at i^{th} layer of the neural network
$\mathbf{f}$	Differential equations representing the dynamics of system components
$\mathbf{f_x}$	Partial derivative of **f** with respect to system state variables
$\mathbf{f_y}$	Partial derivative of **f** with respect to system algebraic variables
$\mathbf{f}_\beta$	Sensitivity of **f** with respect to system parameter
$\mathbf{g}$	Algebraic equations representing the power flow equations
$\mathbf{g_x}$	Partial derivative of **g** with respect to system state variables
$\mathbf{g_y}$	Partial derivative of **g** with respect to system algebraic variables
$\mathbf{g}_\beta$	Sensitivity of **g** with respect to system parameter
$\mathbf{h}$	Nonlinear function vector representing the input-and-output mappings
$\mathbf{x}$	System state variable vector
$\mathbf{x}_{\beta,n}$	Sensitivity of **x** with respect to system parameter at the time instant *n*
$\mathbf{y}$	System algebraic variable vector
$\mathbf{y}_{\beta,n}$	Sensitivity of **y** with respect to system parameter at the time instant *n*
B_{ij}	Imaginary part of the (*i*,*j*) element in the system admittance matrix
E_i	Voltage behind the transient reactance of generator *i*
G_{ij}	Real part of the (*i*,*j*) element in the system admittance matrix
H_{i}	Inertia constant of generator *i*
K_G	Set of dispatchable generators
K_L	Set of load buses subjected to changes
M_i	Inertia of generator *i*
P_{ij}	Active power flow over the line from bus *i* to bus *j*
P_{Gi}	Electrical output power of generator *i*
P_{mi}	Mechanical input power of generator *i*
$P_{ANNi,n}$	Active power injection of the ANN-based equivalent at bus *i* at the time instant *n*
$PTDF_g^{ij}$	Power transfer distribution factor of generator *g* with respect to line from bus *i* to bus *j*
Q_{Gi}	Reactive power output of generator *i*
$Q_{ANNi,n}$	Reactive power injection of the ANN-based equivalent at bus *i* at the time instant *n*
V_i	Voltage magnitude at bus *i*
$\mathbf{A}_{sys}$	System state matrix

$\mathbf{B}$	Node susceptance matrix in DC power flow computation
$\mathbf{D}$	Diagonal generator damping coefficient
$\mathbf{J}_{pf}$	Jacobian matrix in power flow computation
$\mathbf{K}$	Synchronizing power coefficient matrix
$\mathbf{M}$	Diagonal generator inertia coefficient matrix
$\mathbf{M}_{G\mathrm{i}}$	Vector with 1 in the entry of generator *i* and zeros elsewhere
$\mathbf{M}_{l}$	Node-branch incidence vector
$\mathbf{M}_{PLi}$	Vector with 1 in the entry of load bus *i* and zeros elsewhere
$\mathbf{M}_{QLi}$	Vector with 1 in the entry of load bus *i* and zeros elsewhere
$\mathbf{P}$	Active power injection vector in power flow computation
$\mathbf{Q}$	Reactive power injection vector in power flow computation
$\mathbf{S}$	Inverse of Jacobian matrix in power flow calculation
$\mathbf{S}_{ANN,n}$	Power injection vector of the ANN-based equivalent at the time instant *n*
$\mathbf{V}_{ri,n}$	Voltage at bus *i* in the reduced system at the time instant *n*
$\mathbf{V}_{fi,n}$	Voltage at bus *i* in the full system at the time instant *n*
$\mathbf{V}_{ANN,n}$	Terminal voltage vector of the ANN-based equivalent at the time instant *n*
$\mathbf{W}(i)$	Weights matrix at i^{th} layer of the neural network
ATC	Available Transfer Capability
ANN	Artificial Neural Network
DAE	Differential Algebraic Equation
DSA	Dynamic Security Assessment
DYNRED	Dynamic Reduction Program
ISO	Independent System Operator
ISO-NE	ISO New England
LM	Levenberg-Marquardt training algorithm
MLP	Multilayer perceptron-based neural network
NB	New Brunswick
NS	Nova Scotia
NYISO	New York ISO
PMU	Synchronized Phasor Measurement Unit
PSS	Power System Stabilizer
PTDF	Power Transfer Distribution Factor
RMSE	Root Mean Square Error
WECC	Western Electricity Coordinating Council
β	System parameter subject to changes
β_0	Initial value of the system parameter
δ_i	Rotor angle of the generator *i*
θ_i	Voltage phase angle at bus *i*
λ_i	Eigenvalue of i^{th} mode
ω_i	Rotor speed of generator *i* (p.u.)
ω_R	Base frequency (376.99 rad/s)
ω_0	Initial value of the rotor speed of generator *i* (p.u.)
$\boldsymbol{\upsilon}_i$	Row of right eigenvector matrix corresponding to the rotor angle state of generator *i*
ξ	Initial value of the states vector
ϕ_i	Activation function at i^{th} layer of the neural network

$\boldsymbol{\phi}_i$	Right eigenvector corresponding to i^{th} mode
$\boldsymbol{\psi}_i$	Left eigenvector corresponding to i^{th} mode
$\boldsymbol{\Phi}$	Matrix consisting of the right eigenvector of the modes of interest
Δt	Integration time step
$\Delta \mathbf{G}$	Mismatch of eigensolution estimation

1. Introduction

1.1 Background

With the evolution of heavily interconnected electric power systems, it is computationally burdensome to represent the entire system in detail to conduct numerous transient stability studies [1]. This is especially true for real-time power system transient stability assessment because there is a strict limitation on the size of the system that can be simulated. In addition, the generation, transmission and distribution facilities can belong to different owners in the restructured environment [2]. This situation makes it difficult for a single entity to access detailed information about the network and equipment models within the entire system. Therefore, it is necessary to construct a reduced order system which preserves the dynamic property of the specific system that is of interest. To address these challenges, power system dynamic equivalents have been receiving renewed attention recently. As shown in Fig. 1.1, three areas are usually defined in the process of constructing a dynamic equivalent [3]:

- Study area: the core subsystem that is of direct interest and therefore must be retained in detail. For the reduced system to be effective in representing the behavior of the full system, the power flow and dynamic responses in this area are supposed to be the same as that in the full system representation.
- Buffer area: the area that is geographically or electrically close to the retained area. It has significant impact on the study area due to its tight connection to the study area. For better equivalencing accuracy, this area along with the system components is retained in detail.
- External area: this is the portion of the system for which detailed information on the system responses is not required and where the models can be replaced by proper equivalent models.

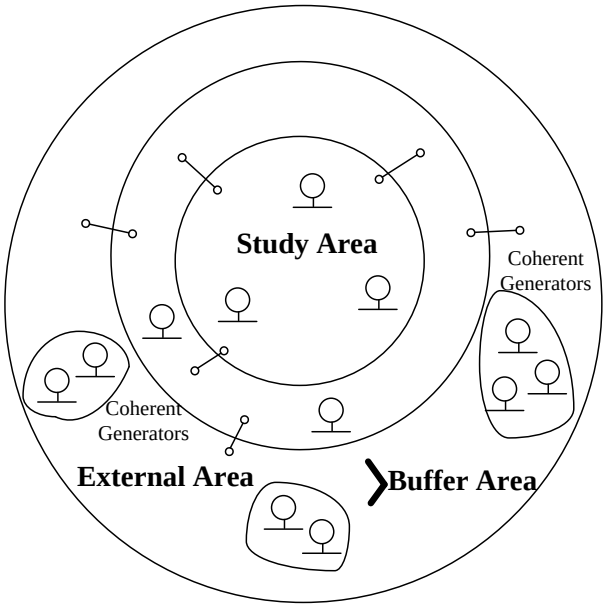

Fig. 1.1 Definitions of study, buffer, and external areas in dynamic equivalents

In this report, the models in the study area and buffer area are retained; therefore both areas are defined as the retained area. After dynamic reduction, the system consisting of the retained area and equivalenced external area is defined as the reduced system.

In the literature, coherency-based dynamic equivalents have been extensively studied. The basic idea is to aggregate the generators in the external area that present similar dynamic characteristics. The extent of the similarity is measured by generator coherency. For example, if two generators present similar rotor angle responses following a system disturbance, they are considered to be tightly coherent. Otherwise, they are considered to be weakly coherent. To evaluate generator coherency, a variety of methods have been proposed. The most intuitive approach is to compare the generator responses following certain system disturbance. Based on this idea, the authors in [4] proposed a linear simulation method. Specifically, two generators are considered to be coherent when the maximum deviation of their rotor angle responses subjected to a specific disturbance is smaller than a threshold value. Even though classical generator models are used, the simulation-based method is still time-consuming when different system disturbances need to be tested. The weak-link method was firstly introduced in [5]. Unlike the linear simulation method, it measures the coupling of generators directly based on the system state matrix. A group of generators are considered to be coherent if the coupling coefficients among them are high. In [6], the slow coherency technique based on the singular perturbation theory was used to separate slow and fast dynamics in large power system and to identify the coherent generators from the perspective of slow dynamic process. As a simplified realization of the slow coherency method, the coherency index is evaluated based on the similarity of the mode shapes associated with a set of specific slow oscillation modes within the system [7].

After coherent generator identification, the parameters of an equivalent generator model are aggregated from individual coherent generators. The frequency-domain method [8] and the structure preserving method [9] have been proposed in the literature. When forming the equivalenced generators with detailed representation, these methods might lead to problematic parameters in certain cases. Therefore the classical aggregation method [7] is widely implemented in practice. By this method, the equivalenced generator is formed in a classical representation. Its inertia is the sum of individual generator inertia, and its transient reactance is the parallel combination of individual transient reactance. The equivalenced damping coefficient is computed based on the user-defined ratio of damping to inertia.

The final step in building the equivalent system is to reduce the network in the external area. During this process, the buses in the external area are eliminated using Gaussian elimination. In the meantime, the load buses are aggregated and replaced by appropriate equivalent load models.

1.2 Overview of the problem

In the coherency-based equivalencing process, the definition of the retained area can significantly impact the equivalencing accuracy of the reduced system. As more components are included in the retained area, more attributes related to the dynamic characteristics of the study area can be retained. Therefore further study is needed to systematically identify an appropriate retained area that not only includes the critical

generators in the external area but also limits the scale of the reduced system after the dynamic equivalent is formed.

It is to be noted that system conditions change frequently in a realistic setting. Generator coherency information obtained under one particular condition might not be applicable to another condition. For a new operating condition, generator coherency needs to be re-evaluated. This process is computationally burdensome, especially for large-scale power systems. Therefore significant strides in developing improved dynamic equivalents can be made if an efficient technique is developed to predict the variations in coherency behavior as system condition changes.

In the conventional dynamic equivalencing, the errors resulting from the generator aggregation cannot be completely eliminated. This is especially true for the classical generator aggregation method. The errors can significantly impact the equivalencing accuracy of the reduced system as the simulation evolves following a system disturbance. This drawback becomes more significant presently as the detailed models in the external area is often inaccessible to a signal entity under the restructured environment. The equivalent system based on the planning cases might lead to inaccurate evaluation results. Therefore a study focused on the improvement of coherency-based equivalent for on-line dynamic security assessment (DSA) is also needed.

1.3 Report organization

The remainder of the report is organized into 4 sections. Section 2 presents the method to identify the critical generators in the initial external area for a specific system condition. Three criteria, namely the power transfer distributions factors (PTDFs), the estimated rotor acceleration during fault duration, and the mode participation factors, are detailed. Section 3 presents a systematic approach to predict the changing patterns of generator slow coherency for different operating conditions. For a new system condition, the predicted coherency patterns are used to adjust the initial retained area boundary and to re-group the coherent generators to be equivalenced. Section 4 details the concept of the hybrid dynamic equivalents and presents a systematical approach to build the artificial neural network (ANN)-based equivalent and to integrate it with existing power system simulation software packages. In Section 5, the conclusions drawn from the analysis are presented.

2. Development of Right-sized Dynamic Equivalents

For a specific operating condition, it is time-consuming to exhaustively test various buffer areas in order to obtain an appropriate reduced system model for transient stability assessment of large-scale power systems. Therefore an analytical method is desired to determine the proper extent of the buffer area for practical implementations. To address this challenge, the algorithm shown in Fig. 2.1 is proposed.

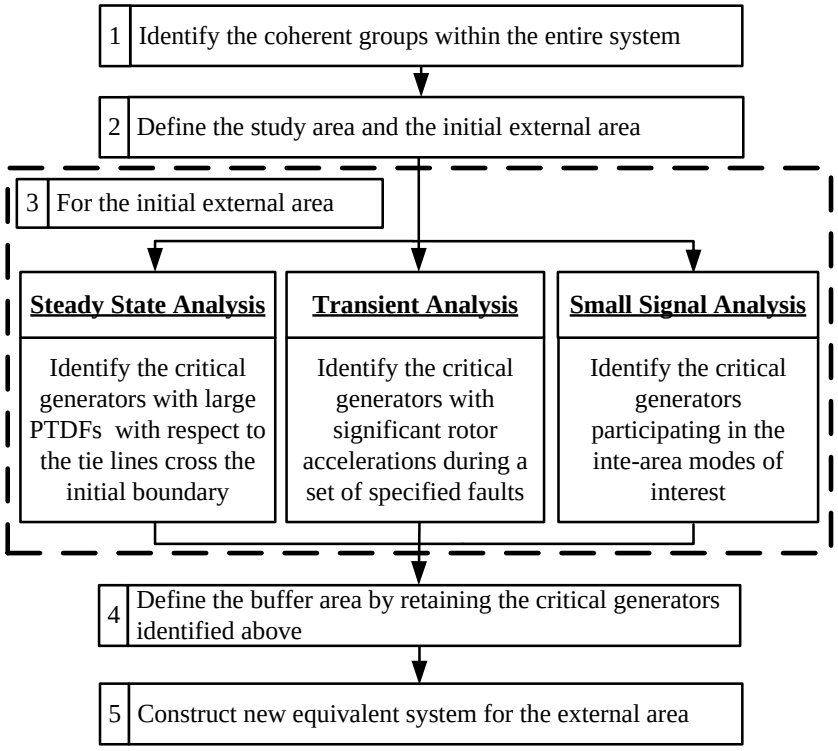

Fig. 2.1 Dynamic equivalent with the analytically determined buffer area

In the proposed algorithm, the entire area, except for the study area, is treated as the initial external area. Then three criteria, namely PTDFs, the estimated generator rotor acceleration in fault duration, and oscillatory mode participation factors, are applied to identify the generators that are critical to the dynamic performance of the study area. The buffer area consisting of these identified generators is then imported into the dynamic reduction program (DYNRED) to construct the equivalent models for the corresponding external area.

2.1 PTDF-based criterion

In dynamic equivalents, the study area is connected to the initial external area through the tie-line interfaces. The dynamic performance of the study area could be significantly impacted by changes in the tie-line flows. In the initial external area, the generators having more impacts on the tie-line flows are expected to be more critical to the study area from both steady state and dynamic performance perspectives. In the proposed algorithm, this impact is evaluated by calculating the DC power flow-based PTDFs. By

definition, the active power flow over the line from bus *i* to bus *j* due to the generation change at bus *g* can be approximated by [10],

$$PTDF_g^{ij} = \frac{\mathbf{M}_l^T \mathbf{B}^{-1} \mathbf{M}_{Gg}}{x_{ij}} \tag{2.1}$$

where **B** is the node susceptance matrix. $\mathbf{M}_l$ is the node-branch incidence vector. $\mathbf{M}_{Gg}$ is the vector with 1 in the entry corresponding to generator *g* and zeros elsewhere. x_{ij} is the primitive line reactance.

Even though PTDF is a steady state index, it provides in-depth insight into the system mutual impacts. Therefore it can be used to judge the effect on the dynamic performance.

2.2 Generator rotor acceleration-based criterion

For a specific contingency within the study area, the generator response in terms of rotor acceleration decreases in magnitude if the generator is located electrically far away from the disturbance. This impact can be interpreted as a measure of the coupling among the generators in the initial external area and the study area.

In the proposed algorithm, the classical generator model with neglect of the damping coefficient is utilized. A three-phase fault is applied at the critical bus in the study area. For a *n*-generator system, the bus admittance matrix is reduced to the generator internal buses. During this process, the faulted bus is also retained. Under the pre-fault condition, the active power output of generator *i* is given by,

$$P_{Gi}(t_0) = \sum_{\substack{j=1 \\ j \neq i}}^{n} E_{i0} E_{j0} B_{ij} \sin\left(\delta_{i0} - \delta_{j0}\right) + E_{i0} V_{f0} B_{if} \sin\left(\delta_{i0} - \theta_{f0}\right) \tag{2.2}$$

where $E_{i0} \angle \delta_{i0}$ is the internal voltage of generator *i*, $V_{f0} \angle \theta_{f0}$ is the voltage of the faulted bus *f*, B_{ij} is the equivalent admittance between the internal nodes of generator *i* and generator *j*, and B_{if} is the equivalent admittance between the faulted bus *f* and the internal node of generator *i*.

At $t = t_0^+$, a three-phase fault is applied, and it is assumed that the generator internal voltages remain constant. Because $V_{f0}^+ = 0$, the acceleration power on the generator *i* is:

$$\Delta P_{Gi} = P_{Gi}\left(t_0\right) - P_{Gi}(t_0^+) = E_{i0} V_{f0} B_{if} \sin\left(\delta_{i0} - \theta_{f0}\right). \tag{2.3}$$

The acceleration of the generator *i* during the fault is:

$$a_i = \Delta P_{Gi} / M_i \tag{2.4}$$

where the generator inertia $M_i = 2H_i/\omega_R$. H_i is inertia constant of generator *i* in s, and ω_R is the base frequency in radians per second (376.99 rad/s).

Assuming that the fault duration is t_f and the acceleration a_i is constant, the rotor angle deviation of generator *i* is given by,

$$\Delta\delta_i = \frac{1}{2}\left|a_i\right| t_f^2 = \frac{1}{2M_i}\left|E_{i0} V_{f0} B_{if} \sin\left(\delta_{i0} - \theta_{f0}\right)\right| t_f^2. \tag{2.5}$$

In the initial external area, the generators having large rotor angle deviations tend to have tight electrical coupling with the faulted area. Therefore retaining these generators will be critical to preservation of the dynamic performance of the study area. It is also noted that the selected generators are sensitive to the fault location. To obtain better results, multiple faults across the study area should be tested.

2.3 Mode participation-based criterion

With the combination of the information contained in the right and left eigenvectors, the following participation factor can be defined [11]:

$$p_{ki} = \phi_{ki}\psi_{ki} \tag{2.6}$$

where ϕ_{ki} is the k^{th} element of the right eigenvector $\boldsymbol{\phi}_i$ that corresponds to the k^{th} state variable. ψ_{ki} is the k^{th} element of the left eigenvector $\boldsymbol{\psi}_i$.

The participation factor p_{ki} provides a measure of the association between the k^{th} state variable and the i^{th} mode. In the proposed algorithm, the participation factors of generator rotor angle states with respect to the inter-area modes of interest are calculated. It is to be noted that some of the identified generators might not be located in the subsystem that is adjacent to the study area. Additionally, the improvement might not be observable in the time-domain simulation if the persevered modes are not properly excited by the specific contingency.

2.4 Test case verification

A large-scale power system with the detailed representation of the US/Canada Eastern interconnection and the simplified representation of the neighboring systems is used. In this test system, the area comprised of ISO New England (ISO-NE), New Brunswick (NB), and Nova Scotia (NS), is treated as the study area. The area representing New York ISO (NYISO) is treated as the initial buffer area. The detailed generator models with exciters, governors, and power system stabilizers (PSSs) are used for all generators in the study and buffer areas. A schematic diagram of the test system is given in Fig. 2.2.

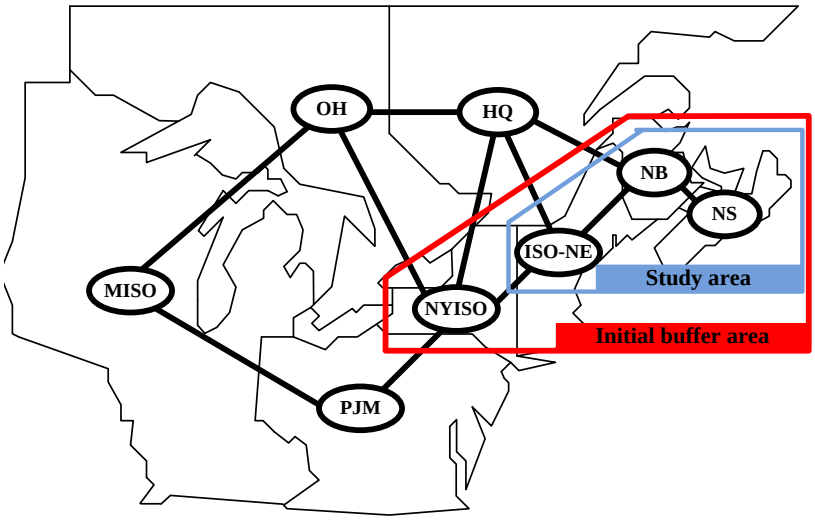

Fig. 2.2 Schematic diagram of the main portion of the test system

In Fig. 2.2, the generators in the initial external area that have a capacity greater than 50 MVA are selected as the candidates. Among these candidates, the proposed criteria are implemented to identify the critical generators to be included in the new buffer area. For different combinations of the criteria, two revised reduced systems, namely ExdCase1 and ExdCase2, are formed as shown in Table 2-1. ExdCase1 uses both PTDF and rotor acceleration as the criteria; while ExdCase2 uses all three criteria. When using the mode participation criterion, only the inter-area modes with a frequency less than 0.9 Hz are considered.

Table 2-1 Summary of the number of generators in the buffer areas

Criteria		ExdCase1	ExdCase2
PTDF	Threshold	3%	3%
	Generator #	45(*37)	45(*37)
Rotor acceleration	Threshold	0.2 degree	0.2 degree
	Generator #	66 (*57)	66(*57)
Mode participation	Threshold	-------	0.5
	Generator #	-------	73 (*1)
Total	Generator #	67	137

*denotes the number of generators which are located in the initial buffer area

In the initial buffer area shown in Fig. 2.2, a total of 233 generators are included. With the proposed algorithm, however, this number decreases to 67 and 137 in ExdCase1 and ExdCase2, respectively. When using the PTDF and rotor acceleration as the criteria, most identified generators have already been included in the initial buffer area. This finding is consistent with the fact that the NYISO system has a tight electrical connection with the study area through the AC tie lines. However, some of the identified critical generators are also located in the initial external area. When using the mode participation-based criterion, most identified generators are located in the remote subsystems. To build new reduced systems, the identified generators are included into the buffer area, and the network in the new external area is reduced except for the terminals of the tie lines across the retained area boundary.

To validate the efficacy of the different reduced systems in the time-domain simulation, a three-phase fault at a 345 kV bus in the southern part of the ISO-NE system is applied at 0.5 s. After 8 cycles, the fault is cleared by opening two 345 kV transmission lines connected to the faulted bus. The entire simulation duration is 20 seconds. The responses of Generator 71126 in the study area are compared in Fig. 2.3.

.

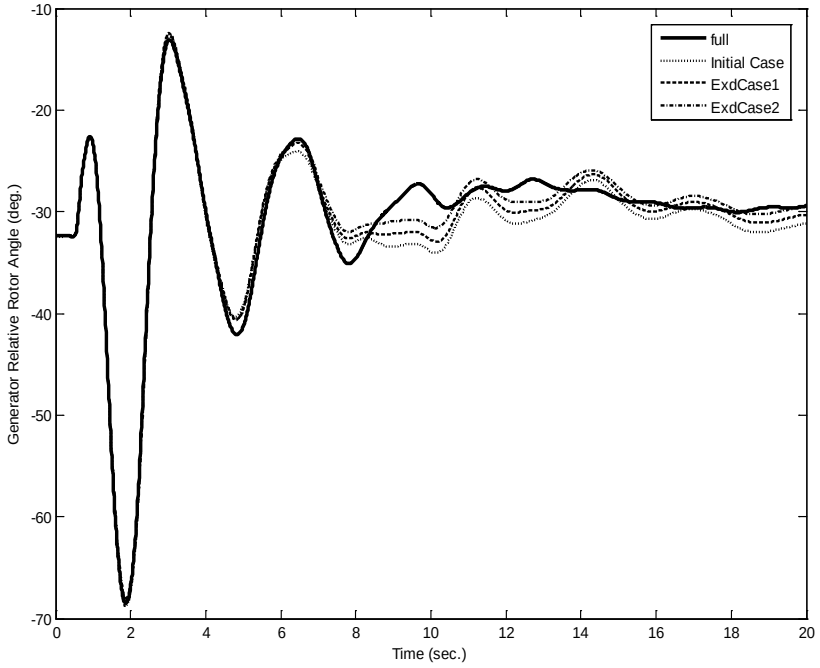

Fig. 2.3 Relative rotor angle responses comparison of Generator 71126

It can be observed in Fig. 2.3 that the responses in the reduced systems using the analytically determined buffer areas are closer to the full system responses than the initial reduced system. The improvement is more significant as the dynamic process evolves. The frequency and damping ratio of the selected inter-area modes in the reduced systems are compared in Table 2-2.

Table 2-2 Small signal analysis results in the reduced systems

Mode		1	2	3	4
Freq. (Hz)/ Damping ratio	Full syst.	0.37 / 8.5%	0.54 / 2.3%	0.56 / 8.1%	0.70 / 8.8%
	Initial Case	0.35 / 8.6%	0.53 / 3.4%	0.55 / 7.2%	0.71 / 4.5%
	ExdCase1	0.35 / 8.9%	0.53 / 3.4%	0.55 / 7.2%	0.71 / 4.5%
	ExdCase2	0.36 /8.0%	0.54 / 2.7%	0.55 / 7.3%	0.71 / 4.6%

It can be seen in Table 2-2 that reduced system in ExdCase1 provides the same modal information as the initial reduced system. As more generators in the remote area are included in the buffer area in ExdCase2, the mismatches, especially for Mode 2, are significantly reduced.

It can be concluded from the former test results that the proposed algorithm is effective in identifying the critical generators to be retained in the buffer area. The resultant reduced system achieves a good balance between equivalencing accuracy and system complexity.

3. Development of Right-sized Dynamic Equivalents for Operating Condition Changes

In this chapter, a systematic approach is developed to predict the variations in generator slow coherency behavior for changing system conditions. The innovative step developed in this report is depicted in Fig. 3.1.

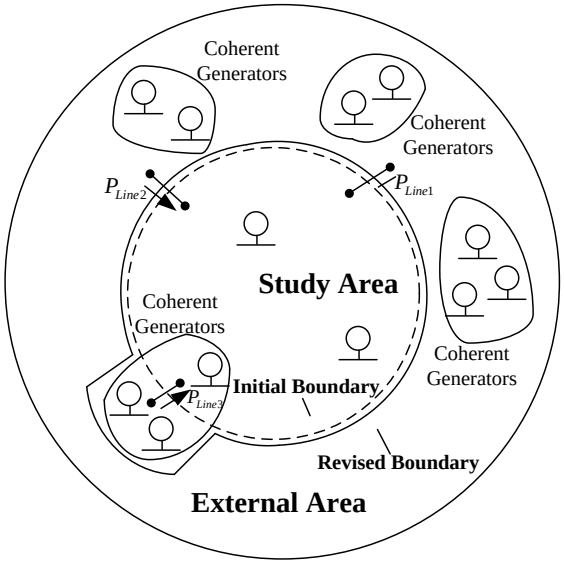

Fig. 3.1 Illustration of the proposed algorithm for operating condition changes

Instead of re-evaluating the slow coherency patterns from scratch under a new operating condition, the critical generators in the initial external area that are predicted to become tightly coherent with the generators in the initial study area are identified. Based on this determination, the revised retained area boundary is formed, and new equivalent system is constructed.

3.1 Slow coherency index

In the proposed algorithm, the classical generator model is used. Then *n*-generator power system can be represented as,

$$\begin{aligned} \dot{\delta}_i &= (\omega_i - \omega_0)\omega_R \\ 2H_i\dot{\omega}_i &= -D_i(\omega_i - \omega_0) + (P_{mi} - P_i),\ i = 1,2,...,n \end{aligned} \tag{3.1}$$

where δ_i and ω_i are the rotor angle and speed of generator *i*, respectively. H_i is the inertia constant. D_i is the damping coefficient. P_{mi} and P_i are the mechanic power input and electrical power output. ω_R is the base frequency (376.99 rad/s), and ω_0 is the initial value of ω_i. *n* is the total number of the generators.

Linearizing (3.1) at the equilibrium point gives,

$$\begin{bmatrix} \Delta\dot{\boldsymbol{\delta}} \\ \Delta\dot{\boldsymbol{\omega}} \end{bmatrix} = \begin{bmatrix} \mathbf{0} & \mathbf{I} \\ -\mathbf{M}^{-1}\mathbf{K} & -\mathbf{M}^{-1}\mathbf{D} \end{bmatrix} \begin{bmatrix} \Delta\boldsymbol{\delta} \\ \Delta\boldsymbol{\omega} \end{bmatrix} \tag{3.2}$$

where $\Delta\boldsymbol{\delta}$ is the generator rotor angle deviation vector. $\boldsymbol{\omega}$ is the generator speed deviation vector. **M** is the diagonal inertia coefficient matrix. **K** is the synchronizing power coefficient matrix. **D** is the diagonal damping coefficient matrix that can be ignored without the loss of accuracy in generator slow coherency analysis

Given the initial value of the state vector in (3.2) following a system disturbance, namely $\boldsymbol{\xi}$, the rotor angle deviations of generator *i* and *j* can be determined by,

$$\Delta\delta_i(t) = e^{\lambda_1}\phi_{i1}\left(\boldsymbol{\psi}_1\boldsymbol{\xi}\right) + e^{\lambda_2}\phi_{i2}\left(\boldsymbol{\psi}_2\boldsymbol{\xi}\right) + \ldots + e^{\lambda_{2n}}\phi_{i2n}\left(\boldsymbol{\psi}_{2n}\boldsymbol{\xi}\right) \tag{3.3}$$

$$\Delta\delta_j(t) = e^{\lambda_1}\phi_{j1}\left(\boldsymbol{\psi}_1\boldsymbol{\xi}\right) + e^{\lambda_2}\phi_{j2}\left(\boldsymbol{\psi}_2\boldsymbol{\xi}\right) + \ldots + e^{\lambda_{2n}}\phi_{j2n}\left(\boldsymbol{\psi}_{2n}\boldsymbol{\xi}\right) \tag{3.4}$$

where ϕ_{ik} is the i^{th} element of $\boldsymbol{\phi}_k$.

It is shown in (3.3) and (3.4) that the generator rotor angle response can be represented as a linear combination of all system modes. For a given disturbance, $\boldsymbol{\xi}$ has the same impact on all state solutions through the left eigenvectors. In (3.3), ϕ_{ij} indicates the contribution of j^{th} mode on $\Delta\delta_i(t)$. If the right eigenvector elements $[\phi_{i1,\ldots,}\ \phi_{i2n}]$ and $[\phi_{j1,\ldots,}\ \phi_{j2n}]$ are identical, the same generator responses in terms of $\Delta\delta_i(t)$ and $\Delta\delta_j(t)$ can be obtained.

To evaluate generator slow coherency, only the slow modes representing the inherent structural characteristics of the system are concerned. It is a common practice to choose a specific number of the slowest modes in the system. This number is primarily dependent on the coherent groups to be formed. Suppose that the matrix $\boldsymbol{\Phi}$ consists of the right eigenvectors associated with *k* slowest modes,

$$\boldsymbol{\Phi} = [\boldsymbol{\phi}_1, \ldots, \boldsymbol{\phi}_k]. \tag{3.5}$$

Then, the slow coherency index between generator *i* and generator *j* can be defined as,

$$d_{ij} = \frac{\boldsymbol{\upsilon}_i \boldsymbol{\upsilon}_j^H}{\left\|\boldsymbol{\upsilon}_i\right\| \left\|\boldsymbol{\upsilon}_j\right\|} \tag{3.6}$$

where $\boldsymbol{\upsilon}_i = [\phi_{i1,\ldots,}\ \phi_{ik}]$ and $\boldsymbol{\upsilon}_j = [\phi_{j1,\ldots,}\ \phi_{jk}]$ are the rows of $\boldsymbol{\Phi}$ corresponding to the rotor angle states of generator *i* and generator *j*, respectively. $\|\ \|$ denotes the 2-norm of complex vector. *H* denotes the conjugate transpose.

In (3.6), the real scalar d_{ij} provides a numeric measure of the generator coherency with respect to the selected slow modes in the system.

3.2 Prediction of slow coherency index for changing operation conditions

The flowchart of the proposed algorithm is shown in Fig. 3.2. The PTDFs are only used to identify the critical generator candidates in the initial external area. For certain cases, this step can be skipped, and then all the generators in the initial external area will be considered.

3.2.1 Estimation of system variable perturbation

To obtain the system state matrix perturbation for a change in system operating condition, the perturbation of network variables needs to be determined first. Assuming that the Jacobian matrix at the base case is $\mathbf{J}_{pf}$, the equation in polar coordinates relating power injection perturbation with voltage perturbation is as follows,

$$\begin{bmatrix} \Delta \mathbf{P}\boldsymbol{\theta} \\ \Delta \mathbf{Q} \end{bmatrix} = \mathbf{J}_{pf} \begin{bmatrix} \Delta \\ \Delta \mathbf{V} / \mathbf{V} \end{bmatrix} \tag{3.7}$$

where $\Delta \mathbf{P} = [\Delta \mathbf{P}_G{}^{\mathrm{T}}\ \Delta \mathbf{P}_L{}^{\mathrm{T}}]^{\mathrm{T}}$ is the active power injection perturbation vector, $\Delta\ \boldsymbol{\theta} = [\Delta \boldsymbol{\theta}_G{}^{\mathrm{T}}\ \Delta \boldsymbol{\theta}_L{}^{\mathrm{T}}]^{\mathrm{T}}$ is the bus voltage phase angle perturbation vector. The subscripts *G* and *L* denote the generator and load buses, respectively. $\Delta \mathbf{Q} = \Delta \mathbf{Q}_L$ and $\Delta \mathbf{V}/\mathbf{V} = \Delta \mathbf{V}_L/\mathbf{V}_L$ are the reactive power injection perturbation vector and the voltage magnitude perturbation vector at load buses, respectively.

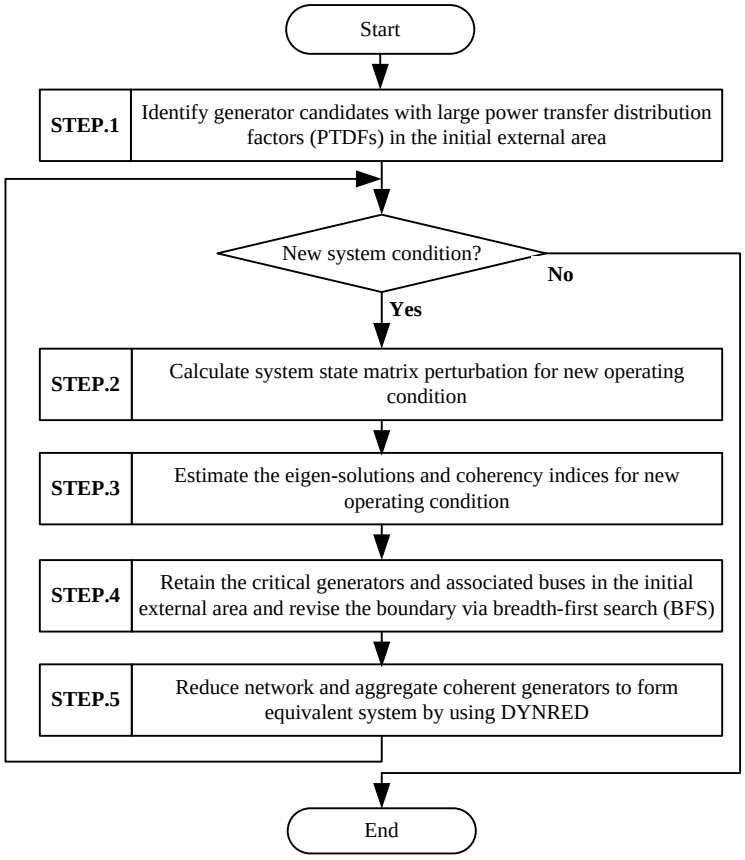

Fig. 3.2 Flowchart of right-sized dynamic equivalent algorithm

In (3.7), the generator bus violating the reactive power limit is treated as a *P*-*Q* bus. Defining the sensitivity matrix $\mathbf{S} = \mathbf{J}_{pf}^{-1}$, the bus voltage perturbation is given by,

$$\begin{bmatrix} \Delta \boldsymbol{\theta}\mathbf{P} \\ \Delta \mathbf{V} / \mathbf{V} \end{bmatrix} = \mathbf{S} \begin{bmatrix} \Delta \\ \Delta \mathbf{Q} \end{bmatrix}. \tag{3.8}$$

Then, the reactive power injection perturbation at generator *i* can be obtained by,

$$\Delta Q_{Gi} = \frac{\partial Q_{Gi}}{\partial \boldsymbol{\theta}\mathbf{V}} \Delta \boldsymbol{\theta}\mathbf{V} \frac{\partial Q_{Gi}}{\mathbf{V} \partial\ /} \left(\Delta \quad / \quad \right) \tag{3.9}$$

where $\Delta \boldsymbol{\theta}$ and $\Delta \mathbf{V}/\mathbf{V}$ can be obtained from (3.8). $Q_{Gi}/\partial \boldsymbol{\theta}$ and $\partial\, Q_{Gi}/(\partial \mathbf{V}/\mathbf{V})$ are the Jacobian matrix elements associated with the reactive power injection at generator *i*.

In the classical generator model, the internal voltage behind the transient reactance of

generator i, namely $E_i \angle \delta_i$, is defined as,

$$E_i = \sqrt{\left(V_i + Q_{Gi} x'_{di} / V_i\right)^2 + \left(P_{Gi} x'_{di} / V_i\right)^2} \tag{3.10}$$

$$\delta_i = \theta_i + \tan^{-1}\left[\left(P_{Gi} x'_{di} / V_i\right) / \left(V_i + Q_{Gi} x'_{di} / V_i\right)\right] \tag{3.11}$$

where x'_{di} is the generator transient reactance. $V_i \angle \theta_i$ is the generator terminal voltage. P_{Gi} and Q_{Gi} are the active and reactive power injections, respectively. Linearizing (3.10) and (3.11) on the assumption that V_i is held constant gives,

$$\Delta E_i = \frac{P_{Gi} x'^2_{di}}{E_i V_i^2} \Delta P_{Gi} + \frac{V_i^2 x'_{di} + Q_{Gi} x'^2_{di}}{E_i V_i^2} \Delta Q_{Gi} \tag{3.12}$$

$$\Delta \delta_i = \Delta \theta_i + \frac{V_i^2 x'_{di} + Q_{Gi} x'^2_{di}}{E_i^2 V_i^2} \Delta P_{Gi} - \frac{P_{Gi} x'^2_{di}}{E_i^2 V_i^2} \Delta Q_{Gi}. \tag{3.13}$$

As shown above, the perturbations of generator internal voltage and rotor angle can be determined once $\Delta \mathbf{P}_G$, $\Delta \mathbf{P}_L$, and $\Delta \mathbf{Q}_L$ for different system conditions are properly defined. It also is noted that in (3.12) and (3.13) only the static transition is considered and the dynamics from one system operating condition to another condition will not be taken into account. The approach to determine the power injection perturbation vector for different operating condition is detailed as follows.

(a) Generation change

Assuming the active power injections at a set of generators are changed under a new operating condition, its impact on the remainder of the system can be simulated by setting $\Delta \mathbf{P}_G$ as,

$$\Delta \mathbf{P}_G = \sum_{i \in K_G} \mathbf{M}_{Gi} \Delta P_{Gi} \tag{3.14}$$

where K_G is the set of dispatchable generators. $\mathbf{M}_{Gi}$ is the vector with 1 in the entry corresponding to generator i and zeros elsewhereΔ P_{Gi} is the amount of generation change.

In (3.14), ΔP_{Gi} is determined by the scheduling methodology for the selected generators when an active power imbalance occurs within the systems.

(b) Load change

The following adjustments to $\Delta \mathbf{P}_L$ and $\Delta \mathbf{Q}_L$ are also made when a set of loads are subject to changes,

$$\Delta \mathbf{P}_L = -\sum_{i \in K_L} \mathbf{M}_{PLi} \Delta P_{Li} \tag{3.15}$$

$$\Delta \mathbf{Q}_L = -\sum_{i \in K_L} \mathbf{M}_{QLi} \Delta Q_{Li} \tag{3.16}$$

where K_L is the set of load buses at which loads are changed. $\mathbf{M}_{PLi}$ and $\mathbf{M}_{QLi}$ are the vectors with 1 in the entry corresponding to load bus i at which load changes and zeros elsewhere. ΔP_{Gi} and ΔQ_{Gi} are the amounts of changes of active and reactive power consumption at load bus i. K_L is the set of load buses subjected to changes.

(c) Line outage

The line outage simulation is commonly used in the available transfer capability (ATC) evaluation to investigate the impacts of line outage on the power flow distribution for a given network. The sensitivity-based method [12] for ATC assessment is applied in this project. The basic idea is to simulate the impacts of line outage by adding an appropriate set of power injection perturbation vectors at the line terminal buses under the pre-outage condition. In the case of tripping the line from bus *i* to bus *j*, the following equation is solved for the equivalent perturbations of power injection at line terminal buses, namely ΔP_i, ΔP_j, ΔQ_i, and ΔQ_j:

$$\begin{bmatrix} \frac{\partial P_{ij}}{\partial P_i}-1 & \frac{\partial P_{ij}}{\partial P_j} & \frac{\partial P_{ij}}{\partial Q_i} & \frac{\partial P_{ij}}{\partial Q_j} \\ \frac{\partial P_{ji}}{\partial P_i} & \frac{\partial P_{ji}}{\partial P_j}-1 & \frac{\partial P_{ji}}{\partial Q_i} & \frac{\partial P_{ji}}{\partial Q_j} \\ \frac{\partial Q_{ij}}{\partial P_i} & \frac{\partial Q_{ij}}{\partial P_j} & \frac{\partial Q_{ij}}{\partial Q_i}-1 & \frac{\partial Q_{ij}}{\partial Q_j} \\ \frac{\partial Q_{ji}}{\partial P_i} & \frac{\partial Q_{ji}}{\partial P_j} & \frac{\partial Q_{ji}}{\partial Q_i} & \frac{\partial Q_{ji}}{\partial Q_j}-1 \end{bmatrix} \begin{bmatrix} \Delta P_i \\ \Delta P_j \\ \Delta Q_i \\ \Delta Q_j \end{bmatrix} = \begin{bmatrix} -P_{ij} \\ -P_{ji} \\ -Q_{ij} \\ -Q_{ji} \end{bmatrix} \tag{3.17}$$

where P_{ij}+jQ_{ij} and P_{ji}+jQ_{ji} are the line power flow measured at bus *i* and bus *j* at the base case, respectively.

The elements of the coefficient matrix in (3.17) can be obtained directly from the original operating condition. For instance, the active power over the line from bus *i* to bus *j* measured at bus *i* is:

$$P_{ij} = V_i^2 g_{ij} - V_i V_j \left(g_{ij} \cos\theta_{ij} + b_{ij} \sin\theta_{ij} \right) \tag{3.18}$$

where g_{ij} is the primitive line conductance, and b_{ij} is the primitive line susceptance.

Taking the partial derivative of (3.18) with respect to P_i gives,

$$\frac{\partial P_{ij}}{\partial P_i} = \left(\frac{\partial P_{ij}}{\partial \theta_i}\right)\left(\frac{\partial \theta_i}{\partial P_i}\right) + \left(\frac{\partial P_{ij}}{\partial \theta_j}\right)\left(\frac{\partial \theta_j}{\partial P_i}\right) + \left(\frac{\partial P_{ij}}{\partial V_i / V_i}\right)\left(\frac{\partial V_i / V_i}{\partial P_i}\right) + \left(\frac{\partial P_{ij}}{\partial V_j / V_j}\right)\left(\frac{\partial V_j / V_j}{\partial P_i}\right) \tag{3.19}$$

where $\partial\theta_i/\partial P_i$, $\partial\theta_j/\partial P_i$, $(\partial V_i/V_i)/\partial P_i$, and $(\partial V_j/V_j)/\partial P_i$ are the corresponding elements of **S** in (3.8). $\partial P_{ij}/\partial\theta_i$, $\partial P_{ij}/\partial\theta_j$, $\partial P_{ij}/(\partial V_i/V_i)$, and $\partial P_{ij}/(\partial V_j/V_j)$ can be calculated with the line parameter and terminal voltages at the base case known

The resultant equivalent perturbations of power injections are then appended to the line terminal buses in the terms of (3.15) and (3.16) to simulate the line outage impacts.

(d) Line addition

When the line from bus *i* to bus *j* is added to the network, a similar sensitivity–based procedure can be developed. Then the following equation is solved for the equivalent power injection perturbation at the line terminal buses:

$$\begin{bmatrix} \frac{\partial P_{ij0}}{\partial P_i}+1 & \frac{\partial P_{ij0}}{\partial P_j} & \frac{\partial P_{ij0}}{\partial Q_i} & \frac{\partial P_{ij0}}{\partial Q_j} \\ \frac{\partial P_{ji0}}{\partial P_i} & \frac{\partial P_{ji0}}{\partial P_j}+1 & \frac{\partial P_{ji0}}{\partial Q_i} & \frac{\partial P_{ji0}}{\partial Q_j} \\ \frac{\partial Q_{ij0}}{\partial P_i} & \frac{\partial Q_{ij0}}{\partial P_j} & \frac{\partial Q_{ij0}}{\partial Q_i}+1 & \frac{\partial Q_{ij0}}{\partial Q_j} \\ \frac{\partial Q_{ji0}}{\partial P_i} & \frac{\partial Q_{ji0}}{\partial P_j} & \frac{\partial Q_{ji0}}{\partial Q_i} & \frac{\partial Q_{ji0}}{\partial Q_j}+1 \end{bmatrix} \begin{bmatrix} \Delta P_i \\ \Delta P_j \\ \Delta Q_i \\ \Delta Q_j \end{bmatrix} = \begin{bmatrix} -P_{ij0} \\ -P_{ji0} \\ -Q_{ij0} \\ -Q_{ji0} \end{bmatrix} \tag{3.20}$$

where P_{ij0}+jQ_{ij0} and P_{ji0}+jQ_{ji0} are the fictitious power flow transmitted over the line to be added on the assumption that the line terminal voltages are the same as the base case.

Similar to the case of line outage, the elements of the coefficient matrix in (3.20) can be obtained under the original operating condition.

3.2.2 Estimation of system state matrix perturbation

In the previous steps, the perturbations of the system variables (i.e. generator internal voltage and rotor angle) can be approximated. Then, the perturbation of synchronizing power coefficient matrix **K** can be obtained by ignoring the higher order terms of the Taylor series,

$$\begin{aligned} \Delta K_{ij}\big|_{i\neq j} = &-\left(\Delta E_i E_j + E_i \Delta E_j\right)\left(-G_{ij}\sin\delta_{ij} + B_{ij}\cos\delta_{ij}\right) \\ &- E_i E_j \left(-G_{ij}\cos\delta_{ij} - B_{ij}\sin\delta_{ij}\right)\left(\Delta\delta_i - \Delta\delta_j\right) \\ &- E_i E_j \left(-\Delta G_{ij}\sin\delta_{ij} + \Delta B_{ij}\cos\delta_{ij}\right) \end{aligned} \tag{3.21}$$

$$\Delta K_{ii} = -\sum_{j=1, j\neq i}^{n} \Delta K_{ij} \tag{3.22}$$

where ΔG_{ij} and ΔB_{ij} are the perturbation of the system admittance matrix reduced to the generator internal buses calculated using the Householder's theorem for line outage and addition cases.

Then, the perturbation of system state matrix for a new operating condition is:

$$\Delta \mathbf{A}_{sys} = \begin{bmatrix} \mathbf{0} & \mathbf{0} \\ -\mathbf{M}^{-1}\Delta\mathbf{K} & \mathbf{0} \end{bmatrix}. \tag{3.23}$$

3.2.3 Estimation of slow coherency index perturbation

For different operating conditions, the key to predicting the changes in generator slow coherency is to estimate the new right eigenvectors associated with selected slow modes. As $\Delta\mathbf{A}_{sys}$ is known from the previous step, a predictor and corrector based approach is applied.

(a) Predictor

Given $\Delta\mathbf{A}_{sys}$ in (3.23), the sensitivities of the eigenvalue and right eigenvector of the i^{th} slow mode are given by,

$$\Delta\lambda_i = \boldsymbol{\psi}_i \Delta\mathbf{A}_{sys}\boldsymbol{\phi}_i \tag{3.24}$$

$$\Delta\boldsymbol{\phi}_i = -\left(\mathbf{A}_{sys} - \lambda_i\mathbf{I} + \boldsymbol{\phi}_i\boldsymbol{\phi}_i^H\right)\left(\Delta\mathbf{A}_{sys} + \Delta\lambda_i\mathbf{I}\right)\boldsymbol{\phi}_i. \tag{3.25}$$

Then the new eigensolution can be approximated by,

$$\lambda'_i = \lambda_i + \Delta\lambda_i \tag{3.26}$$

$$\boldsymbol{\phi}'_i = \boldsymbol{\phi}_i + \Delta\boldsymbol{\phi}_i. \tag{3.27}$$

It can be seen that a unit step length along the direction of$\Delta\lambda_i$ and $\Delta\boldsymbol{\phi}_i$ is used in (3.26) and (3.27). Assuming that the system state matrix under the new operating condition is $\mathbf{A}'_{sys} = \mathbf{A}_{sys}+\Delta\mathbf{A}_{sys}$, the following mismatch of the predictor procedure needs to be justified.

$$\Delta\mathbf{G} = \mathbf{A}'_{sys}\boldsymbol{\phi}'_i - \lambda'_i\boldsymbol{\phi}'_i. \tag{3.28}$$

(b) Corrector

To drive (3.28) to zero, the first-order estimate is applied as follows,

$$\left(\mathbf{A}'_{sys} - \lambda'_i\mathbf{I}\right)\Delta\boldsymbol{\phi}'_i - \boldsymbol{\phi}_i\Delta\lambda_i + \Delta\mathbf{G} = \mathbf{0}. \tag{3.29}$$

For the unit normalization constraint on the right eigenvector, the following equation also holds,

$$\boldsymbol{\phi}'^H_i\Delta\boldsymbol{\phi}'_i = 0. \tag{3.30}$$

Combining (3.29) and (3.30), a set of complex equations is formed to solve for the eigensolution sensitivities indicating the descent direction for $\Delta\mathbf{G}$ in (3.28),

$$\begin{bmatrix} \mathbf{A}'_{sys} - \lambda'_i\mathbf{I} & -\boldsymbol{\phi}_i \\ \boldsymbol{\phi}'^H_i & 0 \end{bmatrix}\begin{bmatrix} \Delta\boldsymbol{\phi}'_i \\ \Delta\lambda'_i \end{bmatrix} = \begin{bmatrix} -\Delta\mathbf{G} \\ 0 \end{bmatrix}. \tag{3.31}$$

Assuming that the step length along the direction of$\Delta\boldsymbol{\phi}'_i$ and $\Delta\lambda'_i$ is a, the best estimate of the new eigensolution can be achieved when the following norm function is minimized

$$f(a) = \left\| \left(\mathbf{A}'_{sys} - (\lambda'_i + \Delta\lambda_i a)\mathbf{I}\right)(\boldsymbol{\phi}'_i + \Delta\boldsymbol{\phi}_i a) - (\lambda_i + \Delta\lambda_i)(\boldsymbol{\phi}_i + \Delta\boldsymbol{\phi}_i) \right\|^2. \tag{3.32}$$

Neglecting the higher order term of $(\Delta\lambda'_i a)(\Delta\boldsymbol{\phi}'_i a)$ gives,

$$f(a) = \left(\Delta\mathbf{G} + \mathbf{e}_i a\right)^H\left(\Delta\mathbf{G} + \mathbf{e}_i a\right) \tag{3.33}$$

where $\mathbf{e}_i = \mathbf{A}'_{sys}\Delta\boldsymbol{\phi}'_i - \lambda'_i\Delta\boldsymbol{\phi}'_i - \Delta\lambda'_i\boldsymbol{\phi}'_i$. To minimize (3.33), the following necessary condition needs to be satisfied,

$$\frac{\partial}{\partial a}\left(\left(\Delta\mathbf{G} + \mathbf{e}_i a\right)^H\left(\Delta\mathbf{G} + \mathbf{e}_i a\right)\right) = 0. \tag{3.34}$$

Then the optimal step length a_{opt} is:

$$a_{opt} = -\left(\mathbf{e}_i^H \mathbf{e}_i\right)^{-1} \mathrm{Re}\left(\Delta \mathbf{G}^H \mathbf{e}_i\right). \tag{3.35}$$

From (3.33) and (3.35), it can be proven that $\mathbf{e}_i = -\Delta\mathbf{G}$, then $a_{opt} = 1.0$. As a_{opt} is known, the updated estimate of the new eigensolutions can be formed as,

$$\lambda''_i = \lambda'_i + a_{opt}\Delta\lambda'_i = \lambda'_i + \Delta\lambda'_i \tag{3.36}$$

$$\boldsymbol{\phi}''_i = \boldsymbol{\phi}'_i + a_{opt}\Delta\boldsymbol{\phi}'_i = \boldsymbol{\phi}'_i + \Delta\boldsymbol{\phi}'_i. \tag{3.37}$$

It is to be noted that the above estimate may not necessarily lead to the minimum error term defined in (3.28) due to the approximation made in (3.32). Then corrector procedure needs to be applied iteratively until the norm of $\Delta\mathbf{G}$ decreases to an acceptable value. In each iteration, λ'_i and $\boldsymbol{\phi}'_i$ in (3.28) and (3.31) will be substituted by λ''_i and $\boldsymbol{\phi}''_i$ from (3.36) and (3.37), respectively. Because the estimate from the predictor procedure is close to the exact solution, only a few iterations will be needed.

Once the best estimates of the right eigenvectors are known, generator slow coherency indices within the system can be updated. The critical generators in the initial external area that become tightly slowly coherent with the existing retained generators can be identified.

3.3 Test case verification

A portion of the Western Electricity Coordinating Council (WECC) system shown in Fig. 3.3 is used to verify the effectiveness of the proposed algorithm.

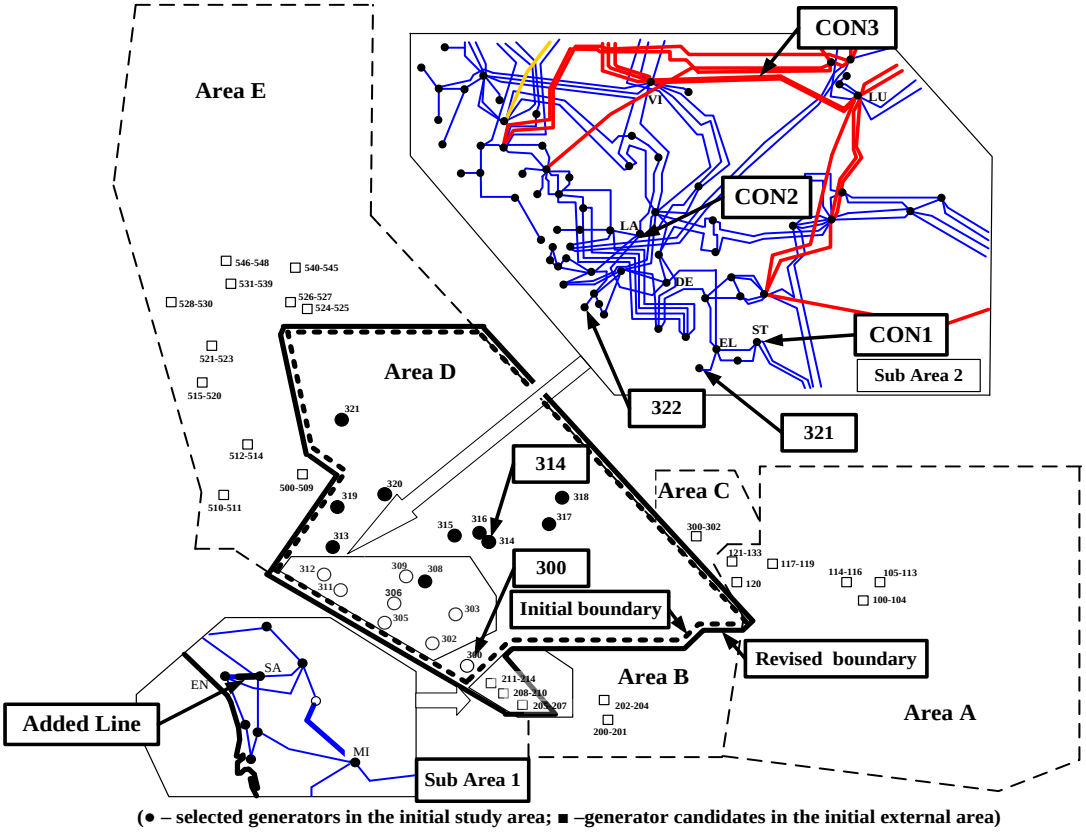

(● – selected generators in the initial study area; ■ –generator candidates in the initial external area)

Fig. 3.3 Schematic diagram of the test system

The system has a total generation of 78170 MW and 9374 MVAr and a total load of 75972 MW and 11666 MVAr. The detailed generator models with exciters, governors, and PSSs are used if applicable. Area D is defined as the initial study area, and 45 slowest modes are selected to be retained.

It is assumed that the 230 kV transmission line from bus EN to bus SA is added, resulting in a new system operating condition. As shown in Fig. 3.3, the generators having PTDFs greater than 0.35 and the capacity greater than 50MVA are selected as the candidates in the initial external area. Using 0.80 as the threshold, Generator 205–214 with the total capacity of 1935 MVA are found to become strongly slowly coherent with the generators in the initial study area after the line EN–SA is added. As a result, a total of 26 buses in the initial external area are retained additionally, leading to new retained area boundary shown in Fig. 3.3. Accordingly, a new equivalent is formed. Table 3-1 compares the size of the full system and equivalent system representations.

Table 3-1 Summary of reduced systems

	Buses	Lines	Loads	Generators in Entire syst.	Generators in External Area
Full syst.	5186	6953	2794	567	431
New equivalent syst.	1208	2253	574	264	119
% of full syst.	23.2%	32.4%	20.5%	46.6%	27.6%

It can be concluded from Table 3-1 that a significant reduction in the system size can be achieved. For the entire system, 53.4% of the generators have been eliminated after dynamic equivalencing. This reduction ratio is even higher considering the generators in the external area. As the number of generators reduces in the equivalent system, the computational effort required for the numerical time-domain simulation can be reduced. The computational time for the proposed method is compared versus formation of the equivalent from the start in DYNRED. As shown in Table 3-2, the proposed method allows a saving of 65.5% of the computational time in comparison to DYNRED when forming the system state matrix and solving for the eigensolutions on an Intel Core2 Duo Processor T6700 (2.66GHz) PC with 2 GB of RAM. Because the calculation of each mode in the proposed method is independent of others, further improvement can be achieved using parallel computation.

Table 3-2 Time consumption comparison of building dynamic equivalents

Steps	Proposed method	DYNRED
Form and calculate state matrix	3.8s	11.0s
Group coherent generators	1.1s	2.3s
Build equivalent system	2.4s	2.4s
Total	7.3s	15.7s

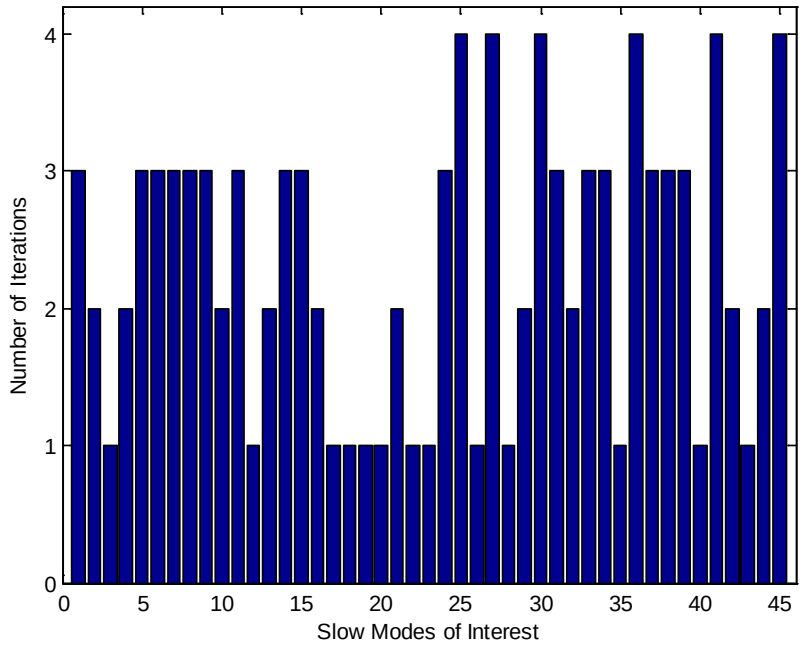

Fig. 3.4 Iteration number for the slow modes of interest in the corrector step

Fig. 3.4 shows that for half of the slow modes the eigensolutions can be obtained in less than two iterations; and even in the worst case, only four iterations are required. To verify the equivalencing accuracy, three 20-second simulations are conducted.

- **Case1**: a three-phase fault is applied at the ST 230 kV bus in Sub Area 2 at 1 second, and it is cleared after 12 cycles by tripping the 230 kV line from ST to EL;
- **Case2**: a three-phase fault is applied at the LA 230 kV bus in Sub Area 2 at 1 second, and it is cleared after 12 cycles by tripping the 230 kV line from LA to DE;
- **Case3**: a three-phase fault is applied to the middle of the 500 kV line from VI to LU, and it is cleared after 4 cycles by tripping this line.

For each simulation, the root mean square error (RMSE) [13] is utilized to measure the mismatch between the responses obtained in the full system and the equivalent system. For generator *i*, the RMSE is defined as,

$$RMSE = \sqrt{\frac{1}{T}\int_0^T \left|\Delta\delta_i^{full}(t) - \Delta\delta_i^{equ}(t)\right|^2 dt} \quad (in\ degree) \tag{3.38}$$

where $\Delta\delta_i^{full}$ and $\Delta\delta_i^{equ}$ are the relative rotor angle deviations of generator *i* obtained from the full system and equivalent system, respectively. *T* is the simulation duration.

For the tested contingencies, the RMSEs of the selected generators are summarized in Table 3-3. The initial equivalent system is formed by using the initial study area shown in Fig. 3.3. Table 3-3 shows that an improvement in the equivalencing accuracy can be obtained when the new equivalent system based on the revised study area boundary is used. However, this improvement varies for different contingencies. For Case 1, the

largest reduction in RMSEs is 2.73 for generator 300; while for Case 2 and Case 3, the improvements are not significant. This finding is consistent with the fact that Case 1 is much closer to the revised retained area boundary than other contingences. Additionally, the generators close to the revised study area boundary, such as Generator 300, 321, and 322, are found to be more sensitive to the study area boundary adjustment in Case 1.

Table 3-3 Comparison of RMSE results

Generator		300	314	320	321	322
RMSEs for CON1	Initial Equivalent syst.	4.33	1.79	0.57	0.79	1.54
	New Equivalent syst.	1.60	0.73	0.55	0.30	0.87
RMSEs for CON2	Initial Equivalent syst.	1.79	0.85	0.55	0.39	0.98
	New Equivalent syst.	0.97	0.83	0.46	0.21	0.90
RMSEs for CON3	Initial Equivalent syst.	1.09	0.99	0.63	0.29	0.78
	New Equivalent syst.	0.95	0.96	0.58	0.24	0.76

The responses of Generator 300 and 322 to the contingency specified in Case 1 are also shown in Fig. 3.5 and Fig. 3.6. A remote generator in Sub Area 2 is chosen as the reference.

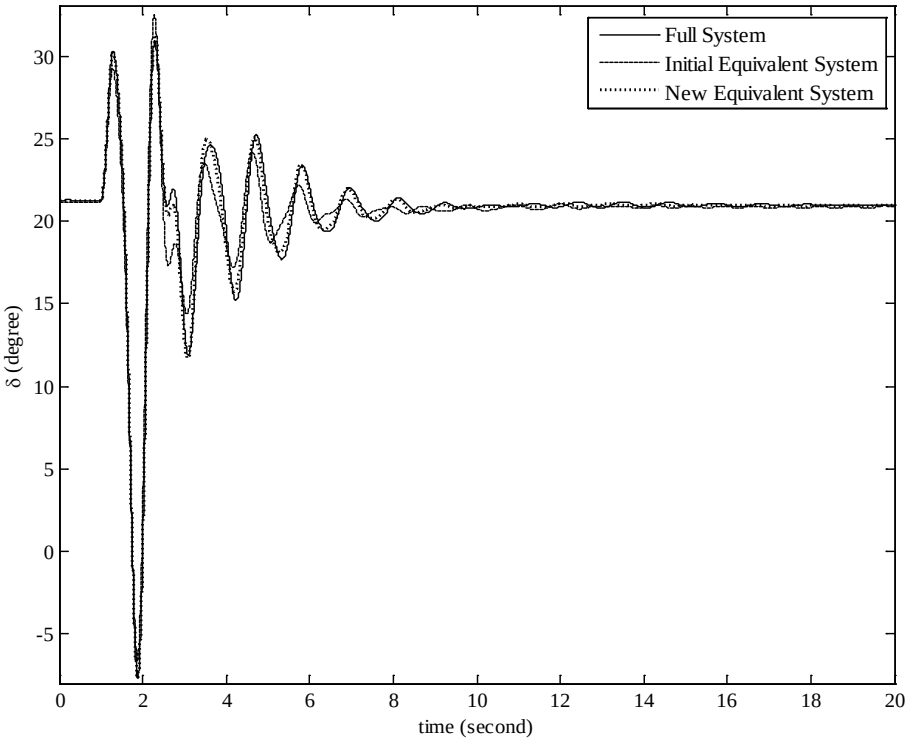

Fig. 3.5 Relative rotor angle responses of Generator 300 in Case 1

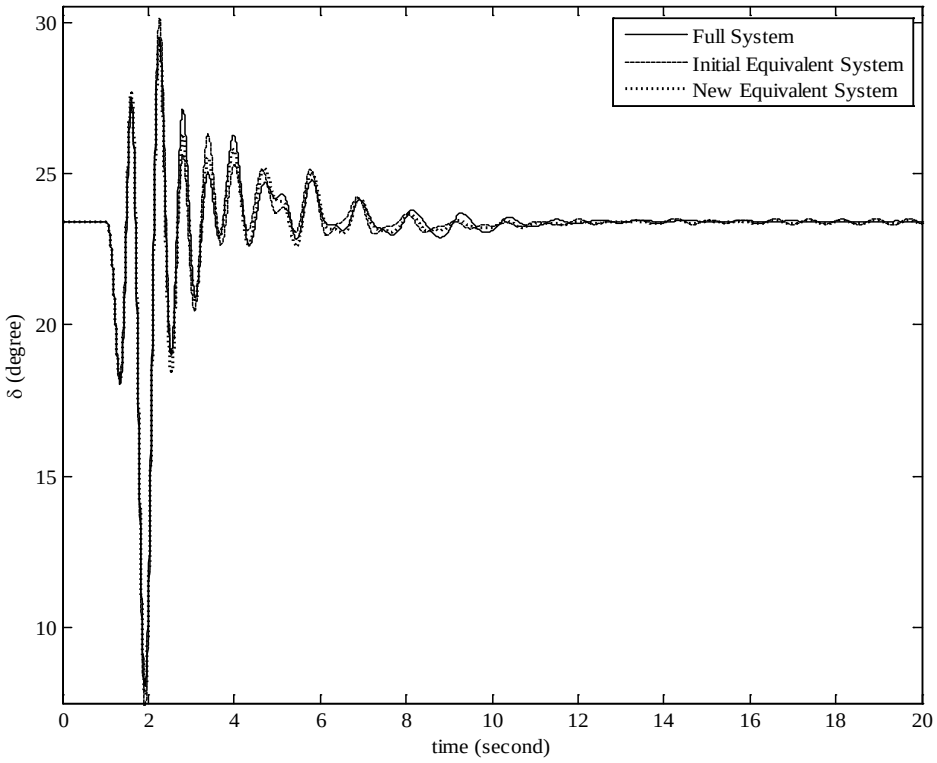

Fig. 3.6 Relative rotor angle responses of Generator 322 in Case 1

The simulation results show that the generator responses in both equivalent systems match the full system for the first few seconds after the contingency. As the dynamic responses evolve, the new equivalent system provides better accuracy than the initial equivalent system later in the simulation. It can also be seen in Fig. 3.5 that the new equivalent system presented a more accurate response in terms of oscillation damping of Generator 300 than the initial equivalent system. On the same PC as described before, the simulation execution time for CON1 has been reduced from 20.2 seconds using the full system representation to 9.3 seconds using the new equivalent system representation. This improvement can be accumulated to a significant saving of computational effort when multiple runs of time-domain simulations are required for on-line DSA.

4. Development of Hybrid Dynamic Equivalents

In the conventional dynamic equivalent discussed in Section 2 and 3, the coherent generators in the external area are aggregated and replaced by appropriate equivalent models. Because of the errors accumulated during the generator aggregation process, a large retained area is commonly used to achieve reasonable equivalencing accuracy. However, this improvement might become insignificant when the retained area itself is already large enough. This limitation becomes more significant presently as the detailed information about the network and component models within the entire system is often inaccessible to a single entity in the restructured environment. To address this challenge, a novel hybrid dynamic equivalent, comprised of both a coherency-based equivalent and an artificial neural network (ANN)-based equivalent, is developed and analyzed in this project as an effort to improve the feasibility of the coherency-based dynamic equivalent method.

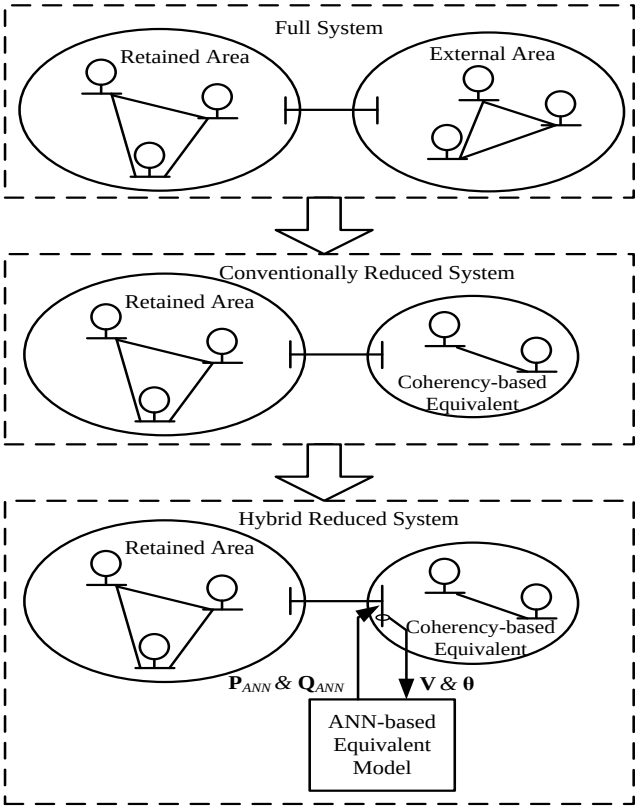

Fig. 4.1 Evolution of the hybrid dynamic equivalent

4.1 Formulation of training set

In the proposed hybrid reduced system shown in Fig. 4.1, the ANN-based equivalent complements the conventional equivalent developed using DYNRED. The appropriate power injections of the ANN-based equivalent at each time instant need to be determined. The trajectory sensitivity method [14],[15] provides an efficient approach to estimate system variable deviations with respect to single or multiple system parameter changes. This method is applied to compute the appropriate power injections of the ANN-based

equivalent that result in a match of the boundary voltage responses in the unreduced and the reduced systems. Typically, a power system can be represented by a set of differential algebraic equations (DAEs) as shown below:

$$\begin{cases} \dot{\mathbf{x}} = \mathbf{f}(\mathbf{x}, \mathbf{y}, \beta) \\ \mathbf{0} = \mathbf{g}(\mathbf{x}, \mathbf{y}, \beta) \end{cases} \tag{4.1}$$

where $\mathbf{x}$ is the state variable vector, $\mathbf{y}$ is the algebraic variable vector, β is a system parameter subject to change, and β_0 is the initial value of β. The differential equations represent the dynamics of system components, and the algebraic equations represent the power flow balance equation at each bus in the system.

For any β that is sufficiently close to β_0, the perturbed trajectory solution can be determined by taking the derivatives of the system state and algebraic variables with respect to β. A new set of linear DAEs can then be formed:

$$\begin{cases} \dfrac{\partial \dot{\mathbf{x}}}{\partial \beta} = \left(\dfrac{\partial \mathbf{f}}{\partial \mathbf{x}}\right)\left(\dfrac{\partial \mathbf{x}}{\partial \beta}\right) + \left(\dfrac{\partial \mathbf{f}}{\partial \mathbf{y}}\right)\left(\dfrac{\partial \mathbf{y}}{\partial \beta}\right) + \dfrac{\partial \mathbf{f}}{\partial \beta} \\ \mathbf{0} = \left(\dfrac{\partial \mathbf{g}}{\partial \mathbf{x}}\right)\left(\dfrac{\partial \mathbf{x}}{\partial \beta}\right) + \left(\dfrac{\partial \mathbf{g}}{\partial \mathbf{y}}\right)\left(\dfrac{\partial \mathbf{y}}{\partial \beta}\right) + \dfrac{\partial \mathbf{g}}{\partial \beta}. \end{cases} \tag{4.2}$$

Assume that the partial derivative matrices $\mathbf{f}_\mathbf{x}=\partial\mathbf{f}/\partial\mathbf{x}$, $\mathbf{f}_\mathbf{y}=\partial\mathbf{f}/\partial\mathbf{y}$, $\mathbf{g}_\mathbf{x}=\partial\mathbf{g}/\partial\mathbf{x}$, $\mathbf{g}_\mathbf{y}=\partial\mathbf{g}/\partial\mathbf{y}$, $\mathbf{x}_\beta=\partial\mathbf{x}/\partial\beta$, $\mathbf{y}_\beta=\partial\mathbf{y}/\partial\beta$, $\mathbf{f}_\beta=\partial\mathbf{f}/\partial\beta$, and $\mathbf{g}_\beta=\partial\mathbf{g}/\partial\beta$, (4.2) can be re-written as:

$$\begin{cases} \dot{\mathbf{x}}_\beta = \mathbf{f}_\mathbf{x}\mathbf{x}_\beta + \mathbf{f}_\mathbf{y}\mathbf{y}_\beta + \mathbf{f}_\beta \\ \mathbf{0} = \mathbf{g}_\mathbf{x}\mathbf{x}_\beta + \mathbf{g}_\mathbf{y}\mathbf{y}_\beta + \mathbf{g}_\beta. \end{cases} \tag{4.3}$$

Similar to (4.1), the implicit method, such as the trapezoidal rule, is applied. At the time instant n, the following linear equations can be formed:

$$\begin{bmatrix} \mathbf{I} - \dfrac{\Delta t}{2}\mathbf{f}_{\mathbf{x},n} & -\dfrac{\Delta t}{2}\mathbf{f}_{\mathbf{y},n} \\ \mathbf{g}_{\mathbf{x},n} & \mathbf{g}_{\mathbf{y},n} \end{bmatrix} \begin{bmatrix} \mathbf{x}_{\beta,n} \\ \mathbf{y}_{\beta,n} \end{bmatrix} = \begin{bmatrix} \mathbf{x}_{\beta,n-1} + \dfrac{\Delta t}{2}\mathbf{f}_{\beta,n} + \dfrac{\Delta t}{2}\left(\mathbf{f}_{\mathbf{x},n-1}\mathbf{x}_{\beta,n-1} + \mathbf{f}_{\mathbf{y},n-1}\mathbf{y}_{\beta,n-1} + \mathbf{f}_{\beta,n-1}\right) \\ -\mathbf{g}_{\beta,n} \end{bmatrix}. \tag{4.4}$$

In (4.4), all the coefficients on the left-hand side have already been calculated when solving for the original trajectory with $\beta = \beta_0$ at the time instant n in (4.1). Based on the specified changing pattern of β, the remaining unknown coefficients can be easily determined. As shown in Fig. 4.1, the algebraic variables of concerns are the boundary bus voltages, and the active and reactive power injections of the ANN-based equivalent are selected as the system parameters. By solving (4.4), V_{ANNi}/P_{ANNj}, θ_{ANNi}/P_{ANNj}, V_{ANNi}/Q_{ANNj}, and θ_{ANNi}/Q_{ANNj} (i=1,..,n_{ANN}, j=1,…,n_{ANN}, n_{ANN} is the total number of boundary buses) can be computed simultaneously at each time instant. For illustrative purposes, it is assumed that the ANN-based equivalent is connected to the reduced system at bus i (n_{ANN}=1). Then, the iterative procedure of determining the power injections of the ANN-based equivalent at time instant n is shown in Fig. 4.2. $\mathbf{V}_{ri,n}$ and $\mathbf{V}_{fi,n}$ are the voltage vectors at bus i, and the subscript r and f denote reduced system and full system, respectively.

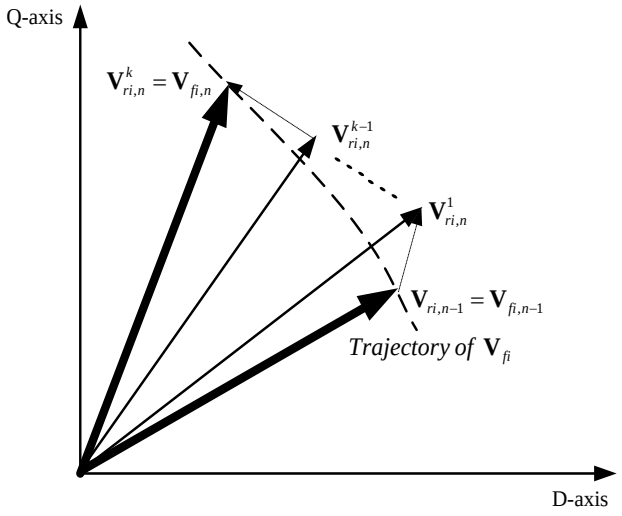

Fig. 4.2 Illustration of the proposed training data formulation

At the k^{th} iteration, the increments of the power injections of the ANN-based equivalent, namely $\Delta P_{ANNi,n}^{k}$ and $\Delta Q_{ANNi,n}^{k}$, are given by,

$$\begin{bmatrix} \Delta P_{ANNi,n}^{k} \\ \Delta Q_{ANNi,n}^{k} \end{bmatrix} = \begin{bmatrix} \dfrac{\partial V_{ri,n}^{k}}{\partial P_{ANNi,n}^{k}} & \dfrac{\partial V_{ri,n}^{k}}{\partial Q_{ANNi,n}^{k}} \\ \dfrac{\partial \theta_{ri,n}^{k}}{\partial P_{ANNi,n}^{k}} & \dfrac{\partial \theta_{ri,n}^{k}}{\partial Q_{ANNi,n}^{k}} \end{bmatrix}^{-1} \begin{bmatrix} V_{fi,n} - V_{ri,n}^{k} \\ \theta_{fi,n} - \theta_{ri,n}^{k} \end{bmatrix}. \tag{4.5}$$

During the process shown in Fig. 4.2, the power injections are updated iteratively to modify the voltage responses at the boundary buses in the reduced system. At the last iteration, the injections match the response obtained in the full system representation.

It can be seen that the proposed algorithm is a type of boundary matching technique specifically for the dynamic simulation. The trajectory sensitivity can be computed without extensively increasing the computational burden. The same procedure is applied throughout the entire simulation duration. Then the training set, consisting of both the power injections and terminal voltages of the ANN-based equivalent, can be formed. To provide sufficient training samples for the neural network, a variety of disturbances need to be investigated.

4.2 Formulation of the ANN-based equivalent

In the proposed hybrid reduced system shown in Fig. 4.1, the inputs are the voltages at the boundary buses, and the outputs are the power injections compensated by the ANN-based equivalent. As a dynamic system, the present outputs of the ANN-based equivalent depend not only on the present inputs but also on the inputs and outputs at previous time instants. To accommodate this characteristic, a fully recurrent neural network (FRNN) [16] is deployed. As shown in Fig. 4.3, both the bus voltages and the power injection predictions are fed into the network through the tapped-delay-line-memories with *l* and *m* delayed units, respectively.

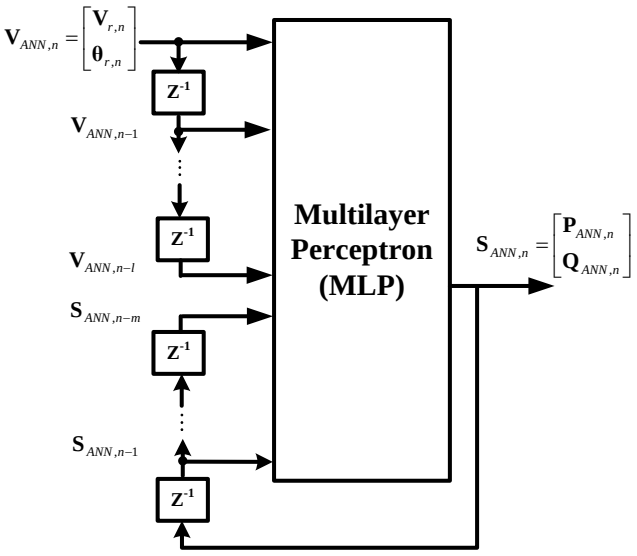

Fig. 4.3 Architecture of the proposed ANN-based equivalent

At the time instant *n*, the ANN-based equivalent can be represented by a nonlinear equation vector defined by,

$$\mathbf{S}_{ANN,n}=\mathbf{h}(\mathbf{V}_{ANN,n},\mathbf{V}_{ANN,n-1},...,\mathbf{V}_{ANN,n-l},\mathbf{S}_{ANN,n-1},...,\mathbf{S}_{ANN,n-m}) \tag{4.6}$$

where $\mathbf{S}_{ANN,n-m}=[\mathbf{P}_{ANN,n-m}{}^{\mathrm{T}}\ \mathbf{Q}_{ANN,n-m}{}^{\mathrm{T}}]^{\mathrm{T}}$ is the power injection vector at the time instant *n-m* and $\mathbf{V}_{ANN,n-l}$ is the voltage vector at the time instant *n-l*. **h** is the vector of nonlinear mapping functions determined by the specific MLP used.

For the FRNN to achieve better capability of capturing the input-and-output mapping stored in the training set and to limit the number of neuron parameters to be optimized, the following three-layer MLP is used.

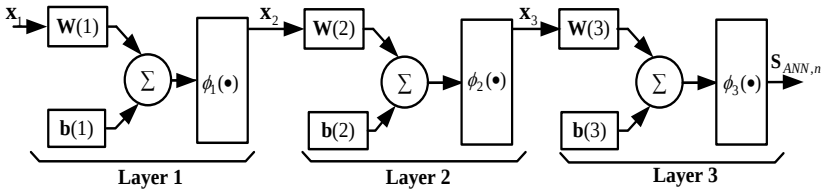

Fig. 4.4 Diagram of MLP in the proposed FRNN

In Fig. 4.4, the input vector is $\mathbf{x}_1=[\mathbf{V}_{ANN,n}{}^{\mathrm{T}}, \mathbf{V}_{ANN,n-1}{}^{\mathrm{T}}, \ldots, \mathbf{V}_{ANN,n-l}{}^{\mathrm{T}}, \mathbf{S}_{ANN,n-1}{}^{\mathrm{T}},\ldots,\mathbf{S}_{ANN,n-m}{}^{\mathrm{T}}]^{\mathrm{T}}$. $\mathbf{x}_2$ and $\mathbf{x}_3$ are the internal state vectors. $\mathbf{W}(1)$, $\mathbf{W}(2)$, and $\mathbf{W}(3)$ are the weighting matrices. $\mathbf{b}(1)$, $\mathbf{b}(2)$, and $\mathbf{b}(3)$ are the bias vectors. ϕ_1, ϕ_2, and ϕ_3 are the activation functions. The subscript 1, 2, and 3 denote layers 1, 2, and 3, respectively in the ANN. Assume that $n_1\times1$, $n_2\times1$, $n_3\times1$, and $n_4\times1$ are the dimensions of $\mathbf{x}_1$, $\mathbf{x}_2$, $\mathbf{x}_3$ and $\mathbf{S}_{ANN,n}$, respectively, then for the layer 1, it can be shown that:

$$x_{2k}=\phi_1\left(\sum_{j=1}^{n_1} w_{kj}(1)x_{1j}+b_k(1)\right),\ k=1,...,n_2 \tag{4.7}$$

where x_{1j} is the j^{th} element of $\mathbf{x}_1$. $w_{kj}(1)$ is the $(k,j)^{\text{th}}$ element of $\mathbf{W}(1)$. $b_k(1)$ is the k^{th} element of $\mathbf{b}(1)$. x_{2k} is the k^{th} element of $\mathbf{x}_2$. Similarly, the following equations hold for layers 2 and 3:

$$x_{3k} = \phi_2\left(\sum_{j=1}^{n_2} w_{kj}(2)x_{2j} + b_k(2)\right),\ k = 1,...,n_3 \tag{4.8}$$

$$S_{ANN,nk} = \phi_3\left(\sum_{j=1}^{n_3} w_{kj}(3)x_{3j} + b_k(3)\right),\ k = 1,...,n_4. \tag{4.9}$$

Then the characteristic equation **h** in (4.6) can be determined uniquely as the combination of (4.7)-(4.9). It is noted that in Fig. 4.3, the exact inputs and outputs at a specific time instant are available in the training set. Therefore for the training purpose, the FRNN can be equivalenced to a static feed-forward network after removing the feedback loop. For the equivalent network, more efficient training methods can be applied. For example, by forming the approximated Hessian matrix of the prediction error with respect to the weights and biases, the Levenberg-Marquardt (LM) back-propagation algorithm can achieve a second-order convergence speed in searching for the optimum weights and biases and thus provides an efficient solution for problems involving the network with up to a few hundred weights [17].

With the inclusion of the ANN-based equivalent, the overall system becomes a hybrid system. It includes the continuous system (described by a set of DAEs) and the discrete system (ANN-based equivalent). The ANN-based equivalent can be regarded as a set of adjustable *P*-*Q* sources using the terminal voltages as inputs. To model the hybrid reduced system, the impacts of the ANN-based equivalent on the power balance equations **g** and the partial derivative matrix $\mathbf{g}_\mathbf{y}$ needs to be considered. Let *B* denotes the set consisting of the connection buses of the ANN-based equivalent, then the new power balance equations at bus $i \in B$ at the time instant *n* are given by:

$$\begin{cases} g_{Pi} = P_{i,n} + P_{ANNi,n} - \sum_{j=1}^{N} V_{i,n}V_{j,n}(G_{ij}\cos\theta_{ij,n} + B_{ij}\sin\theta_{ij,n}) \\ g_{Qi} = Q_{i,n} + Q_{ANNi,n} - \sum_{j=1}^{N} V_{i,n}V_{j,n}(G_{ij}\sin\theta_{ij,n} - B_{ij}\cos\theta_{ij,n}). \end{cases} \tag{4.10}$$

Corresponding to the power injection represented by $P_{ANNi,n}$ and $Q_{ANNi,n}$ in (14), additional partial derivatives, namely$\partial P_{ANNi,n}/\partial V_{j,n}$, $\partial P_{ANNi,n}/\partial\theta_{j,n}$, $\partial Q_{ANNi,n}/\partial V_{j,n}$, and $\partial Q_{ANNi,n}/\partial\theta_{j,n}$ ($j \in B$), needs to be formed. For instance, $\partial P_{ANNi,n}/\partial V_{j,n}$ is given by:

$$\frac{\partial P_{ANNi,n}}{\partial V_{j,n}} = \left(\frac{\partial P_{ANNi,n}}{\partial \mathbf{x}_3}\right)\left(\frac{\partial \mathbf{x}_3}{\partial \mathbf{x}_2}\right)\left(\frac{\partial \mathbf{x}_2}{\partial \mathbf{x}_1}\right)\left(\frac{\partial \mathbf{x}_1}{\partial V_{j,n}}\right). \tag{4.11}$$

Assume ϕ_1 and ϕ_2 are tan-sigmoid activation functions and ϕ_3 is a liner activation function, then the elements of each derivative matrix are given by:

$$\partial P_{ANNi,n}/\partial x_{3m} = w_{km}(3) \tag{4.12}$$

where *k* is the index of $P_{ANNi,n}$ in $\mathbf{S}_{ANN,n}$.

$$\partial x_{3m}/\partial x_{2p} = \left[1-\left(\sum_{j=1}^{n_2} w_{kj}(2)x_{2j} + b_k(2)\right)^2\right] w_{mp}(2) \tag{4.13}$$

where $m = 1,\ldots, n_3$, and $p = 1,\ldots, n_2$.

$$\partial x_{2m}/\partial x_{1p} = \left[1-\left(\sum_{j=1}^{n_1} w_{kj}(1)x_{2j} + b_k(1)\right)^2\right] w_{mp}(1) \tag{4.14}$$

where $m = 1,\ldots, n_2$, and $p = 1,\ldots, n_1$.

$$\partial \mathbf{x}_1/\partial V_{j,n} = [0,...,1,....,0]^T \tag{4.15}$$

where the element of $\mathbf{x}_1$ at the position associated with $V_{j,n}$ is 1 and zeros elsewhere.

The same procedures as shown in (4.10)–(4.15) are followed to account for the impacts of $Q_{ANNi,n}$ but are omitted for the sake of brevity. In addition, to include the power injections of the ANN-based equivalent in (4.10), the additional derivatives are appended to the corresponding entries of the original derivative matrix $\mathbf{g}_\mathbf{y}$ formed using any dynamic simulation software package.

4.3 Test case verification

The system representing a portion of the WECC system is tested to validate the proposed hybrid dynamic equivalent method. A schematic diagram of the test system is shown in Fig. 4.5.

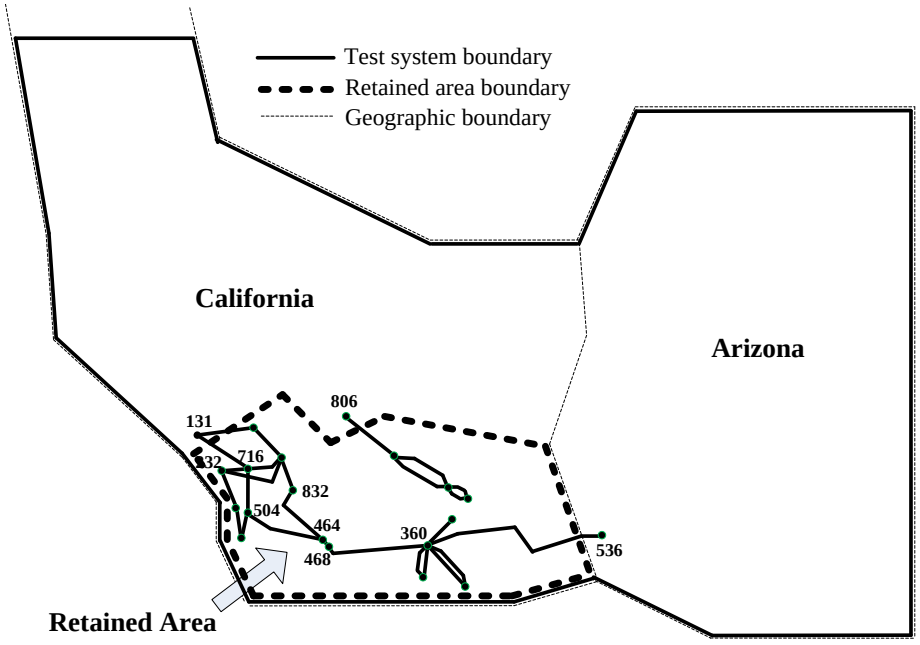

Fig. 4.5 Schematic diagram of the test system

The test system has a total generation of 56944 MW and 7340 MVar and a total load demand of 55476 MW and 6447 MVar. The detailed generator models with exciters, governors, and PSSs are used. The network at 230 kV and above within the retained area is detailed. The remaining part is defined as the external area. After loading the power

flow and dynamic data into DYNRED, the coherent generators are identified using the weak-link method. In the external area, a total of 115 groups of coherent generators are identified with 24 of them have only one generator in each group. Then, the generators in each coherent group are aggregated and replaced by an appropriate equivalent generator using a classical model representation. In the final step, the network in the external area is reduced using Gaussian elimination, and the loads are appropriately aggregated. As a result, the conventionally reduced system, consisting of both the retained area and the equivalenced model for the external area, is formed. The effectiveness of the dynamic equivalent technique in reducing the size of the system to be simulated is illustrated in Table 4-1.

Table 4-1 Summary of full system and conventionally reduced systems

	Full Syst.	Conventionally Reduced Syst.	% of Full Syst.
Buses	2240	806	36.0%
Branches	3015	1573	52.2%
Loads	913	481	52.7%
Generators	342	145	42.4%

It can be seen in Table 4-1 that a significant reduction in the system size can be achieved. In comparison with the full system, 57.6% of the generators have been eliminated in the reduced system. Similar reduction in the number of buses, branches, and loads can also be found. To build the hybrid equivalent for the external area, all the original boundary buses of the retained area, namely 131, 806, and 536, are selected as the connection buses for the ANN-based equivalent. In forming the training set, the typical contingencies summarized in Table 4-2 are evaluated. The simulation duration in each case is 10 s.

Table 4-2 Summary of trained cases

Case #	3-Phase Faulted Bus	Clearance Time (ms)	Line Tripped	
			From Bus	To Bus
1	360	60	360	468
2	360	100	360	468
3	832	100	464	832
4	832	160	464	832
5	716	100	232	716
6	716	160	232	716

For each case in Table 4-2, the trajectory sensitivity-based approach is implemented to determine the appropriate power injections of the ANN-based equivalent. The integration step is fixed at 0.02 s. Therefore, a total of 3006 training samples can be obtained. Take Case 2 for example, the required power injections of the ANN-based equivalent at each boundary bus are shown in Fig. 4.6.

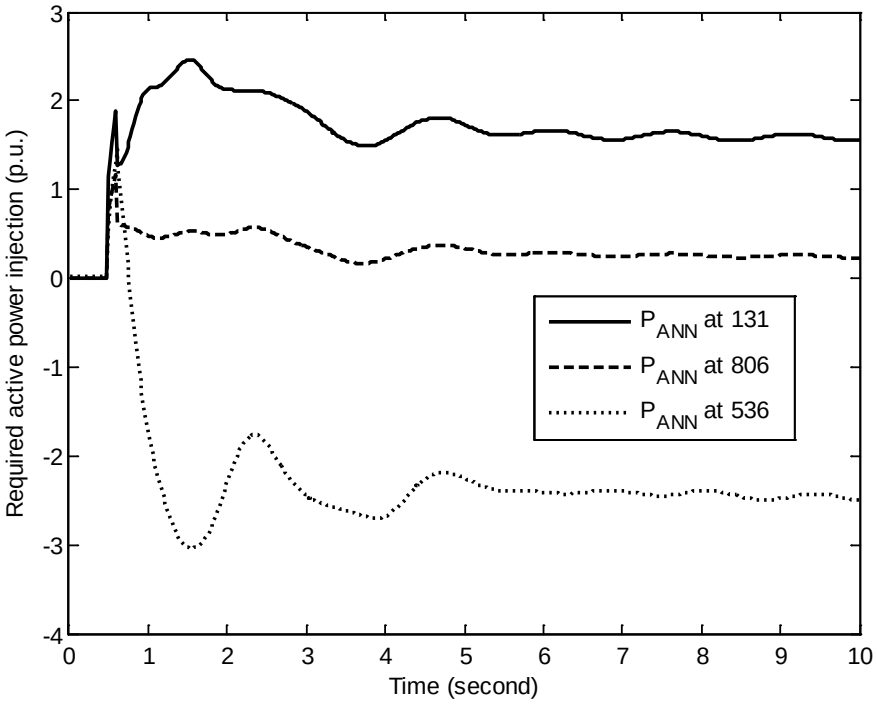

(a) Required active power injections at bus 131, 806, and 536

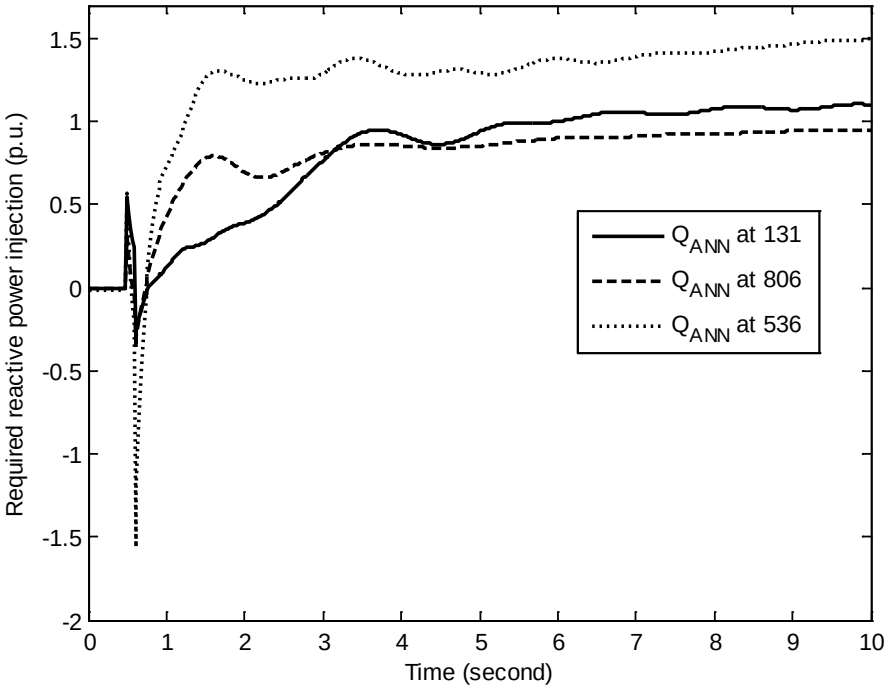

(b) Required reactive power injections at bus 131, 806, and 536

Fig. 4.6 Required active and reactive power injections of the ANN-based equivalent for Case 2

For the same case, the number of iterations in sensitivity approach to converge to the required power injections at each time instant (or *k* in (4.5)), is presented in Fig. 4.7.

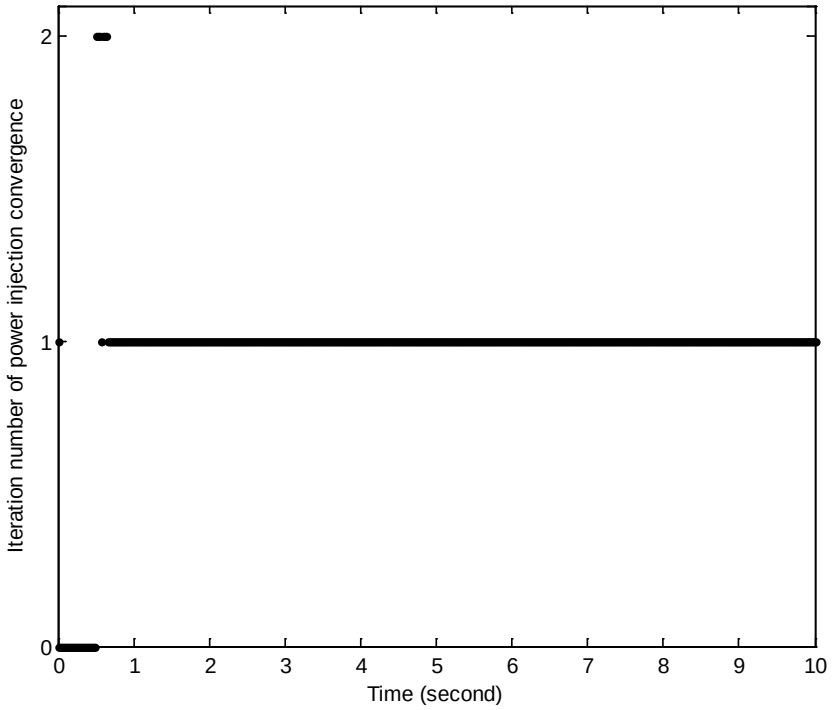

Fig. 4.7 Iteration number of power injection convergence for Case 2

It is seen in Fig. 4.7 that because the trajectory sensitivity provides accurate estimate of the system variable deviation, one iteration of power injections is needed to match the boundary bus voltage responses for the majority of the simulation duration. At the worst scenarios, such as the time instants of fault occurrence and clearance, two iterations are needed.

As for the test system, the FRNN shown in Fig. 4.8 is applied. At the input side, it uses both the present and previous voltage samples at bus i (i=131, 806, and 536) and the delayed feedbacks of the predicted power injections.

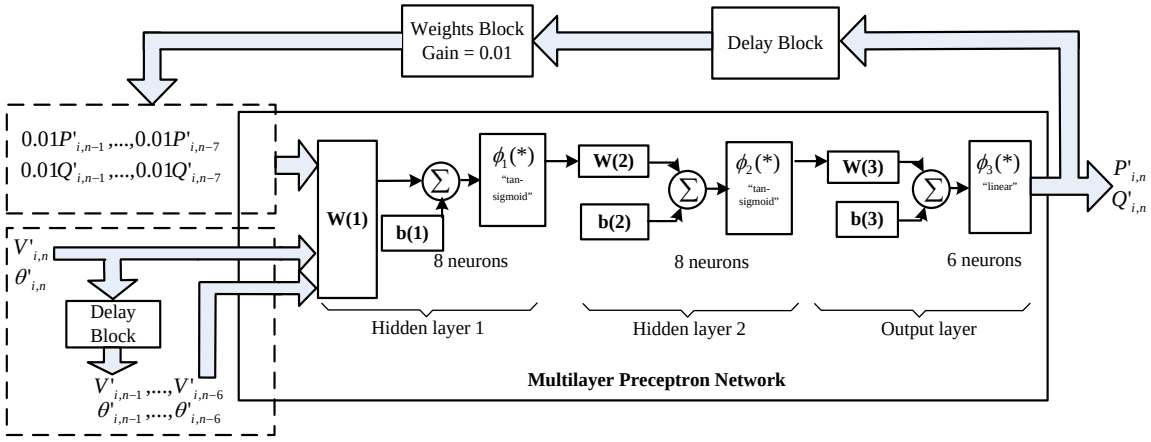

Fig. 4.8 Diagram of the proposed ANN-based equivalent

In Fig. 4.8, tan-sigmoid functions are used as the activation functions at layers 1 and 2, and a linear function is used at layer 3. To make the proposed ANN-based equivalent numerically stable, a gain of 0.01 is applied to the outputs fed back into the input side. To avoid the potential saturation issue with the tan-sigmoid functions, the following pre-processing functions are used,

$$\begin{cases} V'_{ANNi,n} = V_{ANNi,n} / 3 \\ \theta'_{ANNi,n} = \theta_{ANNi,n} / 3 \end{cases} \tag{4.16}$$

$$\begin{cases} P'_{ANNi,n} = P_{ANNi,n} / 6 \\ Q'_{ANNi,n} = Q_{ANNi,n} / 6 \end{cases} \tag{4.17}$$

where $V_{ANNi,n}\angle\theta_{ANNi,n}$ is the voltage at boundary bus i at time instant n. $P_{ANNi,n}+jQ_{ANNi,n}$ is the power injection of the ANN-based equivalent at time instant n. i is the boundary bus number, namely 131, 806, and 536.

When using the pre-processing functions in (4.16) and (4.17), the magnitudes of input and output signals are mapped the unsaturated section of the tan-sigmoid activation function. Given the training set that includes 3006 patterns, the network is trained using the LM routine in MATLAB. On an Intel Core 2 Duo Processor (3.16 GHz) PC with 3 GB of RAM, the total training time is 129 s. After being trained, the ANN-based equivalent is connected to the conventionally reduced system at all the boundary buses.

To validate the proposed hybrid equivalent, the contingency defined in Case 2 is applied to the full system and reduced systems. The relative rotor angle response of generator #15 and voltage response at bus 131 are shown in Fig. 4.9 and Fig. 4.10, respectively.

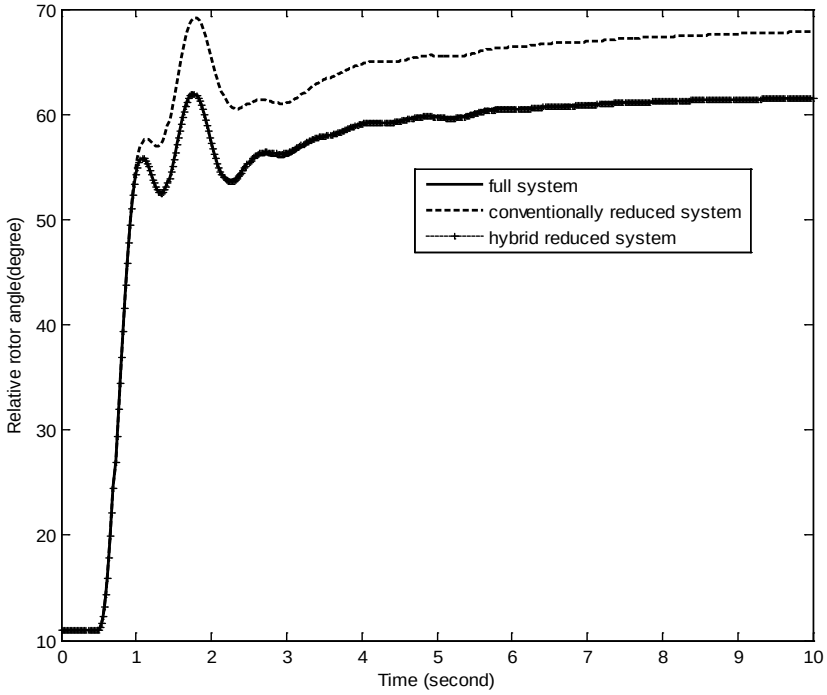

Fig. 4.9 Relative rotor angle responese of genreator #15 for Case 2

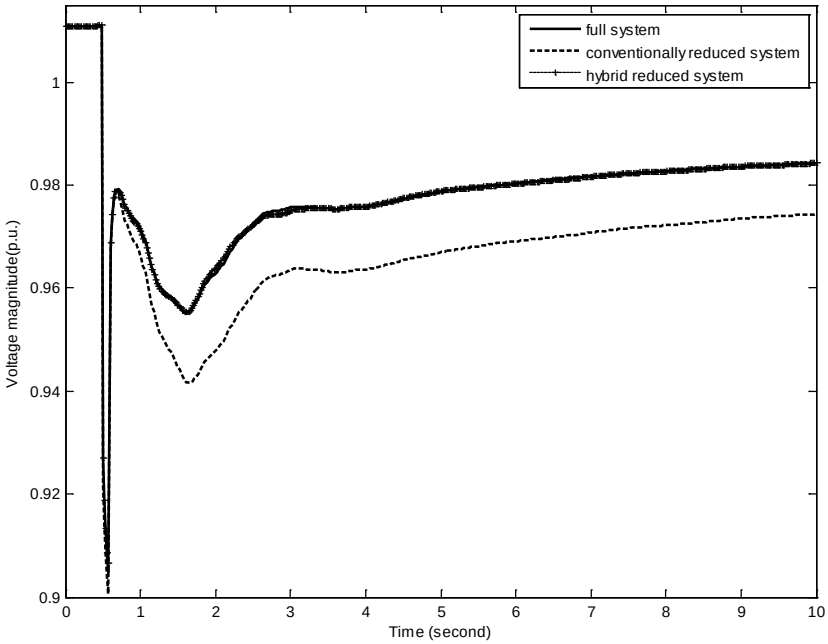

Fig. 4.10 Voltage responses at bus 131 for Case 2

It can be seen in Fig. 4.9 and 4.10 that the mismatches between the full system and conventionally reduced system are well compensated by the ANN-based equivalent as expected. More accurate responses can be obtained in the hybrid reduced system throughout the entire simulation duration. To validate the feasibility of the proposed hybrid equivalent for the cases that are not included in the training set, a 3-phase fault is applied at new bus (bus 504), and it is cleared after 0.10 s by tripping the 230 kV line from bus 504 to bus 464. The results are shown in Fig. 4.11 and Fig. 4.12.

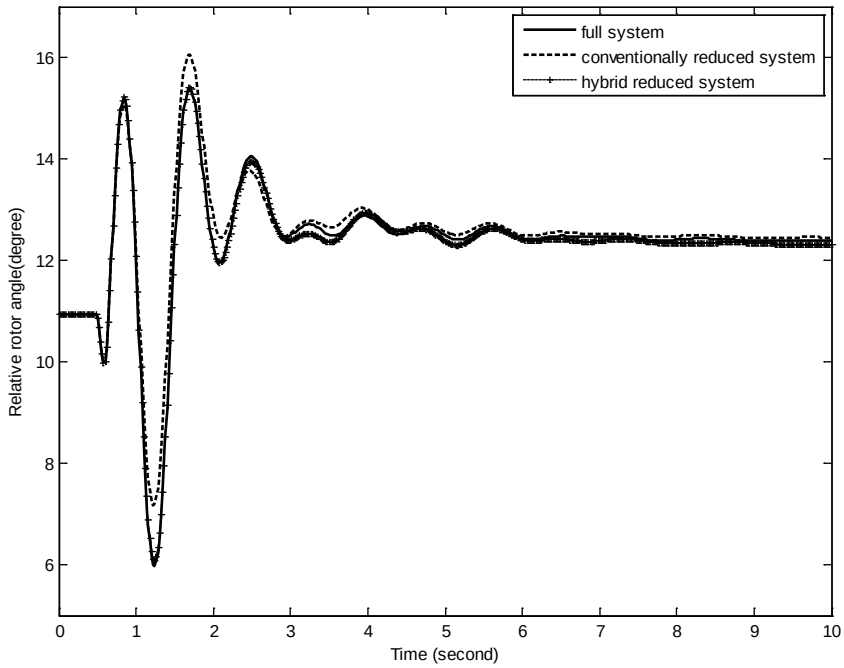

Fig. 4.11 Relative rotor angle responses of generator #15 for the untrained case

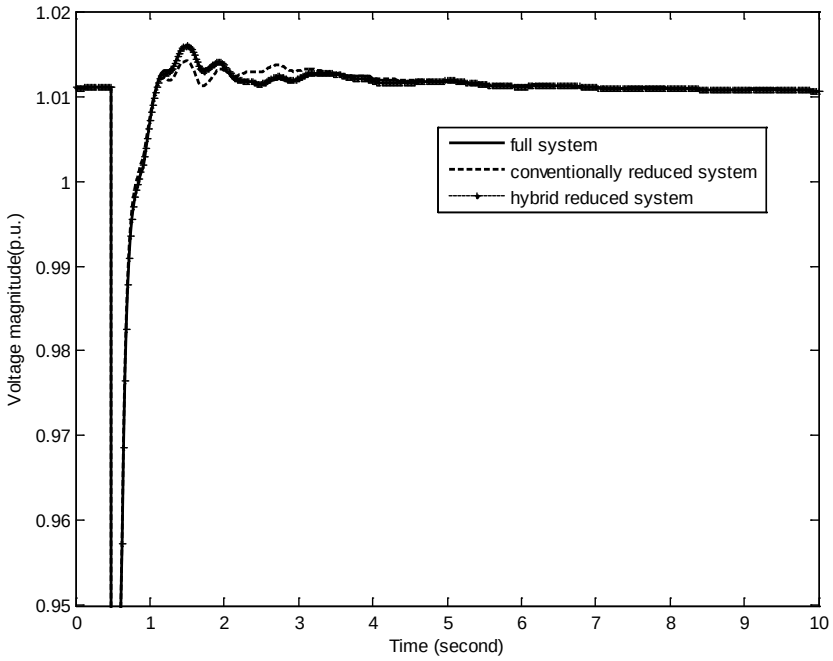

Fig. 4.12 Voltage responses at bus 131 for the untrained case

Fig. 4.11 and 4.12 shows that for the system disturbances that are not included in the training set, the ANN-based equivalent can still improve the equivalencing accuracy by providing essential supplementary compensations to the conventionally reduced system. This is especially true for the period following the disturbances. It is to be noted that the feasibility of the proposed hybrid equivalent can be easily improved by including more samples into the training set. Another prominent advantage of the proposed method is that the PMUs measurements at the boundary buses can be directly used as the reference in determining the training set for the ANN-based equivalent. Real-time measurements collected by PMUs allow the ANN-based equivalent to capture the discrepancies between the planning models that are used for building the conventionally reduced model and the exact system models under realistic operating conditions, leading to improved dynamic models for on-line DSA.

5. Conclusions

Power system dynamic equivalents play a critical role in on-line DSA presently given the increasing scale of interconnected power systems. To improve the feasibility of the conventional coherency-based dynamic equivalents, the following three topics have been discussed in this report.

- A systemic method to determine an appropriate retained area boundary

In the proposed method, the PTDFs-based criterion, the estimated rotor acceleration-based criterion and the mode participation-based criterion have been applied to identify the critical generators in the initial external area that have great impact on the dynamic performance of the study area. The identified generators are retained additionally, leading to a revised equivalent. The proposed approach has been applied to the test system representing the entire US/Canada eastern interconnection. The test results show that the proposed algorithm is capable of identifying the appropriate buffer area and forming improved dynamic equivalent models.

- An efficient method to trace generator slow coherency patterns and to adjust retained area boundary for operating condition changes

A systematic approach based on the eigensensitivity is proposed to evaluate the changing patterns of generator slow coherency as system operating condition varies. The impacts of load change, generation change, line outage, and line addition have been considered. The critical generators in the initial external area that become tightly slowly coherent with the initial study area are identified and retained in forming a new equivalent for a changed system condition. The proposed approach has been applied to a portion of the WECC system. The study shows that the inclusion of the identified critical generators into the retained area is beneficial for the improvement of equivalencing accuracy.

- A novel hybrid dynamic equivalent method

The concept of a novel hybrid dynamic equivalent method has been presented in this report. In the proposed model, the coherency-based equivalent still plays a dominant role, and the ANN-based equivalent is only used to capture additional dynamic characteristics that have been ignored in the conventionally reduced system. The methods to build the training set and to form appropriate neural network for the ANN-based equivalent have been discussed in detail. The test on a portion of the WECC system shows that the ANN-based equivalent can effectively compensate for the discrepancy between the full system and the coherency-based equivalent, leading to improved equivalencing accuracy.

References

[1] S. T. Y. Lee, and F. C. Schweppe, "Distance measures and coherency recognition for transient stability equivalents," *IEEE Trans. Power App. Syst.*, vol. PAS–92, no. 5, pp. 1550–1557, 1973.

[2] R. Billinton, and P. Wang, "Deregulated power system planning using a reliability network equivalent technique," in *IEE Proc.–Gener. Transm. Distrib.*, vol. 153, no. 6, pp. 25–30, Jan. 1999.

[3] L. Wang, and G. Zhang, "DYNRED enhancement project," EPRI, Palo Alto, CA, Tech. Rep. for Software Product ID # 1020268, 2010.

[4] R. Podmore, "Identification of coherent generators for dynamic equivalents," *IEEE Transactions on Power Apparatus and Systems*, Vol. PAS–97, pp. 1344–1354, July/August 1978.

[5] R. Nath, S. S. Lamba, and K. S. P. Rao, "Coherency based system decomposition into study and external areas using weak coupling," *IEEE Trans. Power App. Syst.*, Vol. PAS–104, pp. 1443 – 1449, 1995.

[6] J. H. Chow, J. R. Winkelman, M. A. Pai, and P. W. Sauer, "Model reduction and energy function analysis of power system using singular perturbation techniques," *25th IEEE Conference on Decision and Control*, pp.1206 –1211, 1986.

[7] P. Kundur, G. J. Rogers, D. Y. Wong, J. Ottevangers, and L. Wang, "Dynamic reduction," EPRI TR- 102234 Project 2447–01, 1993.

[8] R. Podmore, and A. Germond, "Development of dynamic equivalent for transient stability studies," EPRI EL–456 Project 763, 1977.

[9] M. L. Ourari, L. A. Dessaint, and V. Q. Do, "Dynamic equivalent modeling of large power systems using structure preservation technique," *IEEE Trans. on Power Syst.*, Vol.21, No.3, pp. 1284 –1295, Aug. 2006.

[10] X. Cheng, and T. J. Overbye, "PTDF-based power system equivalents," *IEEE Trans. on Power Syst.*, vol. 20, no. 4, pp. 1868 – 1876, Sept. 2005.

[11] P. Kundur, *Power system stability and control*, New York: McGraw-Hill, 1994.

[12] Y. K. Wu, "A novel algorithm for ATC calculations and applications in deregulated electricity markets," *Electrical Power and Energy Systems*, Vol. 29, No. 10, pp. 810 – 821, Dec. 2007.

[13] S. K. Joo, C. C. Liu, L. E. Jones, and J. W. Choe, "Coherency and aggregation techniques incorporating rotor and voltage dynamics," *IEEE Trans. on Power Syst.*, Vol. 19, No. 2, pp.1068 – 1075, May, 2004

[14] T. B. Nguyen, and M. A. Pai, "Dynamic security-constrained rescheduling of power systems using trajectory sensitivities," *IEEE Trans. on Power Syst.*, Vol. 18, No.2, pp. 848 – 854, May 2003.

[15] A. Zamora-Cardenas, and C. R. Fuerte-Esquivel, "Multi-parameter trajectory sensitivity approach for location of series-connected controllers to enhance power system transient stability," *Electric Power Systems Research*, Vol. 80, No. 9, pp. 1096 – 1103, Sept. 2010.

[16] S. S. Haykin, *Neural Networks: A Comprehensive Foundation*. Englewood Cliffs, NJ: Prentice-Hall, 1999.

[17] *Neural Network Toolbox, for use with MATLAB User's Guide, Version7*, The Math Works Inc, 2010.

Project Publications

[1] F. Ma, and V. Vittal, "Right-sized power system dynamic equivalents for power system operation," to appear in the *IEEE Trans. on Power Syst*, TPWRS.2011.2138725.

[2] F. Ma, X. Luo, and V. Vittal, "Application of dynamic equivalencing in large-scale power systems," to appear in the proceeding of *IEEE PES 2011 General Meeting*, Detroit, MI, July 24–28, 2011, Paper no. 2011GM0804.

Part II

The Trajectory Sensitivity Analysis Approach to Determine Stability Limits under Changing System Conditions

Vijay Vittal

Guanji Hou – Graduate Student

Arizona State University

Information about this project

Vijay Vittal
Ira A. Fulton Chair Professor
Department of Electrical Engineering
Arizona State University
PO Box 875706
Tempe, AZ 85287-5706
Tel: 480-965-1879
Fax: 480-965-0745
Email: vijay.vittal@asu.edu

Power Systems Engineering Research Center

The Power Systems Engineering Research Center (PSERC) is a multi-university Center conducting research on challenges facing the electric power industry and educating the next generation of power engineers. More information about PSERC can be found at the Center's website: http://www.pserc.org.

For additional information, contact:

Power Systems Engineering Research Center
Arizona State University
577 Engineering Research Center
Tempe, Arizona 85287-5706
Phone: 480-965-1643
Fax: 480-965-0745

Notice Concerning Copyright Material

Table of Contents

List of Figures

List of Tables

Glossary

A	Product of normalized maximum sensitivity and perturbation
B	Shunt capacitor susceptance
D_k	Damping coefficient of generator k
DAEs	Differential algebraic equations
DSA	Dynamic security assessment
E	Error in linear sensitivity approximation
F	Set of system differential equations
F'	Set of system augmented differential equations
f_{ik}	PTDF of generator i on line k
F_{New}	Linearization of F'
F_x	Partial derivative of F with respect to system state variables
F_y	Partial derivative of F with respect to system network variables
F_λ	Partial derivative of F with respect to parameter λ
G	Set of system network equations
G'	Set of system augmented network equations
G_{New}	Set of system augmented network equations
G_x	Partial derivative of G with respect to system state variables
G_y	Partial derivative of G with respect to system network variables
G_λ	Partial derivative of G with respect to parameter λ
GUI	Graphical user interface
H	Generator inertia constant
K_{pm}	Initial active power proportion of the motor loads
M	Set of network buses
g_p	Sets of network equations related to active power
g_q	Sets of network equations related to reactive power
P_{tm}	Active power flow in transmission lines connected at bus m
P_{gm}	Active power generation at bus m
P_{lm}	Active load at bus m
LM	Large inductor motor
PSAT	Power System Analysis Toolbox
P_{mk}	Mechanical power at generator k
P_{ek}	Electrical power at generator k
P_I	Interface real power flow
PSS	Power system stabilizer
PTDF	Power transfer distribution factor
Q_{tm}	Reactive power flow in transmission lines connected at bus m
Q_{gm}	Reactive power generation at bus m
Q_{lm}	Reactive load at bus m
S_{max}	Normalized maximum sensitivity
SM	Small induction motor
ST	Trip induction motor
t_{cl}	Fault clearing time
TS	Trajectory sensitivity
T_v	Voltage trip pick up time for trip motors
U_i	Partial derivatives of x *w.r.t* the *i-th* system changing parameter λ

V_i	Partial derivatives of *y w.r.t* the *i-th* system changing parameter λ
V_{ref}	Generator exciter reference voltage
V_t	Voltage threshold for trip motors
WECC	Western Electricity Coordinating Council
w.r.t	With respect to
X_n^k	The value of *X* at *k-th* iteration step when *t=n*
$X^{New}(t)$	Approximated variable trajectory
$X^{Base}(t)$	Base case variable trajectory
x	Vector of state variables
y	Vector of network variables
ω	Generator rotor speed
δ	Generator rotor angle
δ_{ij}	Relative rotor angle between generator *i* and generator *j*
λ	Set of system parameters that are subjected to change
$\Delta\lambda$	Size of change of the changing parameter
ζ	Efficiency of the cluster
$\Delta\lambda_{max\text{-}lin}$	Linear approximation accuracy constrained maximum perturbation size
$\Delta\lambda_{max\text{-}sta}$	Stability constrained maximum size of perturbation size

1. Introduction

1.1 Background

Existing dynamic security assessment (DSA) tools rely heavily on time-domain simulation to explore the influence of large disturbances on a power system. Currently DSA simulation engines, using time-domain simulation can provide significant amount of information about the dynamic behavior of the system under large disturbances, however, these engines have the following shortcomings:

- For a given specified operating condition and contingency scenario several time-domain simulations must be run to ascertain a particular stability limit
- When the operating condition, such as the network topology, generation, load or control parameters change within a short time, the derivation of the stability limits is computationally burdensome
- Does not provide a quantitative index of the underlying parametric influence on system response
- The accuracy of analysis on a power system depends on the accurate modeling of each component of a power system. In order to account for the uncertainty of parametric values, several time-domain simulations must be run, which is very time consuming and computationally burdensome.

The trajectory sensitivity method is an effective solution to address these drawbacks and can complement the traditional time-domain simulation approach. The concepts of trajectory sensitivity method are well established in [1]–[5].

The most attractive advantage of the trajectory sensitivity approach is that it can provide some valuable insights into system responses due to parameter changes within a very short time at the expense of only a negligible amount of extra computational burden. Detailed descriptions regarding the trajectory sensitivity analysis are provided in chapter 2.

1.2 Literature review

The mathematical introduction to the trajectory sensitivity analysis in differential algebraic systems was first fully described by [1] - [5]. Then M. J. Laufenberg, M. A. Pai, I. A. Hiskens and other scholars applied this method to the field of power systems [6] - [11]. In [6] and [7], the basic theory is introduced and simple examples are given to demonstrate the application of this new method to dynamic security assessment. In [8], some results obtained from the trajectory sensitivity method are compared with the actual recorded data. In [9] the author discusses the application of trajectory sensitivity to hybrid systems. In [10], applications of trajectory sensitivity in system approximation and uncertainty research are presented. In [11], trajectory sensitivity is utilized for system stability boundary uncertainty analysis to quantify the influence of system model uncertainty on dynamic security assessment.

In [12], trajectory sensitivity is used to analyze the Nordel power grid disturbance of January 1, 1997. The voltage and machine angle plots approximated by trajectory

sensitivity are consistent with actual recorded data. The results also show the efficacy of the trajectory sensitivity method in evaluating the influence of various system parameters on the response of the system under a large disturbance. In [13], a detailed discussion of trajectory sensitivity as a tool for dynamic security assessment is presented. The trajectory sensitivity method is also used for the identification of dynamic models, such as exciters and PSSs. In [14], by using trajectory sensitivity, some information on the selection of exciter models and the parameters to be identified, and the appropriateness of the test condition are provided directly in the sensitivity matrix. In [15], trajectory sensitivity is used for PSS design. In [16], trajectory sensitivity is applied to dynamic VAR planning for voltage stability in a large power system. Trajectory sensitivity is also used in generation rescheduling [17], with the sensitivity calculated along the time domain, the selection of the rescheduling choices and the amount of generation that need to be rescheduled are calculated directly. In [19], the trajectory sensitivity analysis is applied to develop a voltage emergency control approach, which has a predictive feature and the system can be stabilized in the early stages after a disturbance by employing only necessary control. The potential applications of trajectory sensitivity in power system are summarized in [20]. Other applications are discussed in [21] - [27].

1.3 Efforts of the report

From the literature survey described above it can be seen that the trajectory sensitivity method has been mathematically proven to be an effective tool to complement the traditional time domain simulation tools. However, there are some important issues that need to be addressed before real applications to realistic large power systems. This report focuses on addressing the following problems:

1) Implementation of various control parameter variations in the trajectory sensitivity approach

In a power system, there are a large amount of control parameters that are aimed at different kinds of control. During this research effort, eight different categories of control parameter sensitivities are implemented and tested. The results show the potential applicability of the trajectory sensitivity method to commercial tools that are widely used in the electric power industry

2) Computational burden reduction

In the formulation of the trajectory sensitivity approach an extra set of sensitivity equations is augmented to the existing system of differential algebraic equations in time domain simulation for every parameter change. As a result the computation burden increases, especially when a large number of parameter sensitivities are calculated. Therefore, the reduction of this computational burden becomes an important issue to be addressed. In the research reported, a high performance cluster based parallel computing platform has been adopted. Using this platform, various types of sensitivity calculations can be conducted in parallel on the fast computers equipped with high speed cores and large amount of memory

3) Linear sensitivity approximation accuracy assessment

The main principle of applying the trajectory sensitivity method in based on linear approximation. However, there is no quantitative guideline relating the parameter change

size and the approximation accuracy. This research effort also addresses this problem. When the perturbation size varies, it is critical to ascertain the accuracy of the trajectory approximation. A technique to characterize the error and quantify it is developed

4) Applicability to various power system problems

Most current research efforts and publications focus on the analytical development of the method. However, very few of these efforts have applied the method to realistic large test systems. To test the applicability of the proposed method, several different power system stability problems have been studied by applying the trajectory sensitivity analysis method to a large WECC system model. The results demonstrate the bright potential of this method.

1.4 Report organization

This section of the report is structured as follows,

- In Chapter 1, related background, literature review, and motivation of the research are presented
- In Chapter 2, the detailed descriptions of trajectory sensitivity, including the formulation of sensitivity equations, the solutions of the augmented DAEs, the main computational effort and the application principle are presented
- In Chapter 3, the implementation of the various sensitivity element calculations and a high performance parallel computing platform are introduced
- In Chapter 4, the accuracy of the implementation is verified by comparing the approximated variable plot obtained using the trajectory sensitivity approach with the actual perturbed plot obtained by running time domain simulation for the changed conditions
- In Chapter 5, the relation between linear approximation accuracy and the perturbation size is addressed
- In Chapter 6, an application of the proposed trajectory sensitivity based generation rescheduling preventive control to the transient angle stability problem is demonstrated
- In Chapter 7, another application demonstrates the application of the trajectory sensitivity analysis approach to the voltage stability problem considering load modeling uncertainties
- In Chapter 8, transient stability constrained interface real power flow limit calculation is tackled using the proposed method
- Conclusions and future work are presented in Chapter 9.

2. Trajectory Sensitivity

2.1 System description

In a conventional time domain transient stability analysis program, a power system is represented by the following set of nonlinear differential-algebraic equations (DAEs).

$$\dot{x} = F(x, y, \lambda) \tag{2-1}$$

$$0 = G(x, y, \lambda) \tag{2-2}$$

where:

x = vector of state variables

y = vector of network variables

λ = vector of parameters that are subjected to change

λ is a parameter characterizing for example, load, generation, transmission line impedance or generator bus initial voltage levels, which is expected to change and affect the operating boundary imposed by dynamic constraints. To account for these changes on the operating boundary, (2-1) which is a set of nonlinear differential equations and (2-2) which is a set of nonlinear algebraic equations are augmented with the following set of equations (2-3) and (2-4)

$$\dot{U}_i = \frac{\partial F}{\partial \lambda_i} = F_x U_i + F_y V_i + F_{\lambda_i} \tag{2-3}$$

$$0 = \frac{\partial G}{\partial \lambda_i} = G_x U_i + G_y V_i + G_{\lambda_i} \tag{2-4}$$

where

$U_i = \frac{\partial x}{\partial \lambda_i}$: Vector of the partial derivatives of x with respect to (w.r.t) λ_i

$V_i = \frac{\partial y}{\partial \lambda_i}$: Vector of the partial derivatives of y w.r.t λ_i

(2-3) is a set of linear differential equations and is referred to as the sensitivity dynamical equations, and (2-4) is the associated set of linear algebraic equations for the solution of the network variables sensitivities with respect to the changing parameter. The set of equations (2-3) and (2-4) are referred to as sensitivity equations. For every parameter which changes, the system equations (2-1) and (2-2) will have to be augmented with a set of sensitivity equations corresponding to (2-3) and (2-4) respectively, which can be solved simultaneously with (2-1) and (2-2) as the time domain trajectory evolves.

2.2 Solutions to the DAEs

An implicit method, such as the trapezoidal method, is recommended for the solution of (2-1) and (2-2) for the reason that implicit methods provide the needed Jacobian matrices which are used to solve the trajectory sensitivity equations (2-3) and (2-4). Assuming that

the trapezoidal implicit method is used in the time domain simulation program, the process of solving the set of sensitivity equation (2-3) and (2-4) is performed as follows, First these two equations are rewritten here for the sake of convenience

$$\dot{U}_i = \frac{\partial F}{\partial \lambda_i} = F_x U_i + F_y V_i + F_{\lambda_i} = F'(U, V, \lambda) \tag{2-5}$$

$$0 = \frac{\partial G}{\partial \lambda_i} = G_x U_i + G_y V_i + G_{\lambda_i} = G'(U, V, \lambda) \tag{2-6}$$

Applying trapezoidal rule to (2-3) and gets

$$U_{n+1} = U_n + \frac{\Delta t}{2}\left[F'(U_{n+1}, V_{n+1}, \lambda) + F'(U_n, V_n, \lambda)\right] \tag{2-7}$$

let

$$F_{new}(U_{n+1}, V_{n+1}, \lambda) = U_{n+1} - U_n - \frac{\Delta t}{2}\left[F'(U_{n+1}, V_{n+1}, \lambda) + F'(U_n, V_n, \lambda)\right] \tag{2-8}$$

and

$$G_{new}(U_{n+1}, V_{n+1}, \lambda) = G_{x(n)} U_{n+1} + G_{y(n)} V_{n+1} + G_{\lambda(n)} \tag{2-9}$$

At solution

$$F_{new}(U_{n+1}, V_{n+1}, \lambda) = 0 \tag{2-10}$$

$$G_{new}(U_{n+1}, V_{n+1}, \lambda) = 0 \tag{2-11}$$

By doing this, the differential equations have been transformed into iterative algebraic equations. Newton's method is then applied to solve (2-10) and (2-11). The iteration formula is as follows,

$$\begin{bmatrix} U_{n+1}^{k+1} \\ V_{n+1}^{k+1} \end{bmatrix} = \begin{bmatrix} U_{n+1}^{k} \\ V_{n+1}^{k} \end{bmatrix} + \begin{bmatrix} \Delta U_{n+1}^{k} \\ \Delta V_{n+1}^{k} \end{bmatrix} \tag{2-12}$$

The following equations are solved to obtain ΔU_{n+1}^k and ΔV_{n+1}^k

$$\begin{bmatrix} -F_{new}(U_{n+1}^k, V_{n+1}^k, \lambda) \\ -G_{new}(U_{n+1}^k, V_{n+1}^k, \lambda) \end{bmatrix} = \begin{bmatrix} \frac{\partial F_{new}}{\partial U} & \frac{\partial F_{new}}{\partial V} \\ \frac{\partial G_{new}}{\partial U} & \frac{\partial G_{new}}{\partial V} \end{bmatrix} \begin{bmatrix} \Delta U_{n+1}^k \\ \Delta V_{n+1}^k \end{bmatrix} \tag{2-13}$$

where

$$\frac{\partial F_{New}}{\partial U} = 1 - \frac{\Delta t}{2} F_x,\ \frac{\partial F_{New}}{\partial V} = -\frac{\Delta t}{2} F_y,\ \frac{\partial G_{New}}{\partial U} = G_x,\ \frac{\partial G_{New}}{\partial V} = G_y.$$

F_x, F_y, G_x and G_y are the Jacobian matrices that are evaluated for solving (2-1) ~ (2-2) by an implicit method, evaluated at $x = x_{n+1}^k$ and $y = y_{n+1}^k$.

Now ΔU_{n+1}^{k} and ΔV_{n+1}^{k} can be obtained from (2-13), then ΔU_{n+1}^{k+1} and ΔV_{n+1}^{k+1} are obtained from (2-12).

2.3 Main computational effort

As mentioned above F_x, F_y, G_x and G_y are the byproducts of the traditional time domain simulation routine when an implicit integration method is used to solve the system of DAEs. The main computational effort to evaluate the trajectory sensitivity is then to compute and update the vectors of F_λ or G_λ according to different types of sensitivity elements at every step of the computation. It is noted that normally F_λ or G_λ are very sparse. This characteristic greatly reduces the computational burden.

For example, if the sensitivities of variables (both state variables and network variables) to change in active generation at generator k are evaluated, the process of setting up the vectors F_λ or G_λ is as follows,

For F_λ, only the derivative of the rotor speed equation of generator k related to the changed variable λ (in this case the changed variable is P_{mk}) is not zero. Other elements of F_λ are zero. The rotor speed differential equation for generator k is given by

$$\dot{\omega}_k = \frac{1}{2H_k}\left(P_{mk} - P_{ek} - D_k\left(\omega_k - 1\right)\right) \tag{2-14}$$

where

ω_k --- Rotor speed

H_k --- Inertia constant

P_{mk} --- Mechanical power input

P_{ek} --- Electrical power output

D_k --- Damping coefficient

Then

$$F_\lambda(i) = \frac{\partial F(i)}{\partial \lambda} = \begin{cases} \dfrac{1}{2H_k} & i = k \\ 0 & i \neq k \end{cases} \tag{2-15}$$

where i is the index of the differential equations.

In (2-15) F_λ is the vector that has to be evaluated for the sensitivity equation (2-3) when the sensitivity to active generation at generator k is evaluated.

As for the evaluation of G_λ, suppose the network equations are of the form of

$$G(x,y) = \begin{bmatrix} g_p \\ g_q \end{bmatrix} = \begin{bmatrix} P_{tm} \\ Q_{tm} \end{bmatrix} - \left(\begin{bmatrix} P_{gm} \\ Q_{gm} \end{bmatrix} - \begin{bmatrix} P_{lm} \\ Q_{lm} \end{bmatrix} \right) \qquad \forall m \in M \tag{2-16}$$

where g_p and g_q are the sets of network equations related to active and reactive power respectively. P_{tm} and Q_{tm} are the active and reactive power flows in transmission lines

related to bus m respectively. P_{gm} and Q_{gm} are the active and reactive power generation at bus m respectively. P_{lm} and Q_{lm} are the active and reactive load at bus m respectively. M is the set of network buses.

Then for G_λ

$$G_\lambda(i) = \frac{\partial G(i)}{\partial \lambda} = \begin{cases} -1 & i = k \\ 0 & i \neq k \end{cases} \tag{2-17}$$

where i is the index of the network equations.

This is the vector G_λ for the sensitivity equation (2-4) when sensitivity to active generation at generator k is evaluated. If F_λ or G_λ are not constant when time evolves, then they should be updated at every computation step. For different types of sensitivity element calculation, F_λ or G_λ should be formulated accordingly. This is the main implementation and computation effort when employing the trajectory sensitivity method.

Another factor in the implementation of the trajectory sensitivity approach is the computational efficiency. This method requires augmenting the original DAEs with a set of extra sensitivity equations for each parameter change. Therefore the computational burden can be significantly increased. The computational burden reduction is a critical issue that needs to be addressed. The independent nature of the sensitivity equations leads to an approach to relieve this computational burden. For a given instant of time in the integration of the original system DAEs, the set of sensitivity equations (2-3) and (2-4) for different parameter changes are independent and can be evaluated in parallel by using distributed parallel computing techniques, which will significantly improve the computational speed.

For example, suppose the sensitivity to active generation at bus j and the sensitivity to active generation at bus k are evaluated simultaneously, and then two sets of equations (2-18) and (2-19) are formed, respectively

$$\begin{cases} \dot{U}_{P_j} = \dfrac{\partial F}{\partial P_j} = F_x U_{P_j} + F_y V_{P_j} + F_{P_j} \\ 0 = \dfrac{\partial G}{\partial P_j} = G_x U_{P_j} + G_y V_{P_j} + G_{P_j} \end{cases} \tag{2-18}$$

$$\begin{cases} \dot{U}_{P_k} = \dfrac{\partial F}{\partial P_k} = F_x U_{P_k} + F_y V_{P_k} + F_{P_k} \\ 0 = \dfrac{\partial G}{\partial P_k} = G_x U_{P_k} + G_y V_{P_k} + G_{P_k} \end{cases} \tag{2-19}$$

These two sets of equations are independent of each other and can be solved in parallel with the same Jacobian matrices F_x, F_y, G_x and G_y being used.

2.4 Application principle

When a change of system parameter occurs, the new value of the system variables (both state variables and network variables) can be approximated linearly based on the base-case value by applying the following formula

$$X^{New}(t) = X^{Base}(t) + \frac{\partial X}{\partial \lambda}(t)\Delta\lambda \tag{2-20}$$

Where:

$X^{New}(t)$: Approximated variable trajectory

$X^{Base}(t)$: Base case variable trajectory

$\frac{\partial X}{\partial \lambda}(t)$: The evaluated sensitivity trajectory

$\Delta\lambda$: The size of change of the changing parameter

Equation (2-20) characterizes the approach to applying the trajectory sensitivity method to evaluate the effect of changes in system parameters. If the changes are large, and linear sensitivity is not applicable, higher order sensitivities may need to be evaluated. The range in which this first order linear sensitivity approach is applicable is system dependent and base-case operating point dependent. During the course of this research, the range of applicability of the linear sensitivity approach will be examined.

2.5 Summary

In this chapter, the fundamentals of the trajectory sensitivity method are presented. In order to account for the parameters that are expected to change and affect the operational stability boundary, the existing DAEs need to be augmented with a set of differential algebraic sensitivity equations. Any implicit integration method can be used to solve the system DAEs in time domain simulation routine since implicit methods provide the needed Jacobian matrices that are required to solve the augmented sensitivity equations. This computation with the implicit method significantly relieves the computational burden. When multiple sensitivity elements are evaluated simultaneously, distributed parallel computation techniques can be applied to further enhance the computational capability. This will be introduced in Chapter 3.2.

3. Software Development

3.1 Trajectory sensitivity routine implementation

The implementation of the approach is based on an open source Matlab based power system analysis software called Power System Analysis Toolbox (PSAT) [37], which was developed primarily by Prof. F. Milano at the University of Castilla – La Mancha, Spain.

During this research effort, eight categories of sensitivity elements have been implemented and tested. They include sensitivity to:

- Active generation change
- Load change, both active and reactive load change
- Generator initial terminal bus voltage changes, which would affect the reference set point for an exciter
- Topology change, including transmission line resistance *R*, reactance *X*, susceptance *B* and shunt compensation change
- Load change, including both the composition and exponent change for voltage/frequency dependent loads
- Generator control parameters, including gains, time constants and other control parameters for exciters, PSSs and turbine governors
- FACTS control parameters
- Load modeling uncertainty, including the uncertainties of the composition of various loads, uncertainties of inductor parameters modeling.

A graphical user interface (GUI) for the trajectory sensitivity method has also been developed as shown in Figure 3-1. Figure 3-2 depicts the GUI panel for general trajectory sensitivity settings. In this panel, users can select the specific sensitivity element to calculate; in addition the perturbation size of the parameter can also be defined.

Figure 3-3 depicts the GUI that provides the interface to the sensitivity trajectory plot after its calculation. All the variable sensitivities can be plotted, exported and edited in this window. Also, there is another interface to plot the approximated variable curve for the perturbed case obtained from (2-20). The perturbation size of the changing parameter can be denoted and changed in this window, as shown in Figure 3-4.

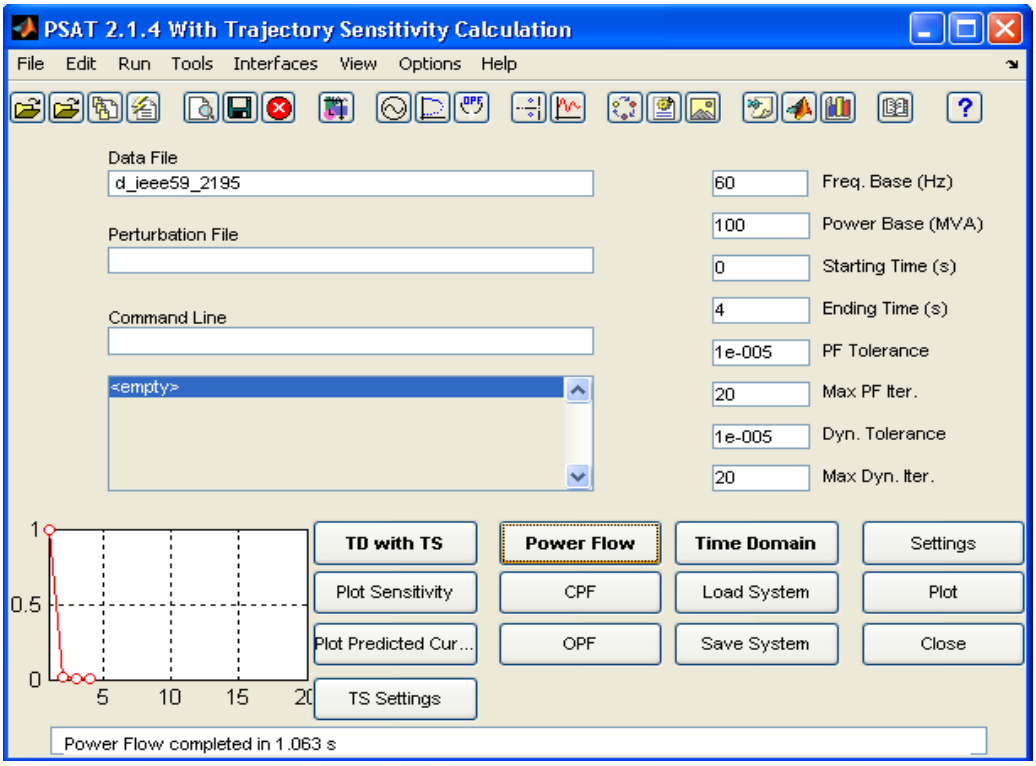

Figure 3-1 Main GUI for the PSAT trajectory sensitivity calculation routine

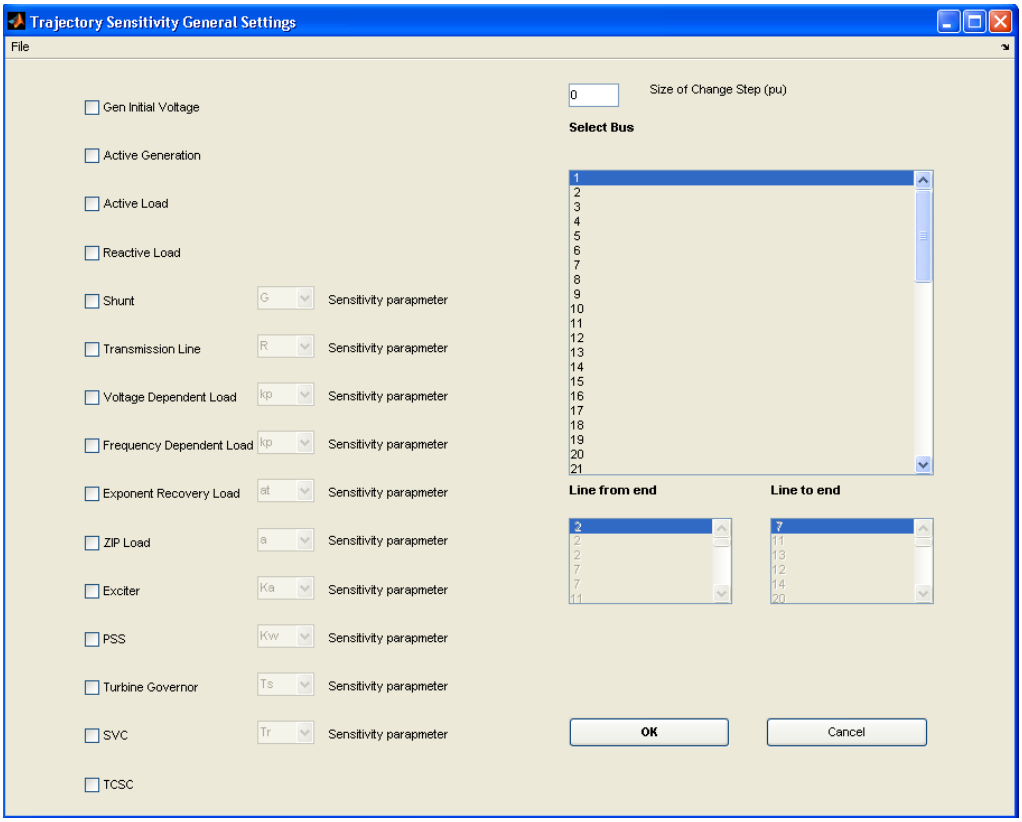

Figure 3-2 GUI for the trajectory sensitivity analysis settings

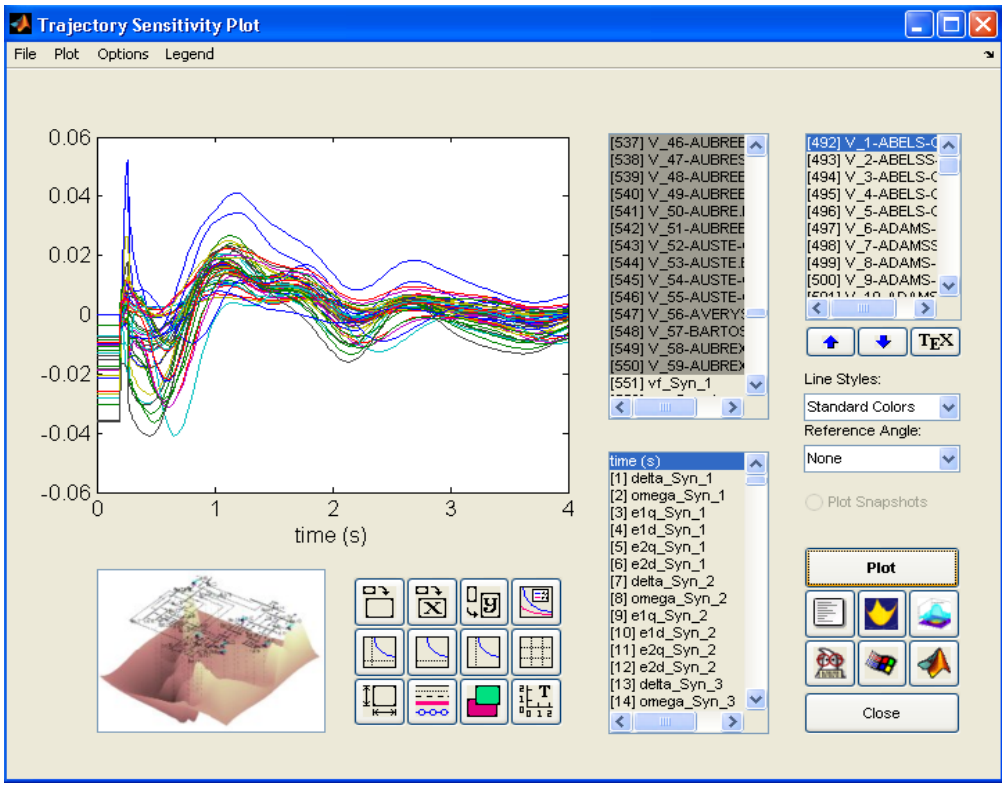

Figure 3-3 GUI for sensitivity trajectory plot

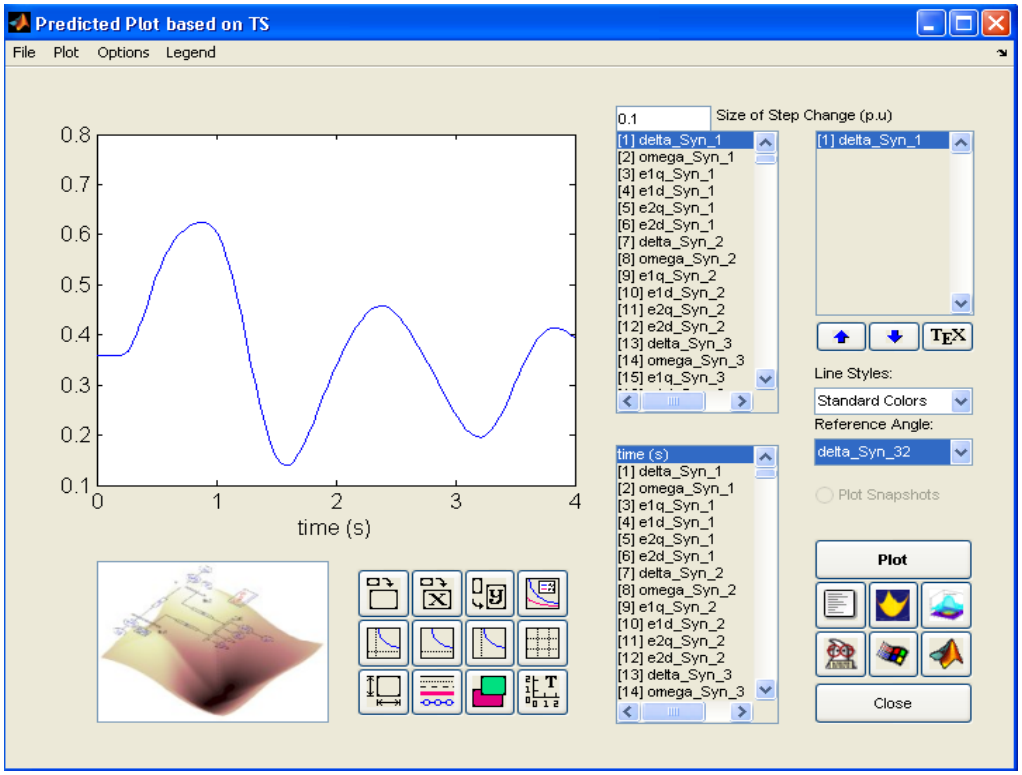

Figure 3-4 GUI for predicted trajectory plot

3.2 Cluster based parallel computing environment setup

To relieve the heavy computational loads after the introduction of extra sensitivity calculations, a parallel computing platform is set-up using the high performance computing initiative (HPCI) Saguaro cluster available at the Ira A. Fulton Schools of Engineering at Arizona State University [41]. The Saguaro cluster has 4560 processing cores available for parallel computing. This cluster is composed of 570 dual quadcore Intel Xeon EM64T nodes, each with 16 gigabytes of RAM. Each node communicates via Cisco Infiniband high speed interconnects and gigabit copper. The cluster also has a partition for running large numbers of serial jobs comprised of 185 nodes with dual Xeon MP 64 bit processors. The total memory in this cluster is 10,240 GB.

This platform uses scripts to control the work flow. Figure 3-5 depicts the architecture of this parallel computing platform.

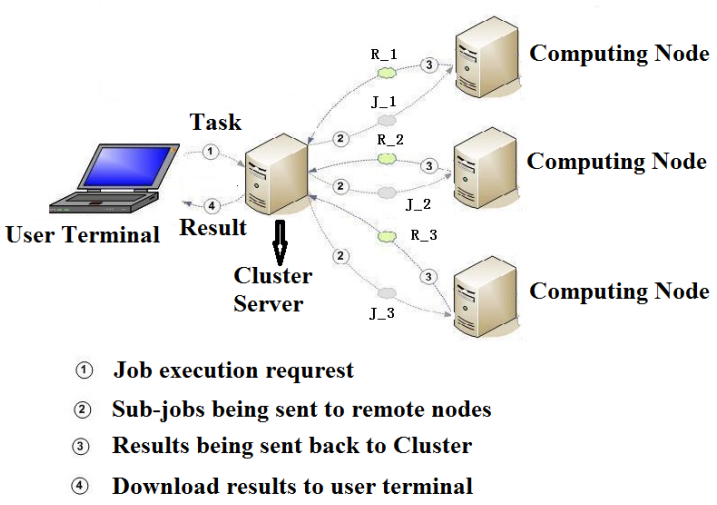

Figure 3-5 Parallel computing platform architecture

1. The user interface consists of a computing platform to write scripts to define tasks that need to be run on the cluster. The scripts are transmitted to the cluster server corresponding to ① in Figure 3-5
2. In the cluster server, the various jobs, J_1, J_2 and J_3 are automatically distributed among the available remote computing nodes. The associated data, such as the stored Jacobian matrix and dynamic states and algebraic variables at each time instant are sent to the remote nodes. This corresponds to ② in Figure 3-5
3. After the computation is completed at each remote node, the results R_1, R_2 and R_3 are transmitted back to the cluster server. This corresponds to ③ in Figure 3-5
4. The results are then transferred back to the user terminal for further analysis. This corresponds to ④ in Figure 3-5.

The computational efficiency of this platform can be assessed using the expression

$$\xi = T_S / T_P \tag{3-1}$$

where: T_S and T_P are the total processing time using the traditional sequential and parallel computation method, respectively. A larger value of ζ indicates that more improvement is achieved.

The total processing time calculation includes the following

- The base case computation time at the cluster server –*T1*
- Data storage time at the cluster server – *T2*
- Data read-in time at the remote computing node –*T3*
- Iteration solution computation time at the remote node –*T4*
- Data transferring over the network –*T5*.

The computational efficiency is evaluated using the WECC system, which is described in 6.1, for a fixed duration time domain simulation of the base case, for different numbers of trajectory sensitivity element calculations (NSC). The total processing times using the conventional sequential computation method and the proposed parallel computation approach are determined and the efficiency ζ is calculated.

Theoretically, T_S is calculated as

$$T_S = T1 + T2 + NSC \times (T3 + T4) + T5 \tag{3-2}$$

When there are sufficient computing nodes in the platform,

$$T_P = T1 + T2 + T3 + T4 + T5 \tag{3-3}$$

For the base case considered, $T1$=480s, $T2$=300s, $T3$=90s, $T4$=500s, and $T5$ varies from 5s ~ 200s depending on the network traffic. $T5$ is 0 for sequential computation mode in (3-2). The efficiency results are shown in Table 3-1.

Table 3-1 Efficiency of the parallel computing platform

NSC	T_s(s)	T_p(s)	ζ
10	6,680	935	7
100	59,780	935	64
500	295,780	968	306
1000	590,780	985	600
1500	885,780	997	888
3000	2,070,780	1060	1,954
5000	2,950,780	1124	2,625

It can be seen from Table 3-1 that compared to the traditional sequential computation method, the parallel computing platform can significantly improve the computational efficiency especially when there are a large number of sensitivity calculations.

4. Implementation of Accuracy Verification

Before demonstrating actual applications of the proposed approach, it is important to verify the accuracy of the implementation. A straightforward approach to examine the accuracy is by comparing the plot of a curve approximated using the sensitivity analysis based on (2-20) with the actual perturbed plot obtained by running the actual time simulation for the changed conditions.

4.1 Test system

A 59-bus test system is used to demonstrate the approach. A one-line diagram for this system is shown in Figure 4-1. The detailed information about the test system used here is as follows,

- 59 buses
- Total active load: 2195 MW
- 31 generators, 30 of which are modeled by a sixth-order model and the swing machine is modeled as a classical machine
- Exciters, PSSs and Turbine-governors are equipped at the machines modeled by detailed models.

The test scenario considered is as follows,

- At 0.2s, a 3-phase permanent fault occurs on line 37 -38
- After 0.1s, the fault is cleared by removing the faulted line.

This scenario is defined as the base case. In the following, two examples are given to show the accuracy of using the trajectory sensitivity method.

4.2 Sensitivity to active generation change

This test case shows the accuracy of the sensitivity approach to an active generation at a certain bus. Consider that an active generation change of 0.1 pu (Machine base, equals to 47.1 MW) at bus 39 is made to the pre-fault base case. Equation (2-20) is applied to approximate the values of all the system variables after this change along the time domain based on the base case. Then the actual perturbed plot is obtained by running the time domain simulation routine again for the changed conditions.

Figure 4-2 shows the sensitivities of all the bus voltages with respect to active generation change at bus 39.

It is found that after the fault is cleared, bus 56 is the most sensitive bus. A ranking of buses according to their sensitivities from high to low is as follow: 56>30>37>28>44>11….

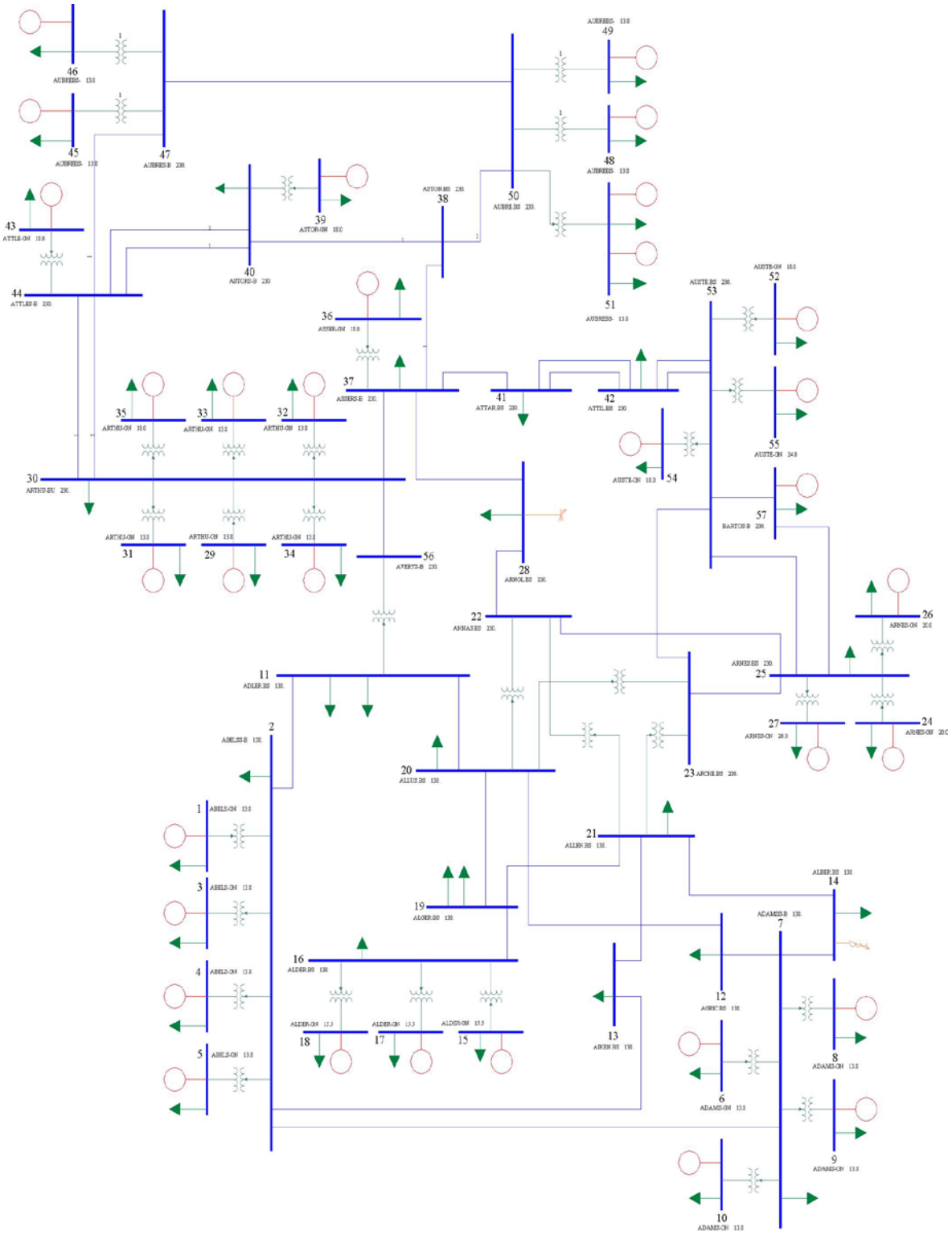

Figure 4-1 Single line diagram of the test system

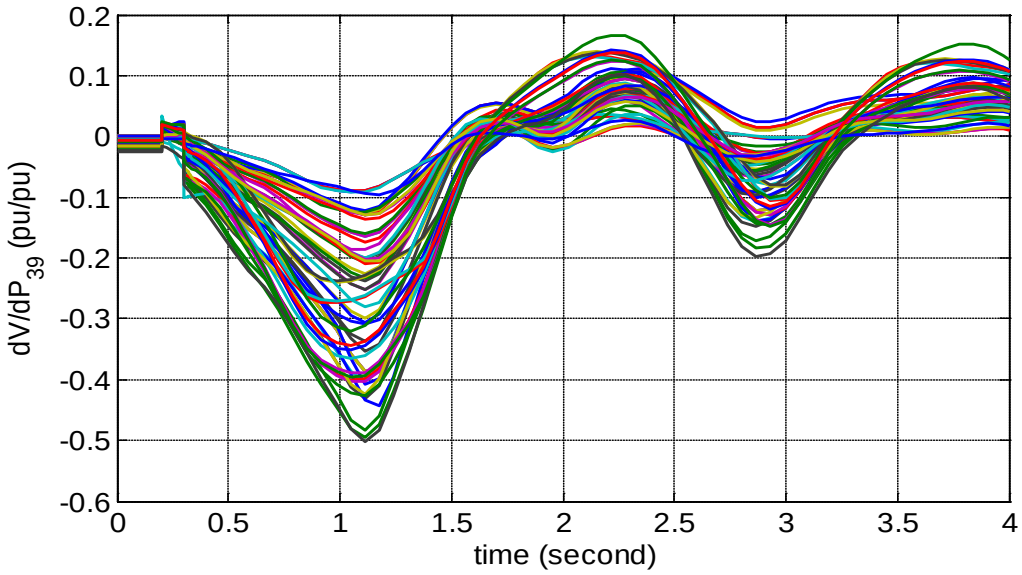

Figure 4-2 Voltage sensitivities to active generation change at bus 39

Figure 4-3 is a topological view of the buses with higher sensitivities and their topology relationship with the fault location

The sensitivity information provides great insight into deciding control strategy. This aspect will be demonstrated in the following chapters.

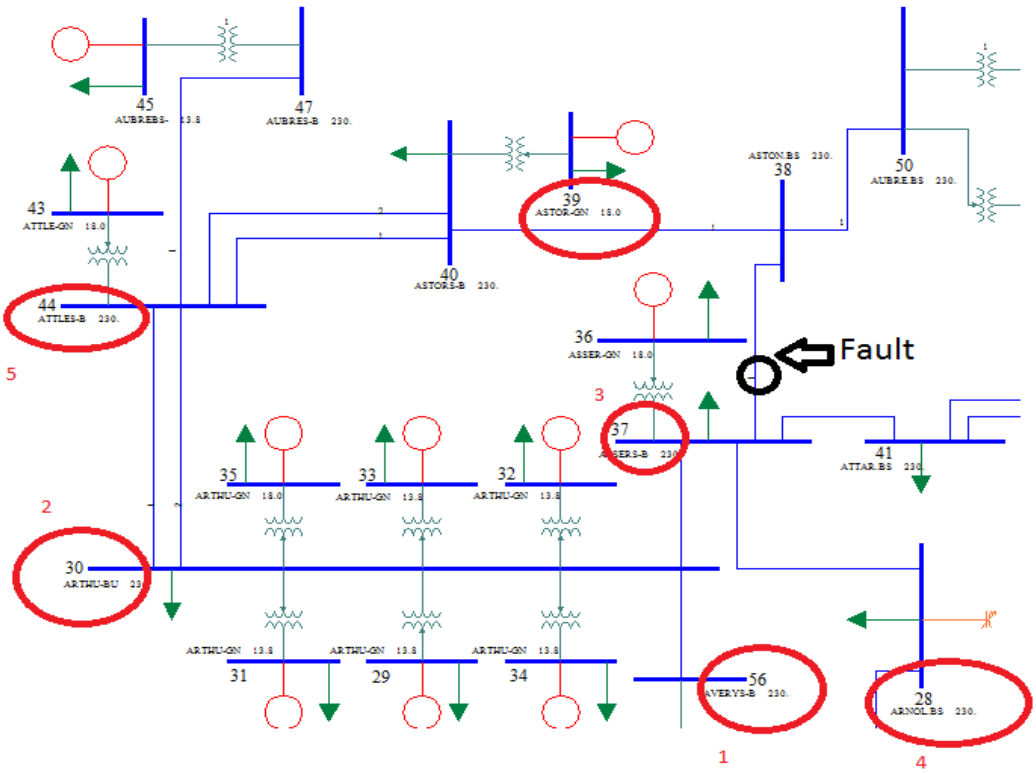

Figure 4-3 Topological view of buses with high sensitivities

Figure 4-4 - Figure 4-7 are a set of comparisons of bus voltage and machine angle plots made at different buses.

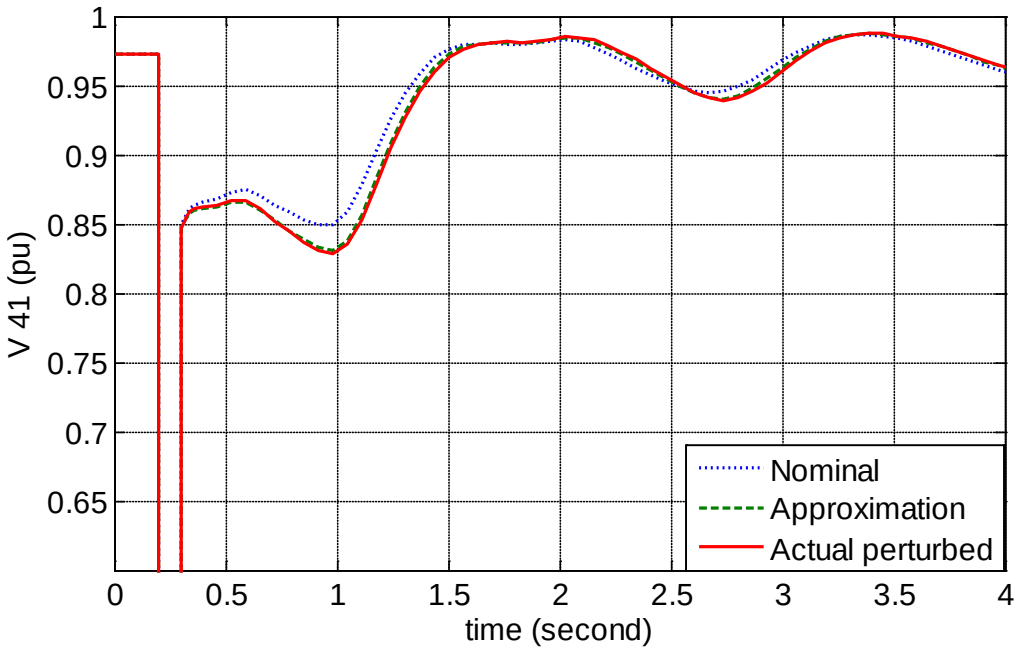

Figure 4-4 Bus 41 voltage result verification

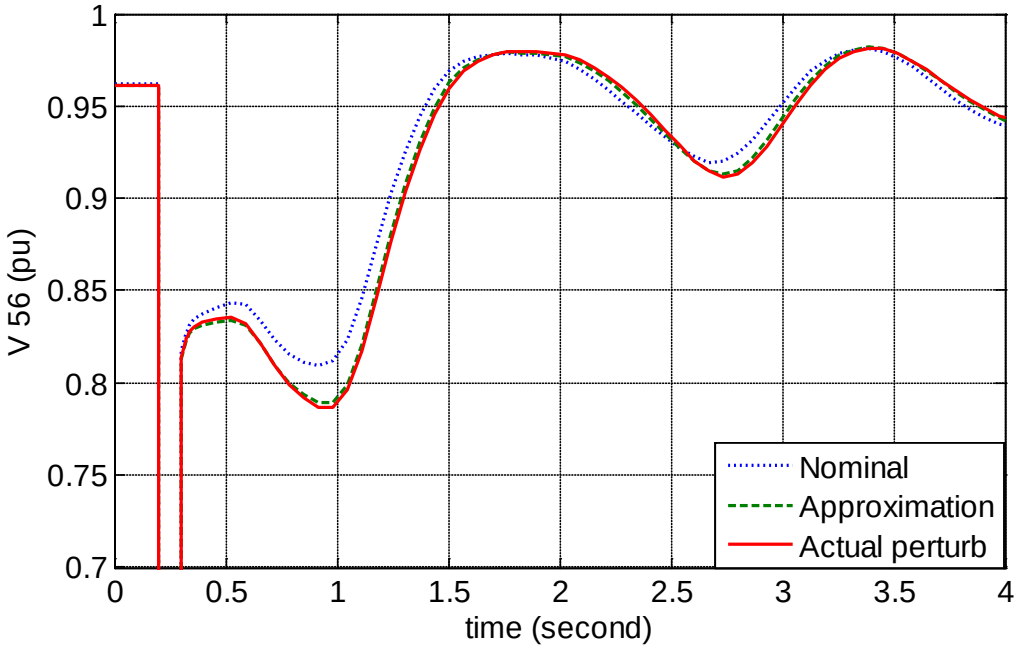

Figure 4-5 Bus 56 voltage result verification

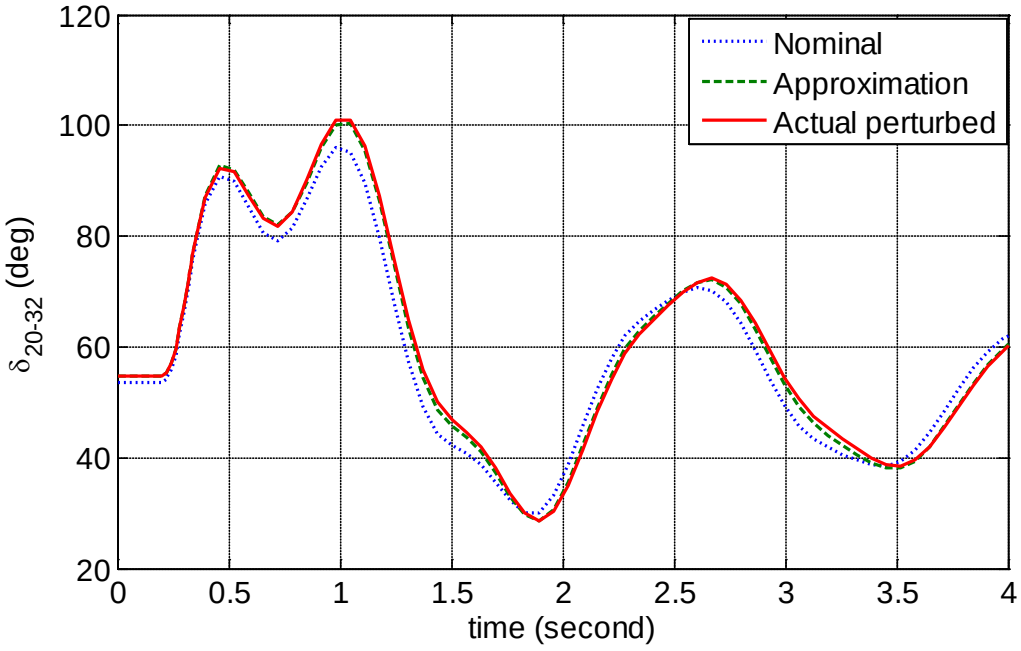

Figure 4-6 Relative rotor angle between generator 20 and generator 32

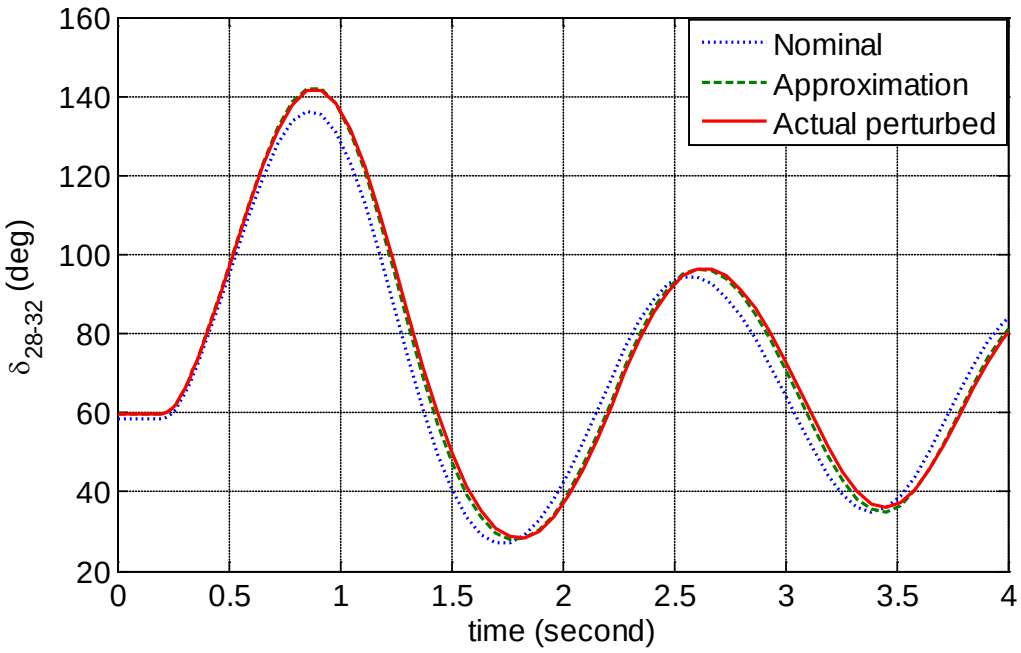

Figure 4-7 Relative rotor angle between generator 28 and generator 32

These comparisons verify the accuracy of the TS calculation. Considering that the size of the change is almost 50 MW, which is quite large, the sensitivity result is satisfactory. It is noted that the size of the parameter change will affect the accuracy of the result, and this will be discussed in detail in Chapter 5.

4.3 Sensitivity to active load change

The load is modeled by a constant power load model when the bus voltage magnitude is within a limit, and represented by a constant impedance model when the bus voltage magnitude limit is violated.

Consider a pre-fault change of active power load at bus 2. The base active power load at bus 2 is 0.75442 pu. When there is a change of -0.5 pu in active power load at this bus; (2-20) is applied to approximate the new values of all the system variables.

Figure 4-8 ~ Figure 4-10 are a set of comparisons of bus voltage and machine angle plots made at different buses.

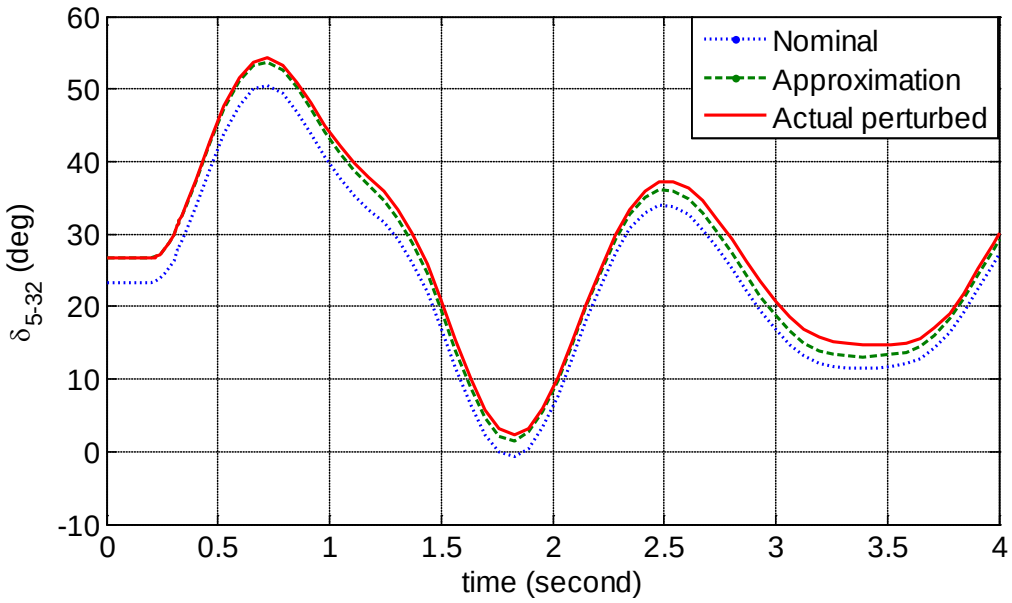

Figure 4-8 Relative rotor angle between generator 5 and generator 32

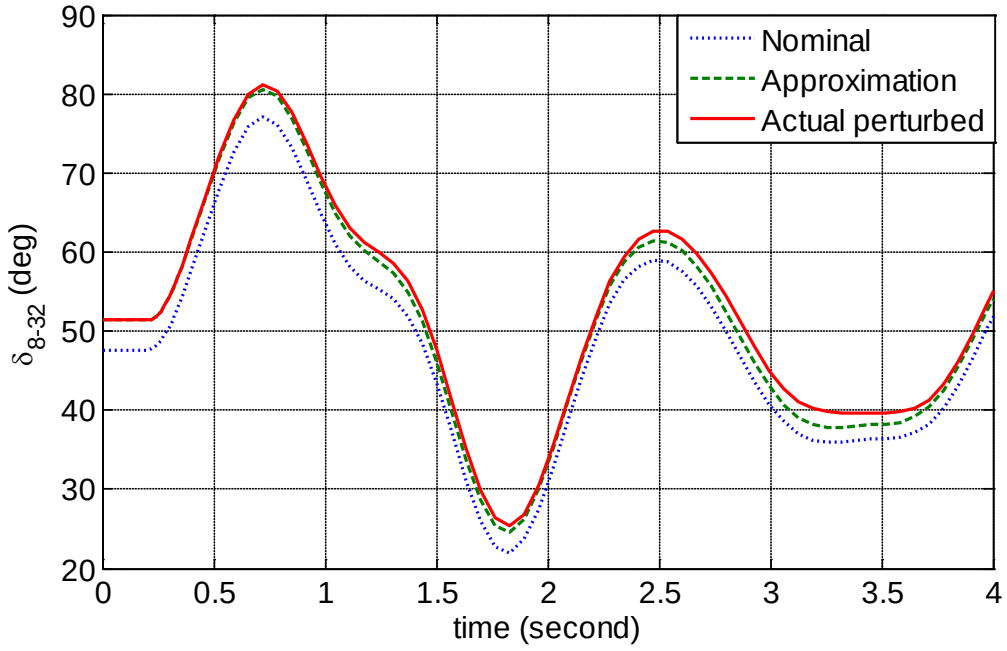

Figure 4-9 Relative rotor angle between generator 8 and generator 32

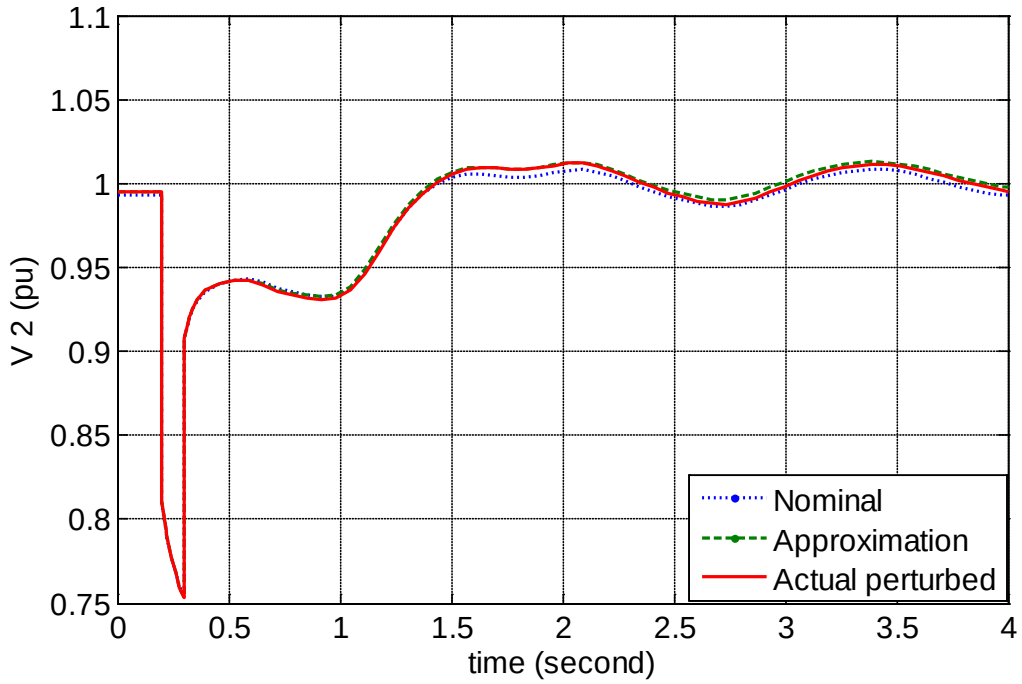

Figure 4-10 Bus 2 voltage result verification

It can be seen from the comparisons that considering the size of change, which is 0.5 pu, the result is satisfactory.

4.4 Summary

In this chapter, the accuracy of using the trajectory sensitivity method to evaluate the perturbed variables are verified by using two examples. The comparison of the approximated values with the actual perturbed values serves as a proof of the accuracy of both the theory and implementation. In the next chapter, the relation between the linear approximation accuracy and the perturbation size is explored.

5. Linear Sensitivity Approximation Assessment

The contemporary method to assess the accuracy of the linear sensitivity approximation is straightforward and evaluated numerically. The accuracy is determined by comparing the approximated trajectory plot obtained using the sensitivity analysis based on (2-20) with the actual perturbed plot obtained by re-running time simulation for the changed condition. The shortcoming of this method is that it is system dependent and operating point dependent, which means that repeated simulations for the changed condition need to be re-run to ascertain the accuracy for each of the following situations:

- When dealing with different network topologies
- For the same network topology, when operating point changes
- For the same network topology with the same operating point, when the perturbation size changes

Moreover, this method neither provides a limit on the size of the perturbation for a certain level of accuracy, nor provides the error bound under certain perturbation.

The principle of trajectory sensitivity approximation is based on the Taylor series expansion as follows,

$$x(\lambda_0 + \Delta\lambda, t) = x(\lambda_0, t) + \frac{\partial x(\lambda_0, t)}{\partial \lambda_0}\Delta\lambda + \varepsilon^{\varphi}(\lambda_0, \Delta\lambda, t) \tag{5-1}$$

where:

$x(\lambda_0, t)$: Base case trajectory

$x(\lambda_0 + \Delta\lambda, t)$: Perturbed trajectory

λ_0 : The base case value of the changing parameter

$\partial x(\lambda_0, t)/\partial\lambda_0$: The sensitivity trajectory evaluated at base case

ε^{ϕ} : The effect of higher order terms

The errors in applying the approximation are caused by neglecting the higher order term ε. It has been widely proven that for linear systems the error term vanishes, thus the approximations are exact. However, for nonlinear systems, such as power systems, the error terms will be small when the perturbation size $\Delta\lambda$ is small [1], [10].

There are however no quantitative measures to determine the size of the parameter perturbation to limit the linearization accuracy of a nonlinear system to an acceptable range. For example, in [17], the authors apply (2-20) to decide the control strategy, which yields the size of control action required in terms of $\Delta\lambda$. However, the issue of whether this $\Delta\lambda$ is small enough or not for the linearization to be valid remains unknown.

The proposed method to deal with this issue is now presented. The exact errors in linearly approximating the trajectory can be assessed by the following equation [10]:

$$E(\lambda_0, \Delta\lambda_0) = \max_{i=1}^{n} \left\{ \left\| \varepsilon_i^{\phi}(\lambda_0, \Delta\lambda_0, t) \right\|_{\infty} \Big/ \left\| x_i(\lambda_0, t) \right\|_{\infty} \right\} \tag{5-2}$$

where n is the number of system variables x.

The norm in (5-2) is defined as

$$\left\| f(t) \right\|_{\infty} = \max_{t_0 \le t \le t_f} \left| f(t) \right| \tag{5-3}$$

where $f(t)$ is a scalar function.

In (5-2), $E(\lambda_0, \Delta\lambda_0)$ is the normalized error. The numerator is the norm of the higher order terms through which errors are introduced in linearly approximating each state i. This error can only be numerically obtained by subtracting the perturbed trajectory from the approximated trajectory as

$$\varepsilon_i^{\varphi}(\lambda_0, \Delta\lambda_0, t) = x_i(\lambda_0 + \Delta\lambda_0, t) - \left[x_i(\lambda_0, t) + \partial x_i(\lambda_0, t) / \partial\lambda_0 \Delta\lambda \right] \tag{5-4}$$

This error term is then normalized in order to be compared for different states. Although the approach described above is accurate, the drawback is obvious since it requires calculation of the exact values for the changed condition. As a result, the advantage of using the trajectory sensitivity method is lost.

Rearrange (5-4)

$$\begin{aligned} \varepsilon_i^{\varphi}(\lambda_0, \Delta\lambda, t) &= x_i(\lambda_0 + \Delta\lambda, t) - x_i(\lambda_0, t) - \partial x_i(\lambda_0, t) / \partial\lambda_0 \Delta\lambda \\ &= \Delta x_i(\lambda_0, t) - \partial x_i(\lambda_0, t) / \partial\lambda_0 \Delta\lambda \end{aligned} \tag{5-5}$$

Define

$$S_{\max}(\lambda_0) = \max_{i=1}^{n} \left\{ \left\| \partial x_i(\lambda_0, t) / \partial\lambda_0 \right\|_{\infty} / \left\| x_i(\lambda_0, t) \right\|_{\infty} \right\} \tag{5-6}$$

$$A(\lambda_0, \Delta\lambda) = S_{\max} \Delta\lambda \tag{5-7}$$

$S_{max}(\lambda_0)$ is the maximum normalized sensitivity for all variables evaluated during the base case simulation.

Once a bound on A, for example $A \le a$ is determined in terms of the accuracy of the linear approximation, the limit on the perturbation size can be determined as follows,

$$\Delta\lambda \le a / S_{\max} \tag{5-8}$$

It is meaningful to examine the term $A(\lambda_0, \Delta\lambda)$ in depth. Mathematically this term denotes the normalized maximum variation of x from its base value when the parameter λ changes from λ_0 to $(\lambda_0 + \Delta\lambda)$. From the theory of linearization, it is known that the size of $\Delta\lambda$ needs to be small in order to achieve a good approximation, especially when the system has significant non-linear characteristics. Therefore, to obtain an accurate linear approximation, the value of $A(\lambda_0, \Delta\lambda)$ should be within a certain bound.

In [10] it has been shown that in a power system the linear approximation is quite accurate when the system is far away from its instability limit. However when the system is close to its instability limit the linear approximation accuracy is dependent on the size of the perturbation $\Delta\lambda$.

It has also been observed that the size of the sensitivity terms $\partial x_i(\lambda_0, t)/\partial \lambda_0$ serve as an indicator of whether the system is operating closer to its limit. When a system is operating far away from its limit $\partial x_i(\lambda_0, t)/\partial \lambda_0$ will be small. Thus, the perturbation size $\Delta\lambda$ can be relatively large for a given measure of linear approximation accuracy. However, when the system is close to its operating limit $\partial x_i(\lambda_0, t)/\partial \lambda_0$ tends to be very large thus requiring a smaller perturbation size $\Delta\lambda$ to obtain the same measure of linear approximation accuracy.

Based on this analysis, it is useful to explore the relationship between the linear approximation error $E(\lambda_0, \Delta\lambda_0)$ and the term $\partial x_i(\lambda_0, t)/\partial \lambda_0 \times \Delta\lambda$, which is denoted by A. To explore this relationship, four different systems of different sizes are used as test systems. These four systems are

1. The two-area-four-machine system [42]
2. A 50 generator system [43]
3. A 59 generator system
4. The WECC system

The exact approximation errors are obtained using (5-2). To achieve a more general conclusion, these test cases take into account different operating conditions in terms of different loading levels and faults with different fault clearing times. A large number of cases have been analyzed. For the sake of brevity ten sample cases are presented. They are listed in Table 5-1.

It is observed that when the error $E(\lambda_0, \Delta\lambda_0) \leq 1$, good approximations are achieved, reference [10] also provides this observation. Therefore, suppose an accuracy requirement is pre-determined as $E(\lambda_0, \Delta\lambda_0) \leq 1$, then from Figure 5-1 it can be seen that when $E(\lambda_0, \Delta\lambda_0) = 1$, $A \leq 1.17$. Therefore, if the chosen value of A is limited to 1.17, then according to (5-8), the maximum perturbation size $\Delta\lambda$ can be determined. Though the $\Delta\lambda$ determined by this method is relatively conservative, it can ascertain the approximation accuracy within an acceptable bound. Therefore, it serves as a general application guide to evaluate the accuracy of the linear approximation.

Table 5-1 Descriptions of test cases

Case	Test System	Total Active load (MW)	Fault Clearing Time (second)
1	1	2,940	0.18
2	1	2,940	0.16
3	2	361,630	0.08
4	2	370,000	0.06
5	3	2,150	0.12
6	3	2,150	0.10
7	3	2,850	0.10
8	4	166,145	0.08
9	4	166,145	0.06
10	4	165,129	0.10

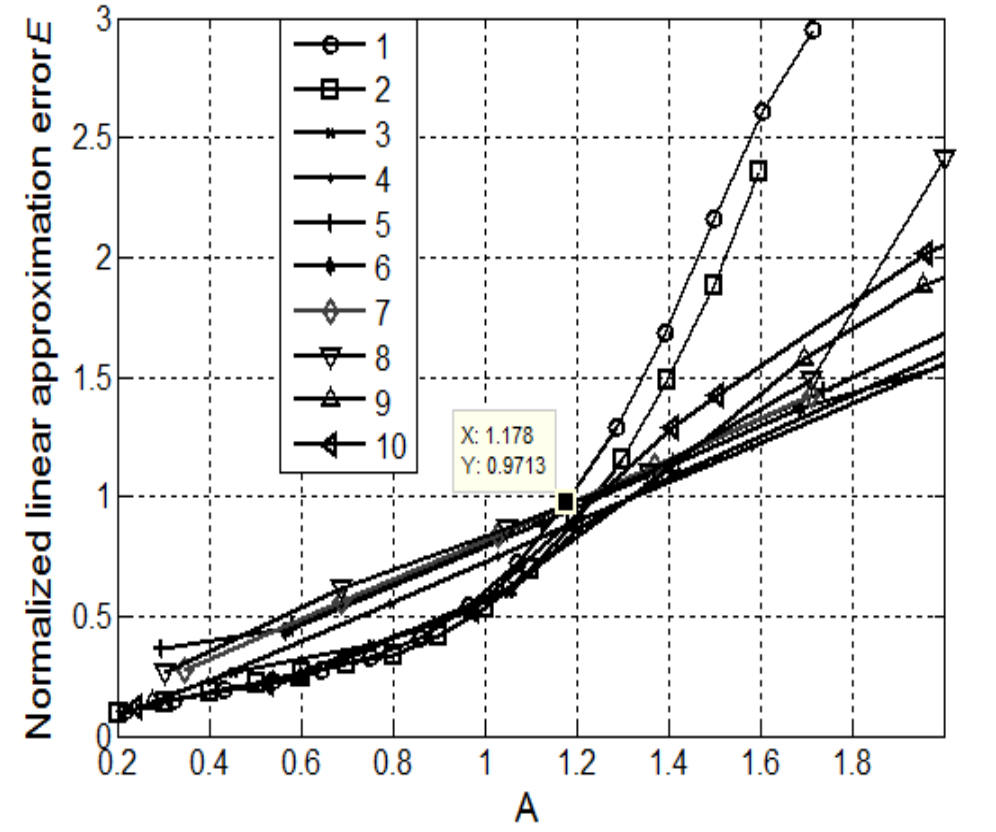

Figure 5-1 Relationship between exact linear approximation error *E* and *A*

6. Application to Angle Stability Problem

As an application to demonstrate the efficacy of the proposed cluster based implementation of the trajectory sensitivity method, a preventive control action in terms of generation rescheduling to maintain the transient angle stability is developed.

6.1 Test system – the WECC system

The 2009 summer peak load case of the WECC system is used in the report to test the performance of the proposed method. The network has 21 areas and 366 zones. The system characteristics are shown in Table 6-1.

All the generators are equipped with a turbine governor, exciter and PSS. The total active generation is 165,129 MW.

Table 6-1 System characteristics of the WECC system

Buses	Lines	Transformers	Generators	Loads
15,437	13,178	5,727	2,059	6,695

6.2 Main procedure

This method, compared to existing trajectory sensitivity based method [17], has the following enhancements:

- It takes advantage of parallel computation techniques to improve the computational efficiency
- Sensitivity information is not evaluated for every contingency. The trajectory sensitivity computation is activated only for unstable contingencies
- Using the proposed error-perturbation evaluation approach, the calculated amount of rescheduled generation ΔP is ascertained to be within a certain prescribed error bound
- The test system used in this analysis is a large realistic representation of the WECC system in comparison to the relatively small system used in [17].

The steps in applying this procedure are depicted in Figure 6-1. The details associated with these steps include:

1. Select a prescribed set of potential contingencies
2. Perform power flow calculation and obtain the steady state operating point
3. Apply contingency k from the prescribed set of potential contingencies
4. Run time domain simulation for this contingency, and monitor the system stability
5. Store the Jacobian matrix, dynamic states x and algebraic variables y at each time instant for use in future trajectory sensitivity calculation
6. If the system is unstable, identify a candidate set of parameters that can be changed as a part of preventive control to alter the stability boundary

7. Use the stored Jacobian matrix, dynamic states and algebraic variables to perform trajectory sensitivity calculations in parallel for the candidate set of parameters to be utilized in preventive control
8. Use the trajectory sensitivity information to identify the most sensitive generator to reduce generation to stabilize the system and the least sensitive generator to compensate for the reduced generation. Calculate the generation shift ΔP
9. Use the approximation accuracy evaluation method introduced in Chapter 5 to ascertain the linear approximation error for this ΔP is within bounds
10. If the error bound is not satisfied the preventive control objective will not be met. Select the largest possible ΔP that is within the required error bound limit as the rescheduled generation, and go to step 1 to recalculate the new value of the shifted generation.

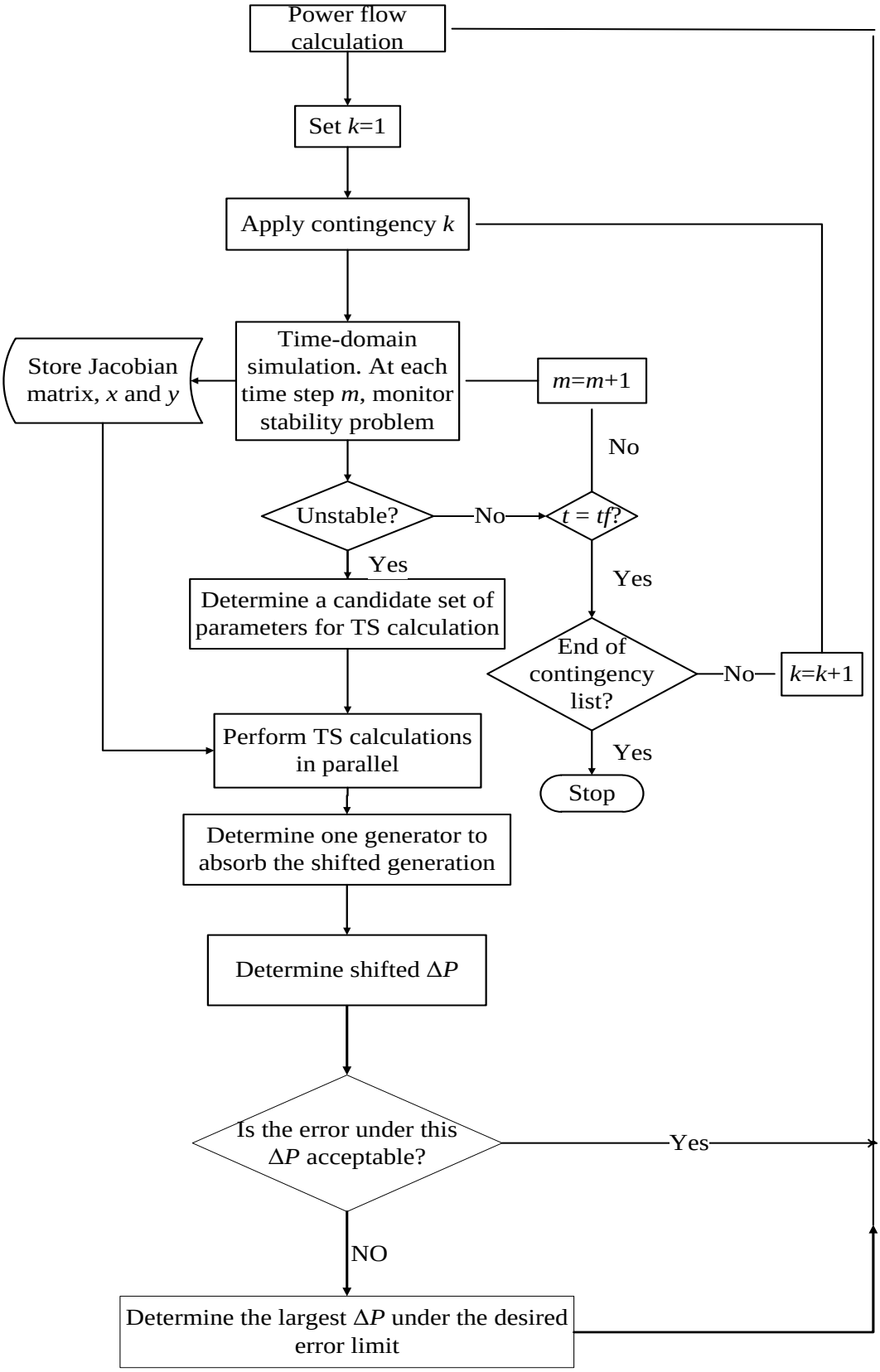

Figure 6-1 Flow chart for trajectory sensitivity based generation rescheduling method

In step 6, since only some of the parameters are controllable, for example, generation at certain areas or zones, exciter parameters for some generators or values of certain loads, a proper candidate set of these potential parameters should be selected before the trajectory sensitivity calculations are performed.

In step 7, if the system is unstable for a given contingency, the trajectory sensitivity calculation is activated. The parallel computing approach proposed in 3.2 is used to perform this calculation. At each computing node, the Jacobian matrix and the dynamic states and algebraic variables are retrieved at each time instant, and the sensitivity equations (2-3) and (2-4) are solved.

The optimal generation rescheduling strategy is determined utilizing the trajectory sensitivity information computed. The transient angle instability problem is considered as an example here.

Based on the standard option in several commercial time domain simulation packages, (e.g. TSAT developed by Powertech Labs) relative rotor angles are used to detect system stability/instability. At each time step, relative rotor angles are monitored during time domain simulation. When the maximum relative rotor angle difference between any two generators $\delta_{ij} = \delta_i - \delta_j$ grows beyond a set limit of 180°, the system is judged to be unstable. Here, generators i and j are referred to as the most and the least advanced generators, respectively.

The sensitivities of the relative angle δ_{ij} with respect to each parameter in the set of candidate parameters are calculated and used to determine the optimal preventive control strategy. Suppose $d\delta_{ij}/dP_i$ has the highest sensitivity and $d\delta_{ij}/dP_k$ has the lowest sensitivity, then a specified amount of generation ΔP is rescheduled from generator i to generator k in the pre-disturbance power flow to stabilize the system. The following expressions are used to determine ΔP.

From (2-20), at a given time instant $t = t_0$

$$\Delta X(t_0) = X^{New}(t_0) - X^{Base}(t_0) = \sum_{i=1}^{n} \frac{\partial X^{Base}}{\partial \lambda_i}(t_0)\Delta\lambda_i \tag{6-1}$$

where n is the number of parameters in the candidate set of controllable parameters.

Accordingly

$$\Delta\delta_{ij}(t_0) = \delta_{ij}^{New}(t_0) - \delta_{ij}^{Base}(t_0) = \frac{\partial \delta_{ij}^{Base}}{\partial P_i}(t_0)(-\Delta P) + \frac{\partial \delta_{ij}^{Base}}{\partial P_k}(t_0)\Delta P \tag{6-2}$$

where δ_{ij}^{Base} and δ_{ij}^{New} are the relative angles between generator i and j before and after ΔP is shifted from generator i to generator k, respectively.

The solution to (6-2) yields a value for ΔP. This value of ΔP should be compared with the perturbation size limit ΔP_{max} for this operating condition, which is obtained from (5-8)

$$\Delta P = \begin{cases} \Delta P & |\Delta P| \le \Delta P_{\max} \\ \Delta P_{\max} & |\Delta P| > \Delta P_{\max} \end{cases} \tag{6-3}$$

The generation at generator *i* and *k* after the shifting generation are as follows,

$$P_i^{New} = P_i - \Delta P \tag{6-4}$$

$$P_k^{New} = P_k + \Delta P \tag{6-5}$$

6.3 **Numerical results**

The WECC system is used here to illustrate this method. A 3-phase short circuit is placed on bus 10011, which is a 230 kV bus in area 1. The fault is cleared at 5 cycles by opening a transmission line between buses 10011 - 10368. The system is unstable under this fault clearing time as shown in Figure 6-2. This is referred to as the base case.

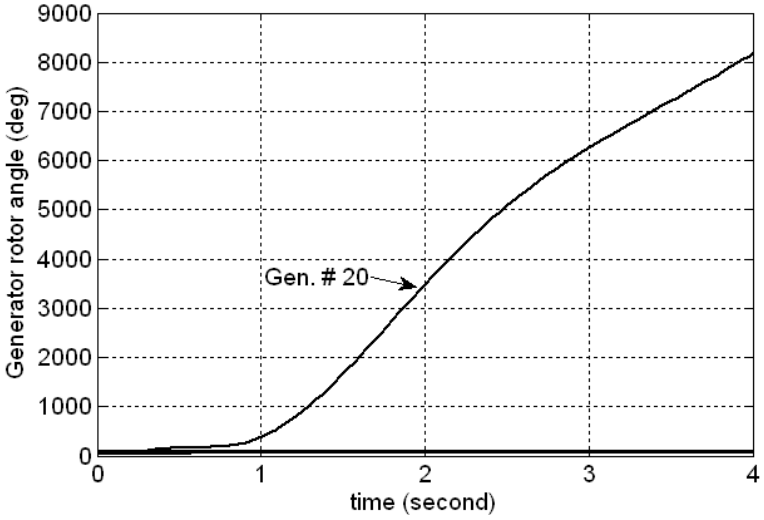

Figure 6-2 Generator angle plots for the base case

It is found that that generator #20 and generator #320 are the most and the least advanced generators, respectively. The relative angle between these two generators reaches the threshold value of instability of 180̊ at time t = 0.5675 s. Generator #20 is in Area 1 but generator #320 is in another area.

Assume that all the generators in area 1 are available to reschedule generation. There are 227 generators in area 1, so 227 cluster computing jobs to evaluate the sensitivities of the maximum rotor angle difference at instability, $\delta_{20\text{-}320}$ with respect to each of these 227 generations $d\delta_{20\text{-}320}/dP_i$ (i=1,2,…,227) are created and run in parallel using the cluster described in 3.2.

If traditional serial computing technique is used, the total processing time is more than 134,710 s. With the proposed parallel computing cluster, this time is reduced to be less than 950 s.

A sample of the ranking of these sensitivities at the time instant t = 0.5675 s in descending order are listed in Table 6-2. From the table it can be seen that generation at generator #20 has the highest sensitivity, which is about 356.132 (deg/pu) at time 0.5675 s. The generator #68 has the lowest sensitivity, which is -0.5652 (deg/pu). Therefore, the

generation rescheduling strategy is to shift a certain amount of generation from generator #20 to generator #68 in the pre-fault power flow.

Table 6-2 Ranking of sensitivities (t = 0.5675 s)

Rank	Gen. No.	Bus No.	Sensitivity (deg/pu)
1	20	12058	356. 132
2	1	10246	8.181661
3	2	10261	7.76204
4	3	10262	6.5490
…	…	…	…
8	16	11116	1.00072
…	…	…	…
226	69	14964	-0.5475
227	68	14963	-0.5652

Here, the generation rescheduling objective is to maintain stability by reducing $\delta_{20\text{-}320}$ to a desired value less than 180° when the fault clearing time is 5 cycles and minimize the amount of control applied.

In the following, two cases with different values of targeted control of relative rotor angles are shown to illustrate the importance of validating the perturbation size.

- Case 1--- Targeted maximum rotor angle difference is 160°

Suppose the targeted maximum rotor angle difference of $\delta_{20\text{-}320}$ after rescheduling is 160° at time 0.5675 s. From (6-2)

$$160° - 180° = 356.132(-\Delta P) + (-0.5652)\Delta P \qquad (6\text{-}6)$$

Solution to (6-6) yields ΔP = 0.056 pu = 5.6 MW. Therefore the amount of generation that needs to be shifted from generator #20 to generator #68 in the pre-fault power flow is 5.6 MW.

From (5-6), the maximum normalized sensitivity can be calculated as S_{max} = 18.54 deg/pu. From Section V, the chosen value of A is limited to 1.1, then from (5-8), the maximum perturbation size is calculated to be ΔP_{max} = 0.0593 pu, so in this case the ΔP calculated from (6-6) is less than ΔP_{max}, which indicates that this chosen value of ΔP will not result in the linear approximation exceeding its desired bounds. The maximum relative rotor angle plot for the same disturbance after rescheduling is shown in Figure 6-3. From Figure 6-3 it can be seen that generator #20 is stabilized and $\delta_{20\text{-}320}$ at 0.5675 s is 164.1°, which is very close to the evaluated value considering the high sensitivity resulting from the system operating at its stability limit.

It should be noted that after rescheduling the maximum of $\delta_{20\text{-}320}$ does not necessarily occur at the same time instant as in the base case [9] - [10].

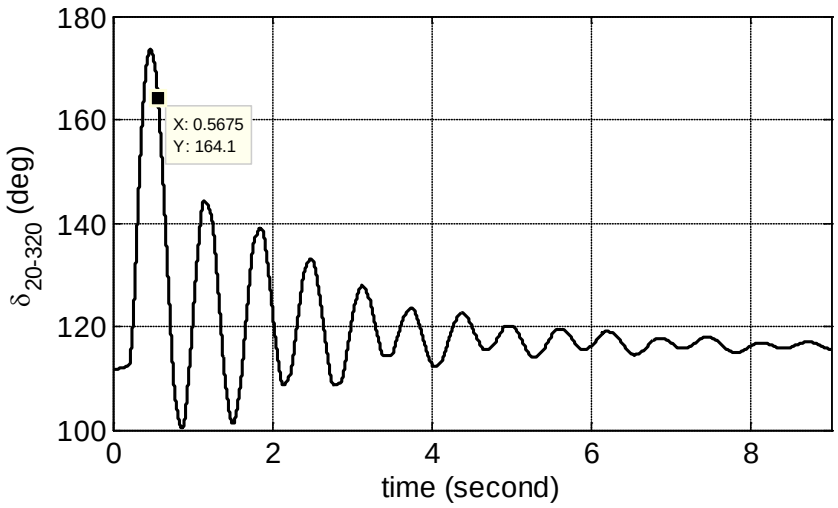

Figure 6-3 Relative angle plot between generator #20 and generator #320 after generation rescheduling of ΔP = 0.056 pu

- Case 2--- Targeted maximum rotor angle difference is 140˚

For this case, suppose the targeted maximum rotor angle difference of $\delta_{20\text{-}320}$ after rescheduling is 140˚. Using the same procedure as in Case 1, the ΔP is calculated to be 0.112 pu.

From case 1 it is known that ΔP_{max} = 0.0593 pu, so ΔP here is much larger than ΔP_{max}, which indicates that the error bounds on the linear approximation will be exceeded. If this ΔP is applied, the angle of $\delta_{20\text{-}320}$ after rescheduling will not be close to the target which is 140˚ for this case. This can be observed in Figure 6-4 where $\delta_{20\text{-}320}$ at 0.5675 s after shifting 11.2 MW from generator #20 to generator #68 and applying the same disturbance is 156.4˚, which is significantly different from the target of 140˚.

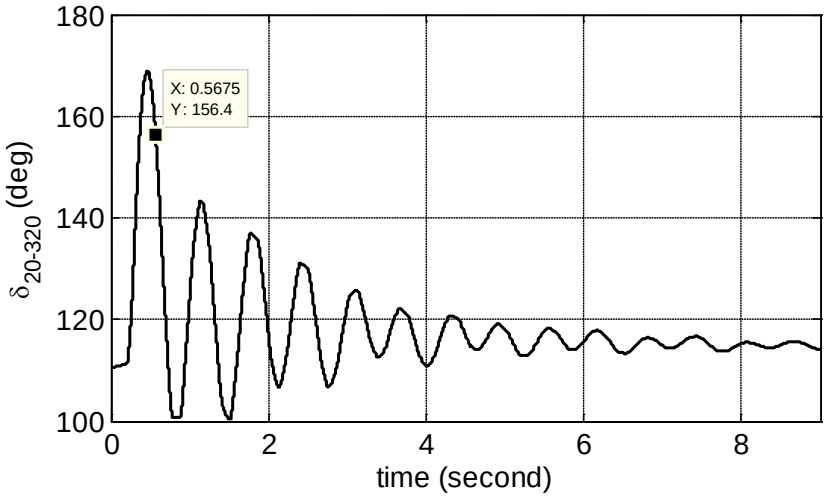

Figure 6-4 Relative angle plot between generator #20 and generator #320 after generation rescheduling of ΔP = 0.112 pu

Hence, the value of ΔP in this case is too large and the linear approximation exceeds the chosen error bounds.

6.4 Summary

The following are some conclusions and features of the test case demonstrated:

1. The applicability of the approach to a large realistic network is demonstrated. This test case applies the trajectory sensitivity analysis method to the WECC system, and the results demonstrate the efficacy of the approach.
2. The cluster architecture of the proposed high performance computing platform together with the formulation of solving different sets of sensitivity equations in parallel greatly enhance the computational efficiency.
3. The constraint of linear approximation accuracy on perturbation size is demonstrated. The test case shows that when linear approximation is applied to estimate the operation curve for the changed condition, this constraint needs to be satisfied to achieve an acceptable approximation accuracy.
4. A systematic preventive control analysis method in terms of generation rescheduling to maintain the transient angle stability is developed and demonstrated. The proposed method, compared to the existing trajectory sensitivity based generation rescheduling approaches, features the following:
    - A more efficient analysis approach is developed. Sensitivity information is not evaluated for every contingency. The sensitivity trajectory computing routine is activated only when the system is unstable for a given contingency, which is more efficient.
    - The computational efficiency is greatly improved with the proposed parallel computing platform.
    - The calculated amount of rescheduled generation ΔP is validated by the proposed error-perturbation evaluation approach. This will ascertain that the linear approximation error is within certain prescribed error bound.
    - The test system used in this analysis is a large realistic representation of the WECC system in comparison to the relatively small system used in other applications of the trajectory sensitivity approach.

7. Application to Voltage Stability Problem Considering Load Uncertainties

Voltage stability problems have become a major concern during the past few decades. It is reported that many major black-outs throughout the world are associated with this phenomenon. It is generally recognized that the voltage instability problem is closely related to the increased use of various types of induction motor loads, and electronically controlled loads and HVDC systems.

The dynamic models of a power system have significant influence on the system response after contingencies. Different types of models for system components such as loads, synchronous machines and their controllers could yield significantly different results. Therefore this suggests different control strategies to maintain system voltage stability. References [16], [44] – [49] study different ways of modeling loads, including ZIP loads, induction loads and a composite loads which include certain percent of ZIP loads, large motor loads, small motor loads and trip motor loads. The system responses under these different load modeling methods vary significantly. It has been reported that different load structures may produce contradictory results in dynamic simulation [44] – [45].

The power system loads are uncertain to a certain extent. Based on measurement and model validation techniques, a load might be modeled accurately at a certain time instant. However, load composition varies in time depending on the demand, so it is very likely that a model developed at one time instant might not be accurate at any other time instant.

Therefore, it is meaningful to account for these uncertainties when analyzing the system dynamic performance and making control strategy decision. Most widely used methods mainly rely on the Monte Carlo type simulation to estimate the probability distribution of the outputs. These methods require repeated simulation for each possible set of values of load models. Therefore, these approaches are computationally intensive.

The trajectory sensitivity analysis can effectively complement time domain simulation. It can provide valuable insights in evaluating limits and account for changes in operating conditions and system parameters. Therefore it provides an alternative approach to analyze load uncertainties in power system voltage stability studies. The possible system operation boundary can be obtained by linear approximation with load parameter sensitivity information evaluated along a base case simulation in the time horizon. According to this operation boundary, the amount of control needed to maintain system voltage stability would not be fixed. Rather it would be defined within a certain range.

Various research efforts have been conducted to study the nature of the voltage instability problem and general solutions have been realized. The most widely used approaches to mitigate voltage instability include:

- Active generation rescheduling
- Generator secondary voltage control
- Shunt VAR compensation
- Load shedding

The first three control strategies fall under the category of preventive control and the last one falls under the category of corrective control. In this part of the report, a method that adopts the trajectory sensitivity approach to take into account the load modeling uncertainty is proposed. Load parameters which have significant influence on the system response will be considered to vary within a certain bounded range instead of a fixed input value. As a result the corresponding system response will operate within a certain bound. Based on this bound of variation, the resulting amounts of preventive and corrective control will also vary within a certain bound. This consideration provides more practical guidelines for both planning and operational decision making. Principles and steps of the proposed analytical approach to develop various optimal controls for the WECC system are presented in the following.

7.1 Load modeling

Various induction motor models are discussed in detail in the literature. In [46], a hybrid model accounting for various induction motor loads and static loads is presented. An update about the application of composite load modeling in the WECC system is reported in [48]. In [49], the authors develop a phasor-based composite model.

In this research effort, a composite load model is developed to capture the effect of various types of induction motor loads as shown in Figure 7-1. Each load is represented as a combination of induction motors and static loads. In Figure 7-1,

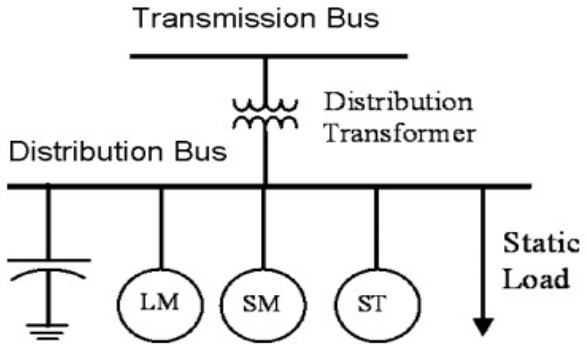

Figure 7-1 Composite load model

- Large motor (LM) – Motor with higher inertia
- Small motor (SM) – Motor with lower inertia
- Trip motor (ST) – Motor with low inertia and will be tripped under lower voltage conditions within certain time constant

The trip motor represents a modern air conditioner in the system equipped with a fast tripping electromagnetic contactor. The trip motor used here is characterized by two parameters

- V_t – Voltage threshold for tripping
- T_v – Voltage trip pick up time

Detailed explanation about this composite model can be found in [16], [46], [47] and [49].For each of the induction motor models, there are 9 parameters that are subject to change and affect the system operation boundary. They are

$$[R_s, X_s, X_m, R_r, X_r, H, T, B, K_{pm}]$$

Besides, there are 4 parameters in the static load models which will affect the system response. They are listed as follows,

$$[P_z, P_p, Q_z, Q_p]$$

where, R_s and X_s are the stator resistance and reactance, respectively. R_r and X_r are the rotor resistance and reactance, respectively. X_m is magnetizing reactance. H is rotor inertia constant. T is torque coefficient related to the square of rotor speed. B is torque coefficient related to rotor speed. P_z and P_p are the proportional coefficient of the constant impedance and constant active power in the static active load, respectively. Q_z and Q_p are the proportional coefficient of the constant impedance and constant reactive power in the static reactive load, respectively. K_{pm} is the initial active power proportion of the motor loads in the composite load.

In all, there are 31 uncertain parameters in this composite load model. If all these parameter uncertainties are taken into account, it will be very computationally intensive to determine sensitivities and provide a meaningful result. Therefore it is important to determine the parameters that are most sensitive to system dynamic responses to minimize the potential set of uncertain parameters. It is generally recognized that K_{pm} and inertia H are the parameters that have significant effects on the system performance. Thus these two parameters are taken into account for the boundary uncertainty study later in this chapter.

For the study cases conducted in this report, the load composition in the WECC system is shown in Table 7-1.

Table 7-1 The load composition of the WECC system

Induction motor load (%)			ZIP load (%)		
70			30		
LM	SM	ST	P_Z	P_I	P_P
10	60	30	33.3	33.3	33.3

The percentage of active motor load of the total active bus load K_{pm} is 70%, and the percentages of large motor, small motor and trip motor at each load bus are 10%, 60% and 30% of the total motor load, respectively. The remaining 30% of the bus load is modeled as ZIP loads with load divided equally among the three components.

In the case of trip motors, the motor will stall, overload and then trip when a motor undergoes a low voltage condition. The typical time for this process is about 15 seconds. However, since we are dealing with fast voltage collapse only, the time frame of interest

is the first few cycles or seconds after the fault. Therefore, V_t = 0.55pu and T_v = 10ms are used for the study cases.

7.2 Determination of operational bound considering load uncertainty

Presently, load is often represented by an aggregate composite model. However, load composition is stochastic, thus a single fixed set of parameters cannot capture the potential expected load variations. Therefore, to better capture the full range of potential system behavior, load should be modeled by a set of possible parameters.

A new method based on the trajectory sensitivity approach is proposed in this research effort to solve this problem. This method can effectively account for the load uncertainty without a large amount of repeated time domain simulations. Sensitivities of system variables to various uncertain load parameters are calculated along the base case time domain simulation. Then with this sensitivity information, the system operational boundary can be estimated by applying the linear approximation (2-20). Details of this method are as follows,

1) Pre-determine a proper base case
2) Pre-select a suitable set of load parameters whose uncertainty is taken into account

It is important to select a proper set of load buses whose modeling parameters are most likely to change and affect the system operational performance. The proposed method for this selection is by calculating the sensitivities of the load buses with the worst voltage magnitude with respect to the reactive load at the load buses. Then for those buses with higher voltage magnitude sensitivities, load model parameters, K_{pm} and H, are selected in the candidate set.

3) Perform the base case time domain simulation
4) Calculate various load parameter sensitivities

Sensitivities of all the load parameters defined in step 2 are calculated in parallel using the parallel computing cluster introduced in Chapter 3.2

5) Estimate the system operational boundary by linear approximation.

From (2-20), the operational bound can be estimated by

$$V_w^{est}(t) = V_w^{base}(t) + \sum_{i=1}^{m} \frac{\partial V_w^{base}}{\partial \lambda_i}(t)\Delta\lambda_i \tag{7-1}$$

where V_w is the voltage magnitude at the bus with the worst voltage performance. $V_w^{est}(t)$ is the estimated value of V_w; $V_w^{base}(t)$ is the value of V_w at base case; $\partial V^{base}{}_w/\partial\lambda_i(t)$ is the sensitivity of V_w with respect to load parameter λ_i evaluated at the base case; $\Delta\lambda_i$ is the perturbation size of load parameter λ_i; m is the number of load uncertain parameters.

Suppose $\Delta\lambda_i$ is within a certain pre-determined range, then when different values of $\Delta\lambda_i$ are applied to (7-1), a bound on V_w can be accordingly obtained. The advantage of this method is that it does not require a large amount of repeated time domain simulations for cases with different possible load parameters. Just one base case simulation is conducted, and then all the sensitivity calculations are performed in parallel using the computing cluster introduced in Chapter 3.2.

7.3 Preventive control scheme for voltage instability considering load uncertainty

When load parameter uncertainty is considered, the system's dynamic responses will lie within a certain bound instead of being characterized by fixed values. Accordingly, the control strategy based on this consideration should be within a certain range rather than being a fixed number. Presently, commonly used methods require determining the control strategy for each possible system operation condition within the boundary. This approach is accurate but inefficient in terms of computing burden and time.

A method based on trajectory sensitivity approach is developed for this purpose. From (2-20), the following equation can be obtained

$$\Delta\lambda = \frac{X^{New}(t) - X^{Base}(t)}{\partial X^{Base}(t)/\partial\lambda} \tag{7-2}$$

Based on different values of X^{base} and for the same control objective X^{New}, different control actions $\Delta\lambda$ can be determined. Therefore, a control range can be determined once the system operational bound is evaluated as detailed in Chapter 7.2. In equation (7-2), the sensitivity term $\partial X^{bas}(t)/\partial\lambda$ is evaluated at the base case.

Here, two different types of preventive control actions are considered: a) active generation rescheduling; b) shunt capacitance compensation.

Details of the proposed method are as follows,

1) Pre-select a suitable set of control parameters for sensitivity calculation

For each control action, a candidate set of parameters that can be changed as a part of the control action to alter the stability boundary needs to be determined. Approaches to determine these sets are varied, and can be decided by operational experience, or by analysis of network topology.

2) Calculate sensitivities of the various control actions. The calculations are performed using the parallel computing cluster introduced in Chapter 3.2
3) Calculate the linear approximation accuracy constrained maximum amount of control action. To ascertain that the size of the control action calculated by (7-2) is within acceptable limits, the linear approximation accuracy constrained maximum amount of control needs to be calculated a priori as detailed in Chapter 5
4) Solve the mathematical optimization problem to obtain the optimal control strategy

Here, active power rescheduling is implemented by adjusting generation active output power P_g and the shunt capacitance compensation is modeled by adjusting the shunt capacitor B_{sh} at certain buses.

To obtain the optimal control effort $\Delta\lambda$ that is needed to enhance the voltage magnitude of bus w from V_w^{base} to an arbitrary value V_w^{new} , the following optimization model can be formulated:

$$\min \quad \Delta f = \sum_{i=1}^{m} \Delta\lambda_i \tag{7-3}$$

s.t.

$$\begin{cases} V_w^{base}(t_0) + \sum_{i=1}^{m} S_i(t_0)\Delta\lambda_i \geq V_w^{new} \\ \Delta\lambda_{\text{imin}} \leq \Delta\lambda_i \leq \Delta\lambda_{\text{imax}} \quad (i = 1,2,\ldots,m) \\ \sum_{i=1}^{m} |\Delta\lambda_i| \leq \Delta\lambda_{\max\_lin} \end{cases} \tag{7-4}$$

where Δf is the total size of the control action applied to all control parameters; λ_i is the i^{th} control parameter; V_w^{base} (t_0) is the voltage of bus w at t_0 before any control is applied; $S_i(t_0)$ is the sensitivity of the voltage magnitude of bus w to various control parameters at t_0 evaluated at the base case; t_0 is one specific time instant of interest; V_w^{new} is the targeted control value; $\Delta\lambda_{imin}$ and $\Delta\lambda_{imax}$ are the lower and upper bound of parameter λ_i; m is the number of λ participating in control; λ_{max_lin} is the linear approximation accuracy constrained maximum bound on the change.

It is noted that only parameters with higher sensitivities will be included in the optimization model (7-3) ~ (7-4). Therefore, this linear programming problem usually has very low dimension even for a large power system.

7.4 Application and results

The proposed method is applied to the WECC system. Details about this application are as follows,

- NERC criteria on voltage performance after disturbance

According to the NERC criteria on the WECC system for post fault system performance [55], the voltage magnitude dip after disturbance should not exceed 20% of the initial voltage magnitude for more than 20 cycles (0.33 seconds).

- Base case description

The WECC system is used as the test system. The fault considered here is shown in Figure 7-2.

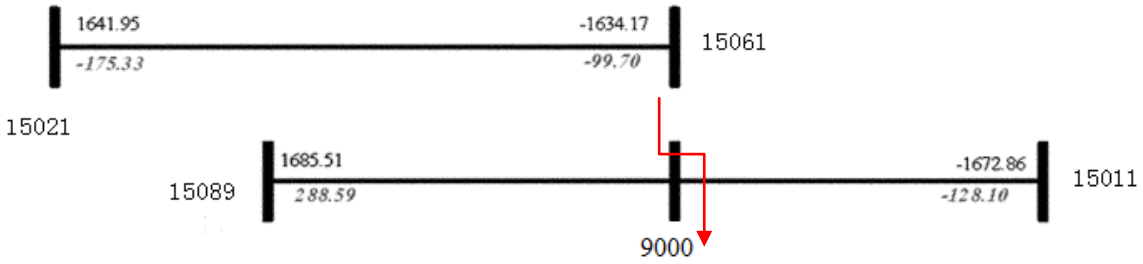

Figure 7-2 Fault description

A three phase fault occurs at t = 0.2 s at bus 9000 and the fault is cleared at t = 0.29 s by removing two lines: line 15021 – 15061 and line 15089 – 15011.And the worst voltage magnitude drop occurs at bus 15050, which is shown in Figure 7-3.

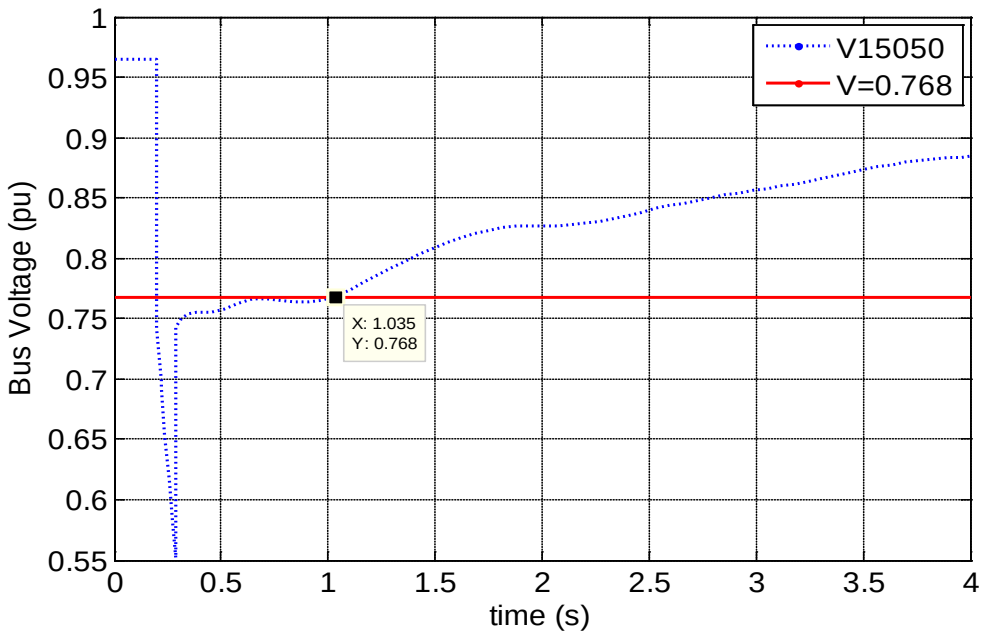

Figure 7-3 Bus 15050 voltage magnitude plot

The initial voltage magnitude at bus 15050 is 0.96 pu. According to the NERC criteria, before the time instant t = 0.29 + 0.33 = 0.62 s, the voltage magnitude should be higher than 0.768 pu. From Figure 7-3 it can be seen that the voltage magnitude does not go up to 0.768 pu until the time instant t = 1.035 s, which violates the NERC criteria.

- Determination of a suitable set of load uncertain parameters

The sensitivities of the voltage magnitude of bus 15050 with respect to reactive loads at buses that are in the same area as the fault location are calculated. 105 load buses with higher sensitivities are selected to examine the load modeling uncertainty. The composite load model introduced in Chapter 7.1 is used for these buses. The composition K_{pm} and inertia of each induction motor H modeled at each of these 105 buses are selected to comprise of the candidate set of load uncertainty parameters. Therefore, in all 630 load parameter uncertainties are taken into account. The sensitivities of bus 15050 voltage magnitude with respect to the 630 load parameters are calculated by the high performance parallel computing platform introduced in Chapter 3.2.

Assume $\Delta\lambda$ which indicates the change in active load composition K_{pm} and inertia H of each induction motor, varies in the range of [-1.25, 1.25] percent of their base value. Then from (7-1) a bound on the voltage magnitude of bus 15050 is formed and shown in Figure 7-4.

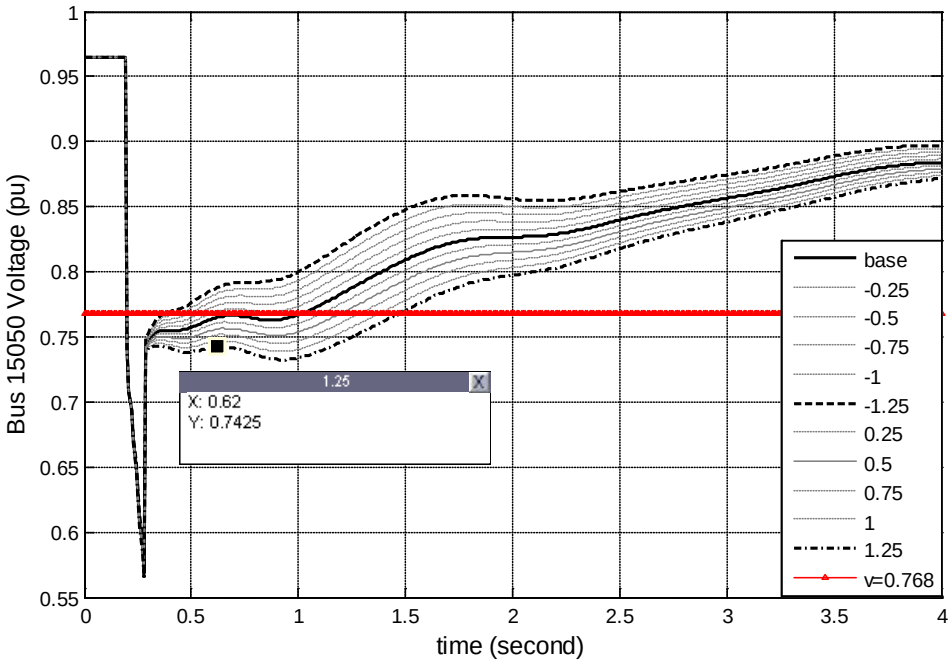

Figure 7-4 Bus 15050 voltage magnitude operational bounds with varying K_{pm} and H

It can be seen from Figure 7-4 that when the load parameters vary, the bus 15050 voltage magnitude operates within a certain bound instead of a fixed value. This behavior suggests that the when making control strategy decisions, not just the base curve, but also the lower bound curve should be taken into account.

The control objective is to guarantee that the entire range of the voltage magnitude of bus 15050 considering load parameter uncertainties satisfies the NERC criterion and also minimize the control effort. From Figure 7-4 it can be seen that voltage magnitude plots for load parameter uncertainty in the range between the base case and the lower bound violate the NERC criteria.

For each control option considered, a set of candidate locations for sensitivity calculation is determined and the number of candidate locations considered for each of these control options is listed in Table 7-2.

Table 7-2 Number of candidate Locations for control options

Control	Generation rescheduling	Shunt compensation
No. of parameters	227	125

Along the base case time domain simulation, the sensitivities of the voltage magnitude of bus 15050 with respect to each of these control parameters at different locations are calculated for each control option listed in Table 7-2. A ranking of sensitivities at t = 0.62 s for each of these control options is conducted. Those locations with higher sensitivities

are accordingly chosen as candidates for applying control. The first 10 locations with higher shunt compensation sensitivities are listed in Table 7-3.

Table 7-3 Bus 15050 voltage magnitude sensitivity ranking – shunt compensation

Sensitivity ranking no.	bus	Sensitivity (pu/pu)	B_0(pu)	B_{max} (pu)	B_{min}(pu)	ΔB_{max} (pu)	ΔB_{min}(pu)
1	15121	0.007408	0.4523	2.5	-2.5	2.0477	-2.9523
2	15119	0.006992	0.3	2.0	-2.0	1.7	-2.3
3	15610	0.006788	1.043	2.0	-2.0	0.957	-3.043
4	15614	0.006463	1.025	3.5	-3.5	2.475	-4.525
5	15608	0.005912	0.5116	1.5	-1.5	0.9884	-2.0116
6	15617	0.005585	0.5429	1.5	-1.5	0.9571	-2.0429
7	15207	0.005393	3.2699	5.5	-5.5	2.2301	-8.7699
8	15612	0.005316	1.0846	3.5	-3.5	2.4154	-4.5846
9	15615	0.005245	0.5303	1.5	-1.5	0.9697	-2.0303
10	15609	0.005143	1.0906	1.5	-1.5	0.4094	-2.5906

Also 10 locations with the highest generation sensitivities and 10 locations with the lowest generation sensitivities are selected and listed respectively in Table 7-4.

Table 7-4 Bus 15050 voltage magnitude sensitivity ranking – generation rescheduling

Sensitivity ranking no.	Highest			Lowest				
	bus	Sensitivity (pu/pu)	P_0 (pu)	bus	Sensitivity (pu/pu)	P_0 (pu)	P_{max} (pu)	ΔP_{max} (*pu*)
1	15928	0.00349	1.42	15923	-0.00262	0.867	1.15	0.283
2	15922	0.002865	0.858	15971	-0.00205	3.89	4.57	0.68
3	15924	0.002851	0.858	15972	-0.00205	3.84	4.57	0.73
4	14924	0.002	1.149	15921	-0.00187	0.844	1.15	0.306
5	14925	0.001999	1.149	15142	-0.00172	2.44	3.2	0.76
6	15919	0.001866	1.55	14902	-0.00168	2.6	3.21	0.61
7	15918	0.001836	0.95	14805	-0.00166	2.35	3	0.65
8	15914	0.001803	0.478	14811	-0.00166	2.35	3	0.65
9	15902	0.001753	1.13	14808	-0.00166	2.35	3	0.65
10	15901	0.001716	1.13	14802	-0.00166	2.35	3	0.65

From Chapter 5, when multiple parameters sensitivities are evaluated, the maximum normalized sensitivity can be determined as

$$S_{\max} = \max_{i=1}^{n} \left\{ \left\| \partial x_i \left(\lambda_j, t \right) / \partial \lambda_j \right\|_\infty / \left\| x_i \left(\lambda_j, t \right) \right\|_\infty \right\} \quad j \in M \tag{7-5}$$

In (7-5), $\partial x_i(\lambda_j,t)/\partial\lambda_j$ is the sensitivity of the i^{th} system variable x with respect to the j^{th} control parameter λ. M is the set of control parameters comprised of the control parameters for the two control actions and n is the number of system variables.

The solution to (7-5) yields: S_{max}=0.914 (1/pu).

Then from (5-8), the maximum perturbation size that satisfies the linear approximation accuracy can be determined

$$\Delta\lambda_{\max\_lin} \le 1.17 / S_{\max} = 1.17/0.194 = 6.03 pu$$

This is the maximum amount of control effort that can be applied to the base case while the linear approximation accuracy requirement is still met.

To achieve the control objective, certain control actions should be applied to the base case to ascertain that the voltage magnitude plots in the range between the base case and the lower bound are in compliance with the NERC requirement.

For each of the two control actions, an optimization problem described by (7-3) and (7-4) is formed and solved respectively to obtain the optimal control effort. The results are as follows,

- For shunt compensation, only two locations will be needed to increase the capacitor susceptance B with the amount listed in Table 7-5

Table 7-5 Changes of preventive control option – Shunt compensation

Bus		15121	15119	Total
Shunt added (pu)	Base case	1.215	0	1.215
	Lower bound	2.0	1.528	3.528

From Table 7-5 it can be seen that different amounts of control should be applied when different operating points are considered. If the control is based on the base case performance, 1.215 pu of shunt capacitance is needed; if the control is based on the lower bound of the voltage magnitude of bus 15050, 3.528 pu of shunt capacitance is needed. The range of control for shunt compensation is [1.215, 3.528] pu.

- For generation rescheduling, the generator with the highest sensitivity is considered with the highest priority to reduce output; and the generator with the lowest sensitivity is considered with the highest priority to increase its output to account for the rescheduled generation. The active generation output after rescheduling for generators participating in rescheduling is listed in Table 7-6

Table 7-6 Generation output after rescheduling

Lower bound				Base case			
High Sensitivity		Low Sensitivity		High Sensitivity		Low Sensitivity	
bus	*Pg*(pu)	bus	*Pg*(pu)	bus	*Pg*(pu)	bus	*Pg*(pu)
15928	0	15923	1.15	15928	0	15923	1.15
15922	0	15971	4.57	15922	0	15971	4.57
15924	0	15972	4.57	15924	0.708	15972	4.57
14924	0	15921	1.15			15921	1.15
14925	0	15142	3.2			15142	2.869
15919	1.16	14902	3.21				
		14805	3				
		14811	3				
		14808	3				
		14802	2.855				
Total(pu)	5.824			Total(pu)	2.428		

From Table 7-6 it can be seen that if the control is based on the base case performance, 2.428 pu of active generation needs to be rescheduled; if the control is based on the lower bound of the voltage magnitude of bus 15050, 5.824 pu of active generation needs to be rescheduled. The range of the control effort for generation rescheduling is [2.428, 5.824] pu.

7.5 Result verification

The results of the control options determined are verified by re-running time domain simulations for the changed cases with the corresponding control actions applied. Both the control strategies for the lower bound control and base case control are verified as follows.

1) **Base Case Control Verification**

Applying the amount of control required considering just the base case voltage magnitude of bus 15050, it is seen from Figure 7-5 and Figure 7-6 that the base case voltage magnitude is higher than 0.768 pu at t = 0.62 s, which is the control objective. However, the lower bound of the voltage magnitude is still violating the NERC criteria.

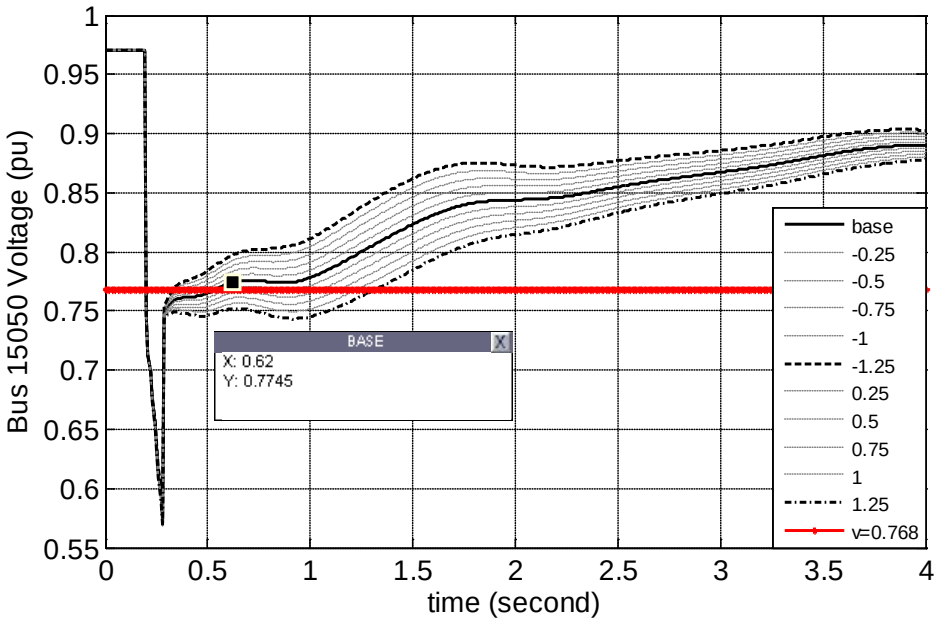

Figure 7-5 Bus 15050 voltage magnitude operational bound – with shunt compensation considering base operating point

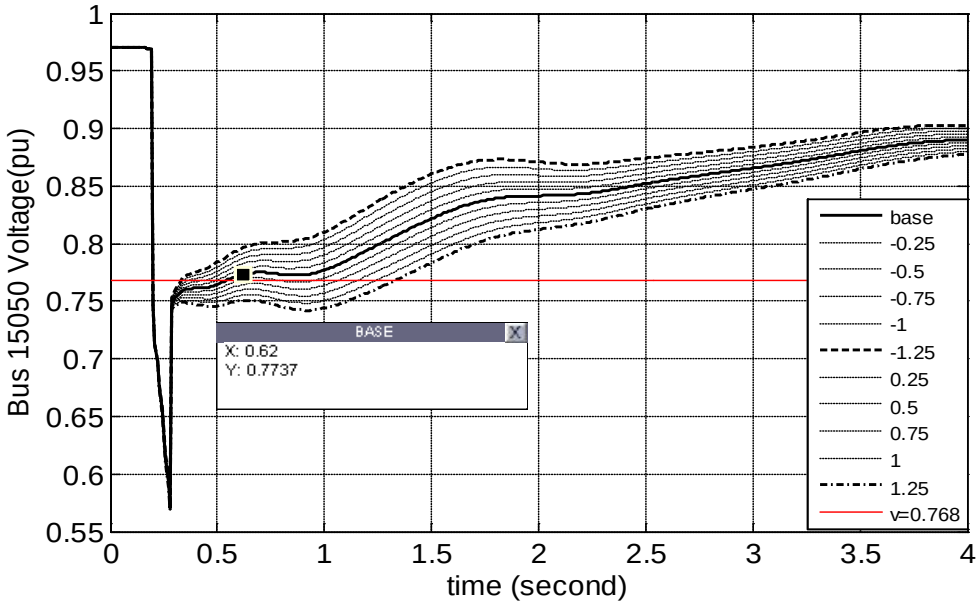

Figure 7-6 Bus 15050 voltage magnitude operational bound – with generation rescheduling considering base operating point

2) **Lower Bound Control Verification**

Applying the amount of control that is required for the control of the lower bound voltage magnitude of bus 15050 it can be seen from Figure 7-7 and Figure 7-8 that the lower bound voltage magnitude is higher than 0.768 pu at t = 0.62 s, which is the control

objective. When these amounts of control effort are applied to the base case, all the voltage magnitudes satisfy the NERC requirement.

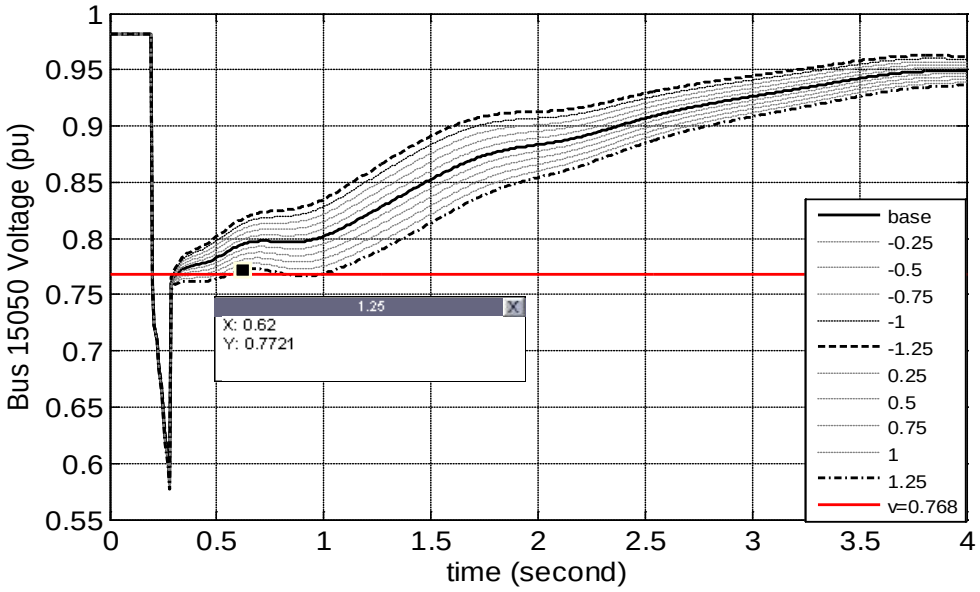

Figure 7-7 Bus 15050 voltage magnitude operational bound – with shunt compensation considering lower bound operating point

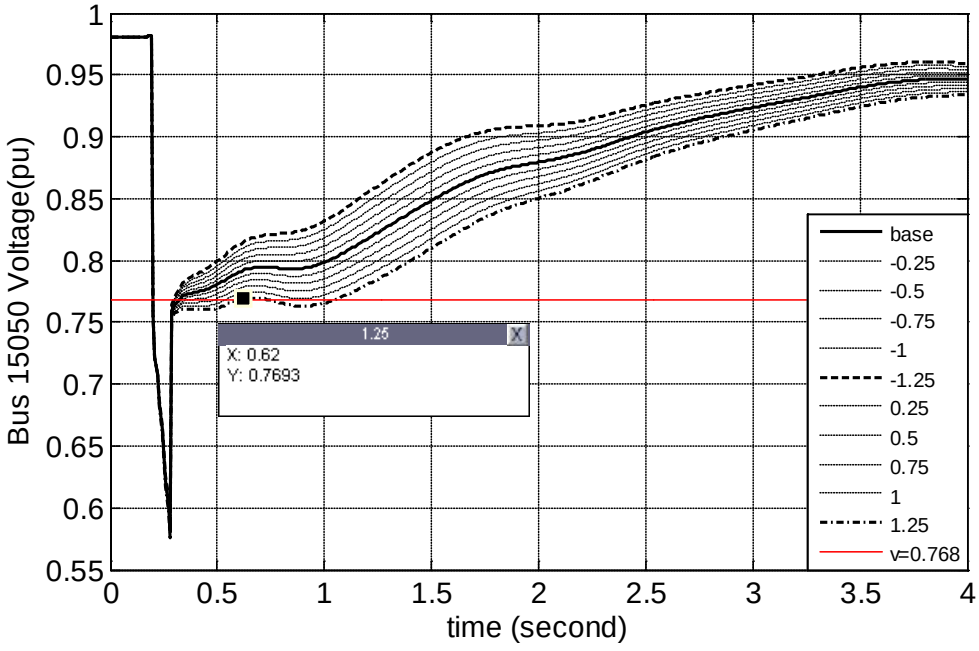

Figure 7-8 Bus 15050 voltage magnitude operational bound – with generation rescheduling considering lower bound operating point

7.6 Summary

This test case demonstrates the merits of applying the trajectory sensitivity analysis method to the voltage stability problem with consideration of the load modeling parameter uncertainties. The main advantages of this method are

1. Load modeling parameters uncertainties can be accounted for in the voltage stability study without a significant computational burden

With the high performance parallel computing platform introduced in 3.2, the calculation of various sensitivities is enhanced significantly. With the sensitivity information, the system operational boundary can be evaluated linearly based on the base value.

2. Control actions for various preventive control methods can be calculated according to the system operational boundary

Traditional methods for voltage control are mainly focused on the current operating point and the amounts of control from these methods are applicable only to the base case. The proposed method can determine the control actions for various preventive control methods based on the system operational bound determined by considering the uncertainties of a power system. This approach provides a measure of the voltage stability boundaries for system operators and planners to decide proper control strategies.

8. Application to Transient Stability Constrained Interface Real Power Flow Limit Calculation

The proposed sensitivity analysis approach is also applied to calculate the interface power transfer limit that meets transient stability constraints.

An interface power flow limit is a limit of real power flow over a cut set of pre-determined transmission lines [50] - [54]. Traditionally, most methods to calculate this limit require repeated time domain simulation by gradually increase the generations at these key generators. These methods are computationally burdensome.

The trajectory sensitivity analysis based approach can provide an efficient solution to this problem. We observe that the limit of flows through an interface is determined by the generations at certain key generators. In other words, these key generators are the main sources of power for these transmission lines. If the maximum generation increment of these key generators can be determined, then with the power transfer distribution factor (PTDFs) of those generators on the interface, the maximum real power flow of the interface can be determined.

The most critical issue of this method is to determine the maximum generation increment of those key generators in an efficient manner. The trajectory sensitivity approach is proposed here to solve this problem. This method can avoid performing a large number of repeated time domain simulations. Details about this proposed method are presented in the following.

8.1 Procedures and details

Current methods that are widely used by various independent system operators (ISOs) for determination of the transient stability constrained interface limit are based on the combination of the direct method and time domain simulation [58]. First, the direct method is used for contingency ranking and screening to identify the critical contingencies. Then for each of those critical contingencies, multiple time domain simulations are performed to determine the transfer limit.

These methods basically monitor the system transient stability while increasing or decreasing the transfer across the interface which is simulated by adjusting the generation and load in the exporting and importing areas. The detailed mechanism for this adjustment varies. For example, one can adjust the generation and load according to a set of scaling factors. For situations evaluating the least-cost transfers, economic dispatch of the system must be taken into account.

Though the contingency screening significantly reduces the computational burden, multiple time domain simulations are still required to determine the transfer limit without violating stability constraints for each contingency considered. To tackle this problem, a new method based on trajectory sensitivity analysis is proposed and presented as follows.

The feature of this method is that it utilizes the trajectory sensitivity analysis method to ascertain that the generation increment at each key generator will not result in the system being unstable. Then a constrained optimization problem can be formulated to calculate the maximum real power flow through an interface of interest.

The detailed procedure for this method is as follows,

1. Pre-determine an interface that is of interest and identify the key generators and transmission lines constitute this cut set
2. Determine a suitable base case

The principle of determining a base case is that this case should be close to its stability limit so that the linear approximation can be applied. For example, in the transient angle stability problem, the commonly used criterion to identify the limit of a system is that the relative rotor angle between any two generators reaches 180°. Thus, for an operating point, when this angle difference is close to 180°, for example 165°, this case can be identified as the base case

3. Identify a set of load buses whose active loads are most likely to change

In the importing area, a set of load buses whose active loads are very likely to change and affect the interface flow needs to be pre-determined. This determination can be based on historical data or operational experience

4. Calculate the sensitivities of interest simultaneously

For interface flow limit calculation, two types of sensitivities are needed: one is the sensitivities of generator rotor angle with respect to active generation change at those key generators; the other one is the sensitivities of generator rotor angle with respect to active load change in the importing area.

5. Calculate the PTDFs of those key generators on those transmission lines that constitute the interface
6. Calculate the maximum interface real power flow

Details about this calculation are as follows,

- Calculate the maximum amount of active generation change ΔP_{max_lin} that meets the linear sensitivity approximation accuracy requirement. Details of this method are discussed in Chapter 5
- Solve the following constrained optimization equations to obtain the maximum changes of the real power flow through the interface.

$$\max \quad \Delta P_I = \sum_{k=1}^{n} \sum_{i=1}^{m} \Delta P_{Gi} \Delta f_{ik} \tag{8-1}$$

s.t.

$$\begin{cases} \delta_{d\_j}^{base}(t_0) + \sum_{i=1}^{m} \Delta P_{Gi} \frac{d\delta_{d\_j}}{dP_{Gi}}(t_0) + \sum_{i=1}^{l} \Delta P_{Li} \frac{d\delta_{d\_j}}{dP_{Li}}(t_0) \le 180^\circ \quad j \in C \\ 0 \le P_{Gi0} + \Delta P_{Gi} \le P_{Gi\max\_cap} (i = 1, 2, ..., m) \\ \sum_{i=1}^{m} |\Delta P_{Gi}| + \sum_{i=1}^{l} |\Delta P_{Li}| \le \Delta P_{\max\_lin} \\ \sum_{i=1}^{m} |\Delta P_{Gi}| = \sum_{i=1}^{l} |\Delta P_{Li}| \end{cases} \tag{8-2}$$

where ΔP_I is the increment of the real power flow through the interface. ΔP_{Gi} is the active generation change at generator *i*. f_{ik} is the PTDF of generator *i* on line *k*. *m* is the number of key generators in the cut set. *n* is the number of transmission lines forming the cut set. *l* is the number of load buses whose active load changes are taken into account. *C* is a set of the most advanced generators. $\delta_{d\_j}(t_0)$ is the generator rotor angle difference between the j^{th} generator in *C* and least advanced generator at time instant $t=t_0$. $\delta_{d\_j}^{base}(t_0)$ is the value of $\delta_{d\_j}(t_0)$ for the base case.$\partial\ \delta_{d\_j}/\partial P_{Gi}(t_0)$ and $\partial \delta_{d\_j}/\partial P_{Li}(t_0)$ are the sensitivity of δ_{d_j} with respect to active generation change at generator *i* and active load change at load bus *i* at time instant $t=t_0$, respectively. ΔP_{Li} is the active load change at load bus *i*. The rotor angle difference 180° is the criteria used to determine the angle stability. P_{Gi0} is the active generation at generator *i* for the base case. P_{Gimax_cap} is the capacity of generator *i*. ΔP_{max_lin} is the total change that can be applied to all key generators and load buses without violating the linear sensitivity approximation accuracy requirement.

In order to solve the optimization problem, in (8-2), it is assumed that the active load of those load buses change proportionally based on some weighting factors as follows:

$$\Delta P_{Lj} = \frac{1}{w_j} \times \Delta P_L = \frac{1}{w_j} \times \sum_{i=1}^{m} |\Delta P_{Gi}| \quad j \in [1, 2, ..., l] \tag{8-3}$$

where w_j is the load increase weighting factor for load bus *j*, and ΔP_L is the total load increment at all the load buses.

The first constraint equation in (8-2) ascertains that the total generation increment at all the key generators will not result in the system instability. It is noted that in this constraint equation, not only the most advanced generator, but also several other advanced generators are taken into account for the reason that the generation increment in these generators might result in the second or third advanced generator become unstable. Therefore, this constraint equation ascertains all the advanced generators are stable when there are generation changes made to the system. The second constraint equation in (8-2) ascertains that the generation increment at each of the key generator will be within its capacity limit. The third constraint equation in (8-2) ascertains that combination of the total generation increment at all generators and the total load change in the load area is within the linear approximation accuracy requirement limit. The fourth constraint equation in (8-2) ascertains that the total generation increment is equal to the total load increment.

Solution of (8-1) - (8-2) yields ΔP_I. Then the stability constrained maximum interface real power flow can be determined as

$$P_{Imax} = P_{I0} + \Delta P_I \tag{8-4}$$

Where, P_{I0} is the interface real power flow for the base case.

8.2 WECC test case and results

The WECC system is used as the test system. An interface of interest is pre-selected as shown in Figure 8-1 and Figure 8-2. There are two major power plants of interest: P1 and P2. Each of these plants contains several generators with high capacity. The configurations of these plants are listed in Table 8-1. There are four transmission lines in this interface. The real power flows on these lines for the base case are listed in Table 8-2.

Table 8-1 Configurations of the two major power plants

Power Plant	P2				P1				
Gen. Bus	118	119	120	121	114	115	111	112	113
Gen. No.	#5	#6	#7	#8	#46	#47	#43	#44	#45
P_{Gi0} (MW)	360	350	544	533.83	750	750	450	400	450
P_{Gimax_cap} (MW)	410	400	594	590	775	775	800	750	800

Table 8-2 Real power flows through the interface for base case

Line	1	2	3	4	Interface
P_{I0} (MW)	190.68	407.18	456.73	508.46	1563.1

The PTDF f_{ik} is defined as follows,

$$f_{ik} = \frac{\Delta P_k}{\Delta P_i} \tag{8-5}$$

Where f_{ik} is the PTDF of generator i on line k. ΔP_k is the real power flow change on line k. ΔP_i is active generation change at generator i.

A PTDF calculation routine has been implemented in PSAT [37]. The results are listed as follows in Table 8-3.

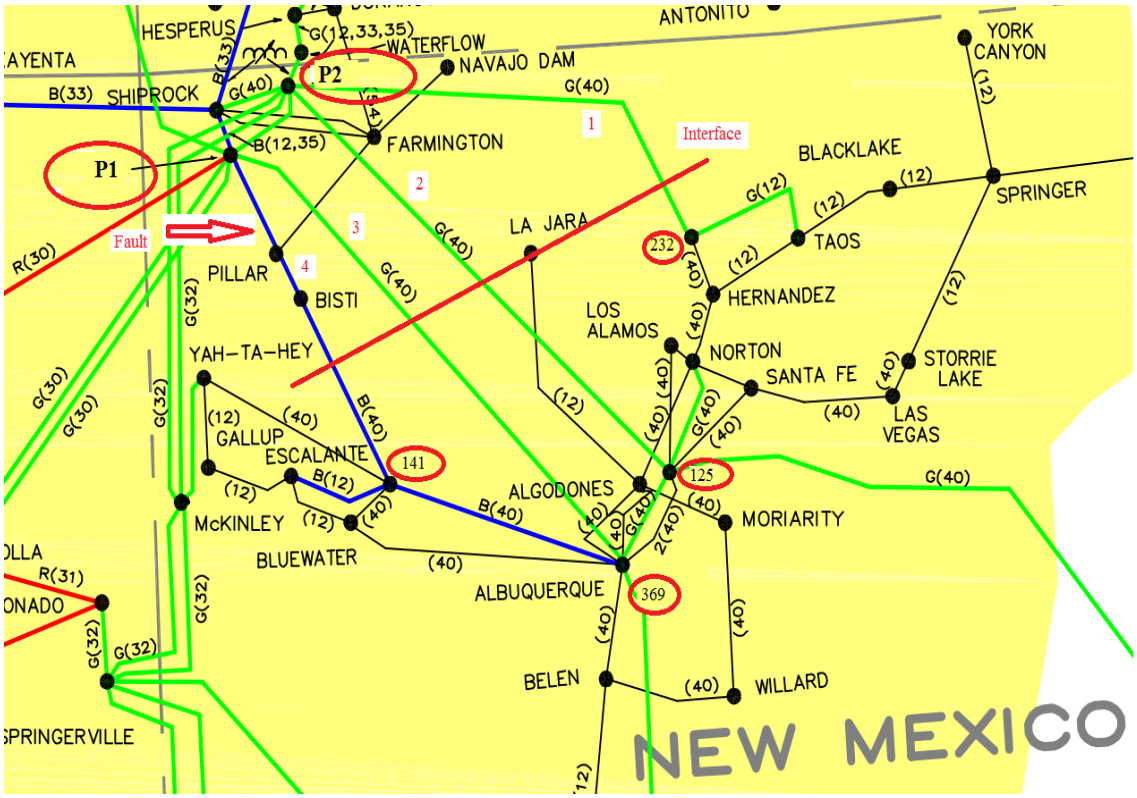

Figure 8-1 The pre-selected interface

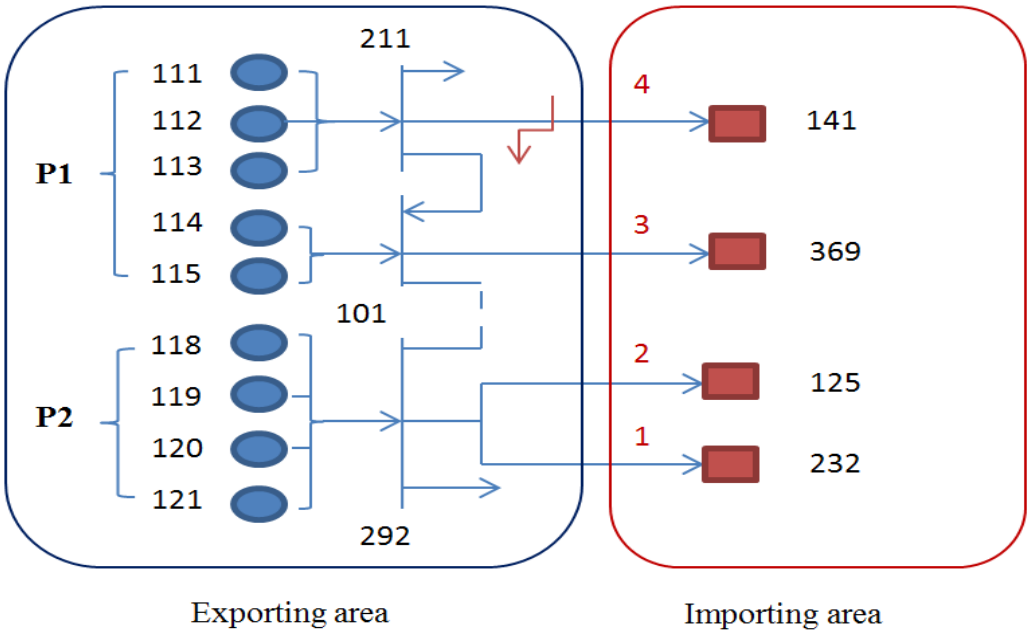

Figure 8-2 Description of the selected interface

Table 8-3 PTDFs of each key generators on the interface

To Load From Gen *i*	PTDF f_{ik} for line *k* (%)			
	1	2	3	4
G1	1.2	2.7	0.2	0
G2	1.2	2.7	0.2	0
G3	1.2	2.7	0.2	0
G4	1.2	2.7	0.2	0
G5	0.9	0.8	2.3	0.5
G6	0.9	0.8	2.3	0.5

The contingency considered is a 3-phase fault on line #4 as depicted in Figure 8-1. The fault occurs at t = 0.2 s and is cleared after 0.06 s. After running time domain simulation for the base case, it is found that Gen. #43, Gen. #44 and Gen. #45 are the most advanced generators, and Gen. #320 is the least advanced generator. Therefore, these three generators are selected as the set of advanced generators C defined in (8-2). The relative angles between these most advanced generators and Gen. #320 are plotted in Figure 8-3.

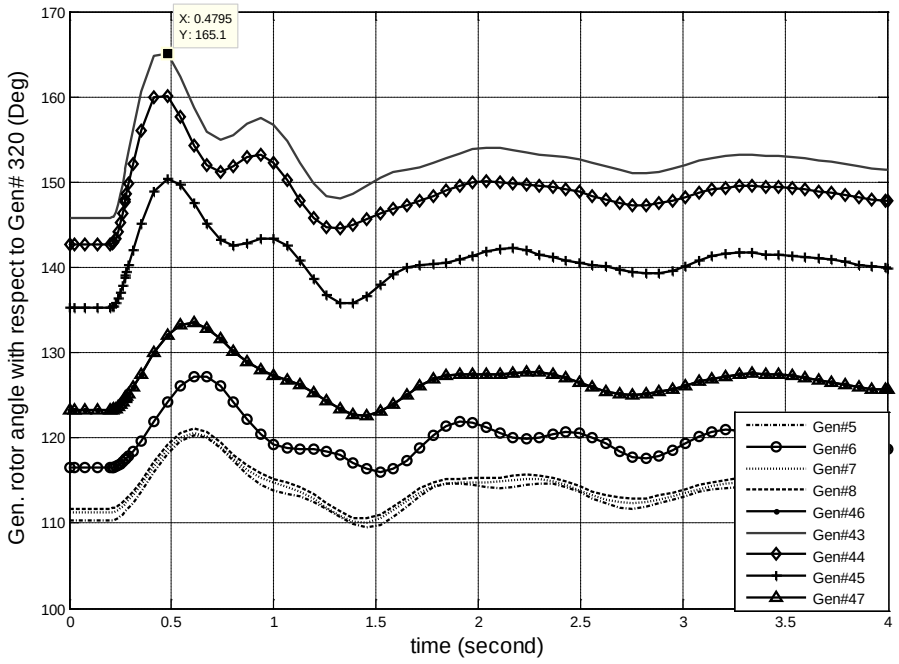

Figure 8-3 Relative angles between the most advanced Gen. and Gen. #320

17 load buses whose active loads are considered to change and affect the interface flow are determined. These 17 load buses are directly supplied by the four interface tie lines.

Based on the standard option in several commercial time domain simulation packages, relative rotor angle values of 180° are used to detect the system stability/instability. The maximum relative rotor angle here is 165.1°, which occurs at t = 0.4795 s. It can be seen that this system operating point is very close to its stability limit.

To solve the optimization problem (8-1) - (8-2), two types of sensitivities are required. They are

- Sensitivities of rotor angles of generators in the set C with respect to active generation change at those key generators depicted in Table 8-1

These sensitivities are calculated using the parallel computing platform described in Chapter 3.2 and they are shown in Figure 8-4 - Figure 8-6.

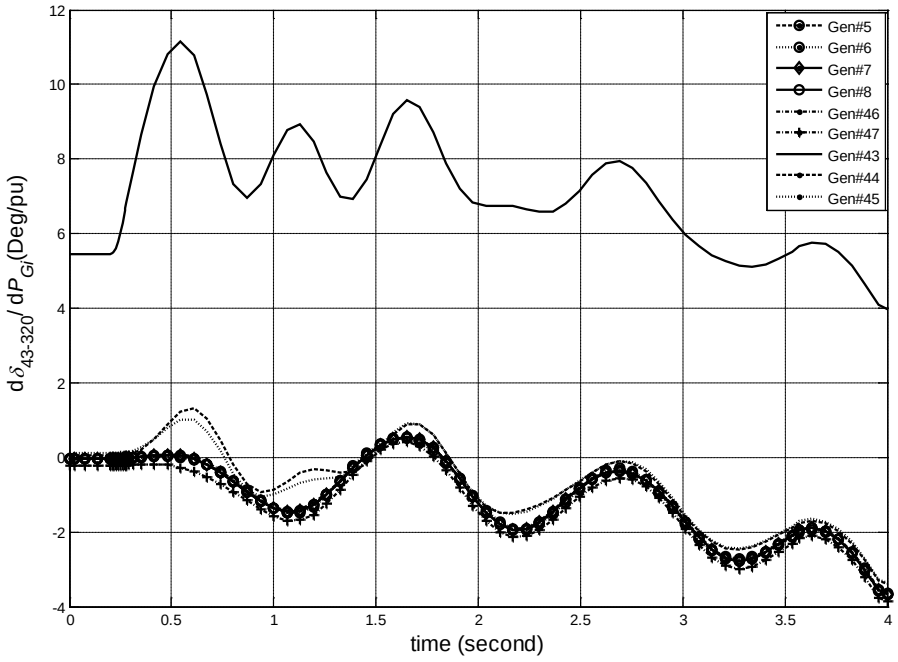

Figure 8-4 Sensitivities of $\delta_{43\text{-}320}$ to active generation of the key generators

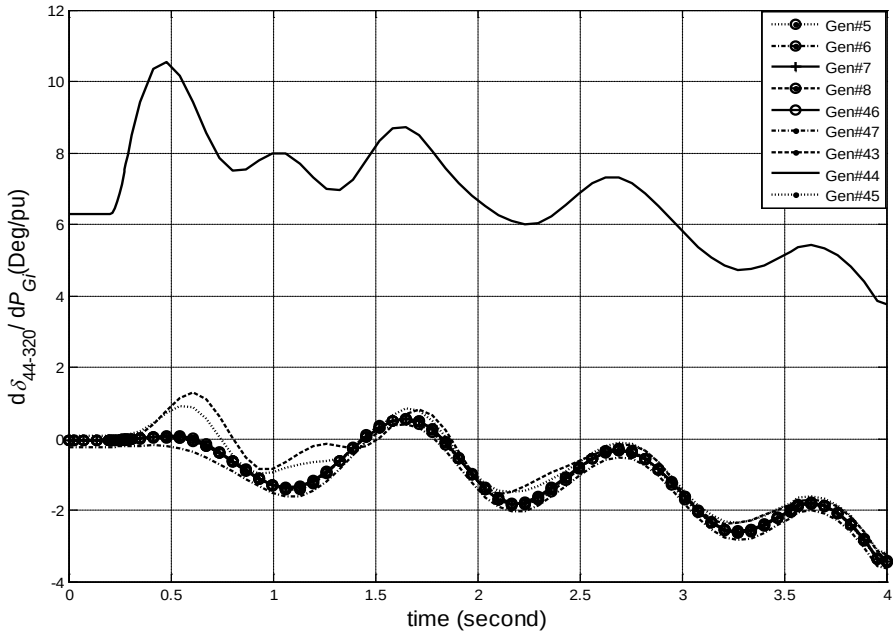

Figure 8-5 Sensitivities of $\delta_{44\text{-}320}$ to active generation of the key generators

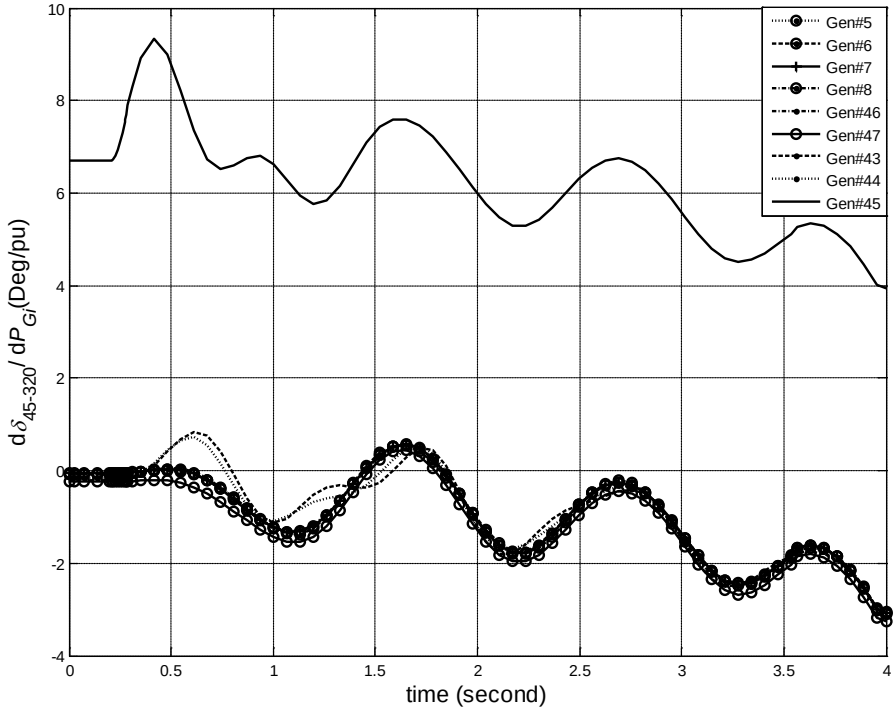

Figure 8-6 Sensitivities of $\delta_{45\text{-}320}$ to active generation of the key generators

It can be seen from Figure 8-3 that the maximum relative rotor angle occurs at time instant t = 0.4795 s, therefore the sensitivity information at this time instant are of interest and they are listed in Table 8-4. The capacities of these key generators P_{imax_cap} are listed in Table 8-1.

Table 8-4 Sensitivity to active generation change at t = 0.4795 s

Generator:	#5	#6	#7	#8	#46	#47	#43	#44	#45
$\partial\delta_{43\text{-}320}/\partial P_{Gi}$ (deg/pu)	0.05	0.03	0.07	0.06	0.1	-0.21	10.9	0.88	0.8
$\partial\delta_{44\text{-}320}/\partial P_{Gi}$ (deg/pu)	0.05	0.03	0.06	0.06	0.09	-0.21	0.78	10.5	0.71
$\partial\delta_{45\text{-}320}/\partial P_{Gi}$ (deg/pu)	0.023	0.005	0.04	0.04	0.05	-0.21	0.4	0.4	9.0

Table 8-5 Sensitivity to active load change at t = 0.4795 s

Bus	$\partial\delta_{43\text{-}320}/\partial P_{Li}$ (deg/pu)	$\partial\delta_{44\text{-}320}/\partial P_{Li}$ (deg/pu)	$\partial\delta_{45\text{-}320}/\partial P_{Li}$ (deg/pu)	Bus	$\partial\delta_{43\text{-}320}/\partial P_{Li}$ (deg/pu)	$\partial\delta_{44\text{-}320}/\partial P_{Li}$ (deg/pu)	$\partial\delta_{45\text{-}320}/\partial P_{Li}$ (deg/pu)
10041	-0.08	-0.01	-0.05	10034	-0.14	-0.14	-0.167
10369	-0.05	-0.05	-0.07	10046	-0.08	-0.08	-0.106
10232	-0.008	-0.01	-0.03	10061	-0.16	-0.15	-0.184
10025	-0.05	-0.05	-0.07	10070	-0.15	-0.15	-0.17
10005	-0.17	-0.2	-0.19	10072	0.13	0.13	0.10
10015	-0.16	-0.15	-0.17	10173	-0.2	-0.2	-0.23
10020	-0.15	-0.14	-0.17	10450	-0.18	-0.2	-0.20
10022	-0.16	-0.15	-0.18	10511	-0.12	-0.12	-0.14
10032	-0.22	-0.22	-0.26				

- Sensitivities of rotor angles of generators in the set C with respect to active load change at the 17 load buses

  The sensitivity information at time instant t = 0.4795 s are listed in Table 8-5.

From Chapter 5, when multiple parameters sensitivities are evaluated, the maximum normalized sensitivity can be determined as

$$S_{\max} = \max_{i=1}^{n} \left\{ \left\| \partial x_i(\lambda_j, t) / \partial \lambda_j \right\|_\infty \Big/ \left\| x_i(\lambda_j, t) \right\|_\infty \right\} \quad j \in M \tag{8-6}$$

In (8-6), $\partial x_i(\lambda_j,t)/\partial\lambda_j$ is the sensitivity of the i^{th} system variable x with respect to the j^{th} changing parameter λ. M is the set of changing parameters and n is the number of system variables.

Solution to (8-6) yields: S_{max} = 0.11538 (1/pu).

Then from (5-8), the maximum perturbation size that meets the linear approximation accuracy requirement can be determined

$$\Delta\lambda_{\max\_lin} \le 1.17 / S_{\max} = 1.17/0.11538 = 10.14\,pu$$

This is the maximum amount of change, including generation change and load change that can be applied to the base case while the linear approximation accuracy requirement is still met.

In order to solve the linear programming problem (8-1) ~ (8-2), the following two assumptions are made:

- In (8-2), it is assumed that ΔP_{Gi} is positive. This indicates that all the key generators are increasing their output
- In (8-2), it is assumed that the load increments are distributed equally among the 17 load buses

The Matlab built-in solver for linear programming problems "linprog" is used to solve the linear programming problem (8-1) ~ (8-2). Solution to (8-1) ~ (8-2) yields ΔP_I = 386.4861 MW. At the solution, the generation increment of each key generator ΔP_{Gi} is listed in Table 8-6.

Table 8-6 The key generator output increment

Generator:	#5	#6	#7	#8	#46	#47	#43	#44	#45	Total
ΔP_{Gi} (MW)	0	0	0	0	17.8	0	88.8	143.09	257.3	507

Then the interface real power flow limit then can be calculated as

$$P_{I0} + \Delta P_{I0} = 1563.1 + 386.48 = 1949.6 \text{ MW}.$$

8.3 Result verification

To verify the results obtained from above, another time domain simulation is run for the changed case with the changes listed in Table 8-6 applied to the pre-fault power flow case. The relative rotor angle plots between the most advanced generators and Gen #320 are shown in Figure 8-7, respectively.

Also, the relative generator rotor angles between the three most advanced generator and Gen. #320 at time instant t = 0.4795 s are also verified and listed in Table 8-7. In the table, the results in the row "From linear programming solution" are the results obtained by solving the linear programming problem (8-1) ~ (8-2). The results in the row "From

time domain simulation for changed case" are the results obtained from running time domain simulation for the changed condition.

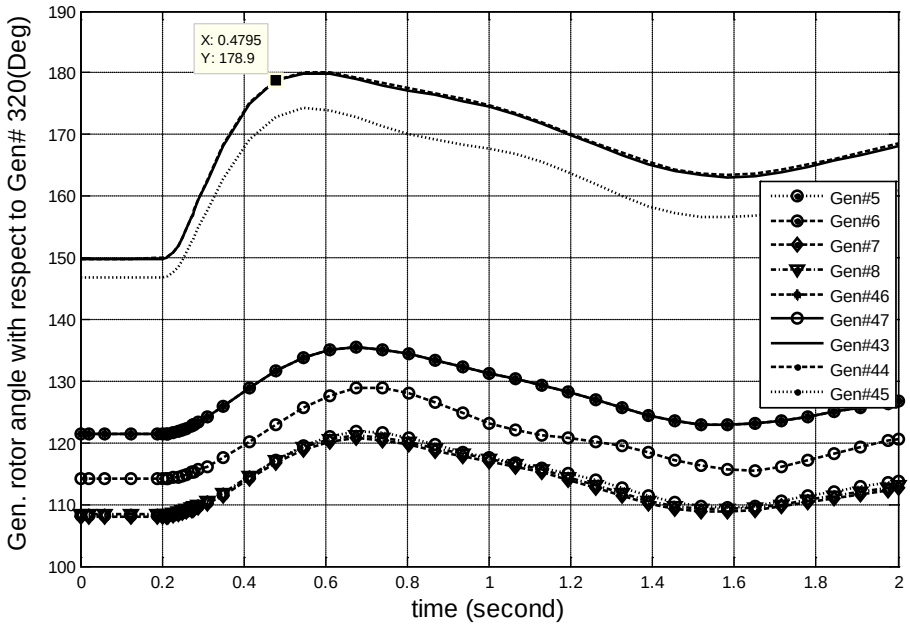

Figure 8-7 Relative angle plots between the most advanced generators and generator #320 for the changed case

Table 8-7 Comparison of the relative generator rotor angles at t = 0.4795 s

	$\delta_{43\text{-}320}$(deg)	$\delta_{44\text{-}320}$(deg)	$\delta_{45\text{-}320}$(deg)
From linear programming solution	177.4	177.03	173.4
From time domain simulation for changed case	178.7	178.9	172.9

Table 8-8 Comparison of the real power flows through the interface

Line	#1	#2	#3	#4	Interface
P_{I0} (MW)	190.68	407.18	456.73	508.46	1563.1
P_I – From linear programming solution (MW)	235.30	537.83	612.38	564.03	1949.6
P_I – From time domain simulation for changed case (MW)	234.07	527.11	599.64	580.71	1941.5

Also, the real power flows in the four tie lines are verified and they are listed in Table 8-8. It can be seen from Figure 8-7 that the relative rotor angles at t = 0.4795 s are very close to 180°. And it is seen from Table 8-7 and Table 8-8 that the results from the solution to (8-1) ~ (8-2) are very close to the actual results from time domain simulation for the changed case.

Then the interface real power flows are increased slightly higher than the amount obtained using the proposed method by 3.5 MW to 390 MW, the relative angle plots are shown in Figure 8-8. It is seen from the figure that three generators are swinging away from the rest of the generators, which indicates that the system is unstable.

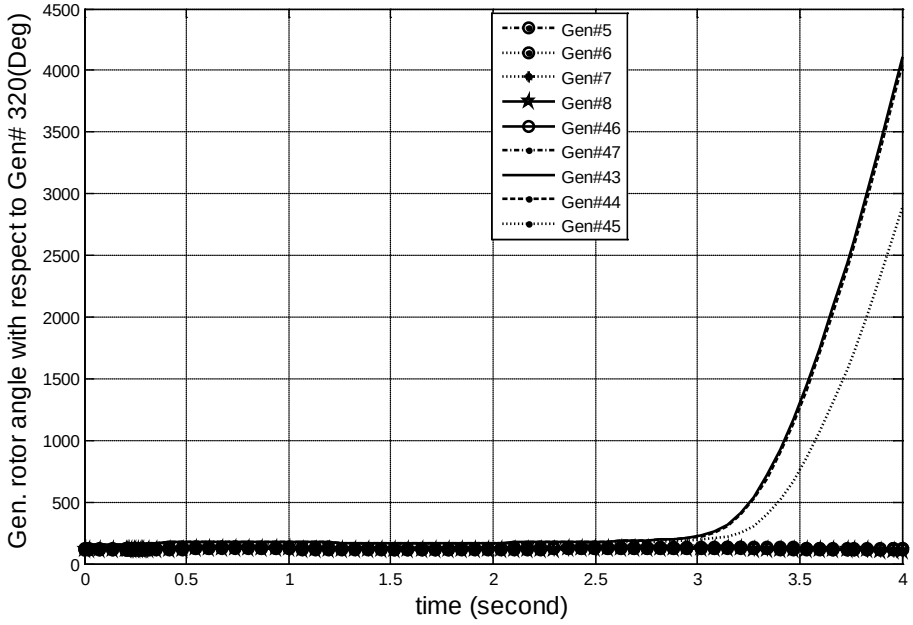

Figure 8-8 Relative angle plots between the most advanced Gen. and Gen. #320 – with interface flow P_I = 390 MW

Thus the result verifies the correctness of the proposed method.

8.4 Summary

This test case demonstrates the trajectory sensitivity based approach to calculate the transient stability constrained interface real power flow limit. Compared to the commonly used methods, this method avoids repeated time domain simulations. Thus, it can significantly reduce the computational burden and provide a good alternative for the calculation of interface flow limit. The result verification part has shown the great accuracy of the proposed method.

9. Conclusions

In this work, the potential applications of the trajectory sensitivity method are explored. Some important issues regarding the method are addressed. The following are the main conclusions and features of the work:

1. The trajectory sensitivity calculation can be integrated into existing time domain simulation tools with moderate implementation effort. The method can be implemented as a plug-in routine and be activated on request.
2. Programs to calculate various system parameter sensitivities have been developed and tested. The test results show good performance of both the method and the implementation.
3. The linear approximation accuracy issue is also addressed. It is found that there is a relationship between the bound on the linear approximation error and the bound on the product of the maximum normalized sensitivity and the perturbation size. This relationship appears to be system independent and system operating point independent. Thus, the error-perturbation size analysis method based on this finding serves as a general application guide to evaluate the accuracy of the linear approximation.
4. A parallel computing platform is developed to solve the sensitivity equations in parallel. The cluster architecture together with the formulation of solving different sets of sensitivity equations in parallel greatly enhance the computational efficiency.
5. The uncertainty problem of power system modeling can be addressed by the trajectory sensitivity method. An example to study the uncertainty of the composite load modeling and its effect on the system voltage stability problem is provided.
6. The applicability of the trajectory sensitivity approach to a large realistic network is demonstrated in detail. This work applies the trajectory sensitivity analysis method to the WECC system. Several typical power system stability problems have been addressed, including the angle stability problem, the voltage stability problem considering load uncertainties and the transient stability constraint interface real power flow limit calculation.

The next phase of this work aims at the following aspects:

1. Explore the possibility of the implementation of the trajectory sensitivity method in commercial software. Current implementation on a research grade software has demonstrated the great performance of the method, therefore the next step is to seek opportunities to commercialize it.
2. Study in more depth the control strategy decision making utilizing the trajectory sensitivity method. Currently the method does not take into account the cost of the control; therefore the next step is to develop an optimization model that involves economic considerations.
3. Explore other possible applications of the trajectory sensitivity method to power systems, such as system component modeling parameter validation.

References

[1]. R. Tomovic, Sensitivity Analysis of Dynamic Systems, New York, McGraw Hill, 1963.

[2]. P. Frank, Introduction to System Sensitivity Theory. New York: Academic Press, 1978.

[3]. W. Feehery, J. Tolsma, P. Barton, "Efficient sensitivity analysis of large-scale differential-algebraic systems," *Appl. Number. Math.*, v. 25, pp. 41 – 54, 1997.

[4]. J. Cruz Jr., System Sensitivity Analysis. Stroudsburg, PA: Dowden, Hutchinson and Ross, 1973.

[5]. S. Li, L. Petzold, W. Zhu, "Sensitivity analysis of differential-algebraic equations: a comparison of methods on a special problem," *Appl. Number. Math.*, v. 32, No. 8, pp. 161 – 174, 2000.

[6]. M. J. Laufenberg, M. A. Pai, "Sensitivity theory in power systems: application in dynamic security analysis," *Proceedings of the IEEE International Conference on Control Applications*, pp. 738 – 743, Dearborn, Michigan, Sept. 15 – 18, 1996.

[7]. M. J. Laufenberg, M. A. Pai, "A new approach to dynamic security assessment using trajectory sensitivities," *IEEE Trans. Power Syst*., v. 13, No. 3, pp. 953 – 958, 1998.

[8]. I. A. Hiskens, M. A. Pai, "Sensitivity analysis of power system trajectories: recent results," *Proc. of IEEE International Symposium on Circuits and Systems*, v. 3, pp. 439 – 443, June 1998.

[9]. I. A. Hiskens, M. A. Pai, "Trajectory sensitivity analysis of hybrid systems," *IEEE Trans. Circuits Syst. I, Fundam. Theory Appl.*, v. 47, No. 2, pp. 204 – 220, Feb, 2000.

[10]. I. A. Hiskens, J. Alseddiqui, "Sensitivity, approximation, and uncertainty in power system dynamic simulation," *IEEE Trans. Power Syst*., v. 21, No. 4, pp. 1808 – 1820, Nov. 2006.

[11]. I. A. Hiskens, M. A. Pai, T. B. Nguyen, "Bounding uncertainty in power system dynamic simulations," *IEEE PES Winter Meeting*, v. 2, pp. 1533 – 1537, 2000.

[12]. I. A. Hiskens, M. Akke, "Analysis of the Nordel power grid disturbance of January 1, 1997 using trajectory sensitivities," *IEEE Trans. on Power Syst.*, v. 14, No. 3, pp. 987 – 994, Aug. 1999.

[13]. T. B. Nguyen, M. A. Pai, I. A. Hiskens, "Trajectory sensitivity as a tool for dynamic security assessment," *in Proceedings of the International Symposium on Bulk Power System Dynamics and Control – V*, Onomichi, Japan, Aug. 2001.

[14]. S. M. Benchluch, J. H. Chow, "A trajectory sensitivity method for the identification of nonlinear excitation system models," *IEEE Trans. on Energy Conversion*, v. 8, pp. 159 – 164, June, 1993.

[15]. S. Q. Yuan, D. Z. Fang, "Robust PSS parameters design using a trajectory sensitivity approach," *IEEE Trans. on Power Syst.*, v. 24, No. 2, May, 2009.

[16]. B. Sapkota, V. Vittal, "Dynamic VAr planning in a large power system using trajectory sensitivities," *IEEE Trans. on Power Syst.*, v. 25, No. 1, pp. 461 – 469, Feb. 2010.

[17]. T. B. Nguyen, M. A. Pai, "Dynamic security-constrained rescheduling of power system using trajectory sensitivities," *IEEE Trans. on Power Syst.*, v. 18, No. 2, pp. 848 – 855, May, 2003.

[18]. R. M. Pereira, C. M. Ferreira, F. P. Barbosa, "Dynamic voltage stability assessment of an electric power system using trajectory sensitivity analysis," *IEEE Bucharest Power Tech conference*, pp. 1 -6, June – July, 2010.

[19]. M. Zima, P. Korba, G. Anderson, "Power system voltage emergency control approach using trajectory sensitivities," *Proceedings of IEEE Conference on Control Application*, v. 1, pp. 189 – 194, 2003.

[20]. I. A. Hiskens, M. A. Pai, "Power system applications of trajectory sensitivities," *IEEE PES Winter Meeting*, 2002, v. 2, pp. 1200 – 1205.

[21]. D. Chatterjee, A. Ghosh, M. A. Pai, "Trajectory sensitivity analysis in distributed generation systems," *International Conference on Power Electronics, Drives and Energy Systems*, pp. 1- 6, 2006.

[22]. A. Ghosh, D. Chatterjee, P. Bhandiwad, M. A. Pai, "Trajectory sensitivity analysis of TCSC compensated power system," *IEEE PES GM*, v. 2, pp. 1515 – 1520, 2004.

[23]. C. Ferreira, J. Pinto, F. Barbosa, "Transient stability assessment of an electric power system using trajectory sensitivity analysis," *39th University Power Engineering Conference*, v. 2, pp. 1091 – 1095, 2004.

[24]. D. Chatterjee, A. Ghosh, "Using trajectory sensitivity for stability assessment of a Ward- PV equivalent power system," *IEEE PES GM*, pp. 1- 7, 2007.

[25]. I. A. Hiskens, M. A. Pai, P. W. Sauer, "An iterative approach to calculating dynamic ATC," *in Proc. Int. Symp. Buck Power System Dynamics Control –IV*, Santorini, Greece, Aug. 1998.

[26]. T. B. Nguyen, M. A. Pai, I. A. Hiskens, "Direct computation of critical clearing time using trajectory sensitivities," *IEEE PES Winter Meeting*, 2000, v. 1, pp. 604 – 608, 2000.

[27]. E. Cari, L. Alberto, N. Bretas, "A novel methodology for power angle estimation of synchronous generator based on trajectory sensitivity analysis," *IEEE PES GM*, pp. 1 – 6, 2009.

[28]. D. Chamiotis, M. A. Pai, I. A. Hiskens, "Sensitivity analysis of differential-algebraic systems using the GMRES method- application to power systems," *in Proc. IEEE Int. Symp. Circuits Syst.*, 2001.

[29]. V. Vittal, E. Z. Zhou, C. Hwang, A. A. Fouad, "Derivation of stability limits using analytical sensitivity of the transient energy margin," *IEEE Trans. on Power Syst.*, v. 4, pp. 1363 – 1372, Nov. 1989.

[30]. A. A. Fouad, J. Tong, "Stability constrained optimal rescheduling of generation,"

IEEE Trans. on Power Syst., v. 8, No. 1, pp. 105-112, Feb. 1993.

[31]. W. Shao, V. Vittal, "Corrective switching algorithm for relieving overloads and voltage violations," *IEEE Trans. on Power Syst.*, v. 20, No. 4, pp. 1877-1885, Nov. 2005.

[32]. D. Kuo, A. Bose, "A generation rescheduling method to increase the dynamic security of power systems," *IEEE Trans. on Power Syst.*, v. 10, pp. 68- 76, Feb. 1995.

[33]. M. La Scala, M. Trovato, C. Antonelli, "On-line dynamic preventive control: an algorithm for transient security dispatch," *IEEE Trans. on Power Syst.*, v. 13, pp. 601 - 610, May 1998.

[34]. P. W. Sauer, M. A. Pai, Power System Dynamic and Stability. Englewood Cliffs, NJ: Prentice – Hall, 1998.

[35]. P. Kundur, Power System Stability and Control, McGraw – Hill, 1994.

[36]. I. A. Hiskens, A. J. A. Koeman, "Power system parameter estimation," *J. Electr. Electron. Eng. Aust.*, v. 19, No. 1, pp. 1 – 8, June, 1999.

[37]. F. Milano, "An open source power system analysis toolbox," *IEEE Trans. on Power Syst.*, v. 20, No. 3, pp. 1199 – 1206, Aug. 2005.

[38]. L. Vanfretti, F. Milano, "Application of the PSAT, an open source software, for educational and research purpose," IEEE PES, GM, Tampa, USA, 24- 28 June 2007.

[39]. F. Milano, "PSAT documentation", available at: http://www.power.uwaterloo.ca/~fmilano/psat.htm.

[40]. M. Stifter, F. Milnao, "An example of integrating open source modeling frameworks: the integration of GIS in PSAT," IEEE PES GM, Calgary, Canada, July 2009.

[41]. High Performance Computing Initiative. [Online]. Available: http://hpc.asu.edu/

[42]. S. Liu, A. R. Messina, V. Vittal, "A normal form analysis approach to sitting power system stabilizers (PSSs) and assessing power system nonlinear behavior," *IEEE Trans. on Power Syst.*, v. 21, No. 4, pp. 1755 – 1762, Nov. 2006.

[43]. IEEE Committee Report, "Transient stability test systems for direct stability methods," *IEEE Trans. on Power Syst.*, v. 7, No. 1, pp. 37 – 43, Feb. 1992.

[44]. W. Kao, "The effect of load models on unstable low-frequency oscillation damping in Taipei system experience w/wo power system stabilizers," *IEEE Trans. Power Syst.*, v. 16, No. 3, pp. 463 – 472, 2001.

[45]. H. Dong, R. He, "Uncertainty analysis of load models in dynamic stability," *IEEE PES General Meeting*, July, 2008, pp. 1 – 6.

[46]. P. Pourbeik, B. Agrawal, "A hybrid model for representing air-conditioner compressor motor behavior in power system studies," *Proc. IEEE PES General Meeting*, July, 2008, pp. 1 - 8.

[47]. D. Kosterev, A. Meklin, J. Undrill, B. Lesieutre, W. Price, D. Chassin, R. Bravo, S.

Yang, “Load modeling in power system studies: WECC progress update,” *Proc. IEEE PES General Meeting*, July, 2008, pp. 1 - 8.

[48]. B. Lesieutre, D. Kosterev, J. Undrill, “Phasor modeling approach for single phase a/c motors,” Proc. *IEEE PES General Meeting*, July, 2008, pp. 1 - 8.

[49]. D. Han, J. Ma, R. He, Z. Dong, “A real application of measurement-based load modeling in large-scale power system grids and its validation,” *IEEE Trans. Power Syst*., v. 24, No. 4, pp. 1756 – 1764, 2009.

[50]. B. Lee, H. Song, S. Kwon, G. Jang, J. Kim, V. Ajjarapu, ‘A study on determination of interface flow limits in the KEPCO system using modified continuation power flow (MCPF).' *IEEE Trans. Power System*, v. 17, No. 3, pp. 557 – 564, 2003.

[51]. S. Kim, H. Song, B. Lee, S. Kwon, ‘Enhancement of interface flow limit using static synchronous series compensators,’ *IEEE PES Transmission and distribution conference and exhibition*, pp. 714 – 720, May 2006.

[52]. R. Austria, X. Y. Chao, N. Reppen, D. Welsh, ‘Integrated approach to transfer limit calculation,’ *IEEE Comput. Appl. Power*, v. 8, pp. 48 – 52, Jan. 1995

[53]. G. Ejebe, J. Tong, J. G. Waight, J. G. Frame, X. Wang, W. F. Tinney, ‘Available transfer capability calculations,’ *IEEE Trans. Power Syst*., v. 13, pp. 623 – 634, Nov. 1998

[54]. L. Wang, C. Y. Chung, ‘Increasing power transfer limits at interface constrained by small-signal stability,’ *IEEE PES Winter Meeting*, v. 2, pp. 1184 – 1196, 2002

[55]. NERC, ‘TPL – (001 thru 004) – WECC – 1 – CR – System Performance Criteria,’, NERC, available at: http://www.nerc.com/page.php?cid=2|20

[56]. PowerWorld, available at: http://www.powerworld.com/

[57]. DSATools, available at: http://www.dsatools.com/

[58]. NYISO, “NYISO interface stability limit analysis for all lines I/S and outage conditions,” [on line] available at: http://www.nyiso.com/public/webdocs/documents/studies_reports/operating_studies/interface_stability_limit_analysis.pdf

Project Publications

[1] G. Hou, and V. Vittal, "Cluster computing-based trajectory sensitivity analysis application to the WECC system," *IEEE Trans. on Power Syst*., v. 26, No. 3, pp. 1 – 8, 2011.